UNIVERSITÀ DI PARMA

UNIVERSITA' DEGLI STUDI DI PARMA

DOTTORATO DI RICERCA IN INGEGNERIA INDUSTRIALE

CICLO XXXVIII

Bolt Preload Effects in Insulated Rail Joints: Numerical Modelling, Static–Dynamic Testing, and Modal-Based Condition Assessment

Coordinatore:

Chiar.mo Prof. Alessandro Tasora

Tutore:

Chiar.mo Prof. Luca Collini

Dottorando:

Francesco Benelli

Anni Accademici 2022/2023 – 2024/2025

Table of contents

1 Introduction

1.1 Background

Among land transport modes, the train is arguably the fastest and most comfortable. Nowadays, it is essential for our society to focus on the environmental impact of mass transportation systems: an increasing number of people feel the need to cover long distances in a short time, for several reasons (work, leisure).

It is therefore worth emphasizing that rail transport currently represents one of the most ecological solutions to this challenge: the use of electric traction, ideally sourced from renewable energy, its intrinsic energy efficiency due to the reduced rolling resistance between wheel and rail, and its high carrying capacity make the train the quintessential “green” mode of transport.

Furthermore, railway transport is synonymous with safety: numerous European studies and statistical reports indicate that, after commercial aviation, rail transport has the lowest fatality risk per passenger-kilometer traveled [1]

This important level of safety has been achieved, decade after decade, thanks to technical standards and regulations. For instance, standards such as EN 50126, EN 50128, and EN 50129 govern the reliability, availability, maintainability, and safety (RAMS) of railway systems, including software and signalling.

Some of these infrastructural and maintenance standards specifically concern a very critical component of the railway superstructure: the insulated rail joint (IRJ), a system that connects two consecutive rails by means of plates and bolts. The relevant standards—EN 13146, EN 13230, and EN 13674—define the requirements for fatigue resistance, electrical insulation, and the service life of the joint.

IRJs act as a safety valve within railways, serving as a fundamental component of the signalling system to determine the position of the train. Unfortunately, by introducing material discontinuity, they reduce the service life of that section of rail by up to one tenth [2]

Due to its complex structure, the mechanical performance of insulated rail joints is governed by a combination of structural and operational factors. The condition and stiffness of the ballast play a fundamental role, as insufficient support can amplify stress concentrations and accelerate joint deterioration [3]. The geometry and material properties of the fishplates also influence the distribution of loads across the joint, affecting both stiffness and fatigue resistance [4]. Train-related variables such as axle load and running speed directly impact the magnitude and frequency of dynamic stresses transmitted to the joint [5]. Collectively, these factors determine the service life and reliability of IRJs, highlighting the importance of integrated design, monitoring, and maintenance strategies to avoid catastrophic accidents, such as the well-known Pioltello case [6] In this disastrous event, a crack that had formed around the bolt holes propagated all the way to the railhead: with the passage of multiple trains, an entire section of the rail detached, causing the derailment of a passenger train, resulting in three fatalities and two hundred injuries.

The worst problem in insulated rail joints is that structural defects like these are not easily detectable, particularly through routine visual inspections, since the cracks can remain hidden beneath the joint plates and insulating material. One of the primary limitations of traditional visual inspections or experimental methods lies in the difficulty of detecting specific structural weaknesses and the need for prior knowledge regarding the location and nature of potential damage. Consequently, in recent years, Structural Health Monitoring (SHM) has emerged as a crucial field across industrial, aerospace, and civil engineering sectors. SHM encompasses a broad range of approaches aimed at identifying, evaluating, and mitigating structural damage. This field seeks to transform conventional practices for inspection, maintenance, and criticality assessment—traditionally dependent on human observation or localized testing—by leveraging data-driven techniques and machine learning to enable more accurate and proactive structural evaluation.

1.2 Aim of the thesis

After briefly describing the background related to the insulated rail joint, it is now necessary to clearly outline the scope and positioning of this PhD research.

Another critical factor, still scarcely explored in the literature, concerns the loss of preload in the bolts responsible for clamping the joint. This phenomenon, which can occur spontaneously

and with high frequency, causes a significant alteration of the joint's mechanical response to applied loads, leading to a deterioration of operational conditions and an acceleration of wear processes.

Therefore, the aim of this study is to identify and monitor the critical parameters of the joint under progressive bolt preload loss, with the ultimate objective of improving an on-site structural health monitoring system capable of supporting predictive maintenance and complementing the visual inspections currently in use.

In order to achieve robust and reliable results, a comprehensive methodology was adopted, combining numerical simulations based on the finite element method with experimental investigations conducted under both static and dynamic conditions. Within the experimental framework, multiple measurement strategies were implemented through the use of state-of-the-art instrumentation, ensuring a high level of accuracy and reproducibility in the acquired data.

1.3 Outline

The thesis is organized as follows:

- **Section 2**: an in-depth analysis is dedicated to the insulated rail joint (IRJ), which, being the central focus of this study, deserves a prominent space within this work. First, the general railway context will be outlined, highlighting its importance within the transport sector and the associated maintenance costs. Subsequently, the typical railway superstructure will be briefly described, leading to the role that IRJs have played and continue to play within it. The structure, geometries, and materials of the joint will then be presented, followed by its applications across different types of railway lines and the way in which the mechanical and operational challenges vary accordingly. A significant part of this section will be devoted to describing the main mechanisms of wear, degradation, and malfunction that may affect the joint. In addition, the operational conditions under which IRJs must function will be addressed, including environmental and climatic factors, loads, speeds, track geometry, and stability. Finally, several case studies will be examined, which unfortunately entered history as catastrophic accidents that resulted in the loss of human lives.

- **Section 3**: a review of main methodological approaches used to study IRJ. It covers numerical techniques, particularly finite element simulations, as well as experimental methods, including both static and dynamic tests. Measurement strategies are discussed, from traditional sensors such as strain gauges to advanced technologies like vision-based systems, with considerations on laboratory versus field set-ups. The chapter also addresses common data processing and analysis methods, including signal filtering, modal analysis, and data-driven approaches.

- **Section 4**: this part of the study presents the finite element analysis (FEM) of IRJ, focusing on the effect of bolt preload on its mechanical response. The development of the numerical model is described, including geometry, material properties, boundary conditions, and loading scenarios. Mesh generation and convergence studies are addressed to ensure accuracy and reliability.

- **Section 5**: the work, here, presents the static testing campaign conducted on insulated rail joint, once again, with particular focus on the influence of bolt preload. The chapter begins with a description of the test standards and guidelines, including reference to RFI norms and any adaptations applied. The preparation of the test specimens is detailed, covering joint modifications and the layout of sensors and instrumentation. The testing procedure is then outlined, with emphasis on load application, the four-point bending test, and measurement strategies. Results are presented in terms of displacement-time and load-displacement curves, providing comparisons with FEM predictions. The chapter concludes with a discussion of the implications for IRJ performance, durability, design, and maintenance, as well as the limitations of the experimental approach.

- **Section 6**: the presentation of dynamic modal tests on IRJ focus on vertical and horizontal excitations. This section emphasizes the test setup, particularly on the layout employed for the accelerometers and LiDAR. The test procedure covers impact hammer excitation, measurement strategies, and modal analysis. Results highlight natural frequencies, mode shapes, and the influence of bolt preload, with comparisons to FEM and static tests.

- **Section 7**: the closing chapter discusses and summarizes the integration of numerical and experimental results on IRJs, emphasizing the influence of bolt preload and identification of critical zones. Key findings from FEM, static, and dynamic tests are presented, highlighting implications for joint design, durability, and predictive maintenance. Limitations of the study are addressed, and future research directions are proposed, including improved monitoring systems and investigation of additional influencing factors.

2 Insulated Rail Joint (IRJ)

2.1 Background on Railway Transport

2.1.1 Rail transport importance

Rail transport today plays a central role in European mobility and logistics, combining rising passenger demand with significant freight throughput and strong policy support for modal shift to more sustainable transport. Passenger rail reached a record level in the European Union in 2023, with about 429 billion passenger-kilometers (pkm), an 11.2% increase compared to 2022 and slightly above the pre-pandemic 2019 level. Freight rail, while more volatile, remains essential for long-distance cargo: main undertakings transported roughly 378 billion tonnes-kilometers (tkm) in 2023. These figures confirm the importance of rail both for passengers and goods, especially in the context of decarbonization strategies and sustainable transport policies [7].

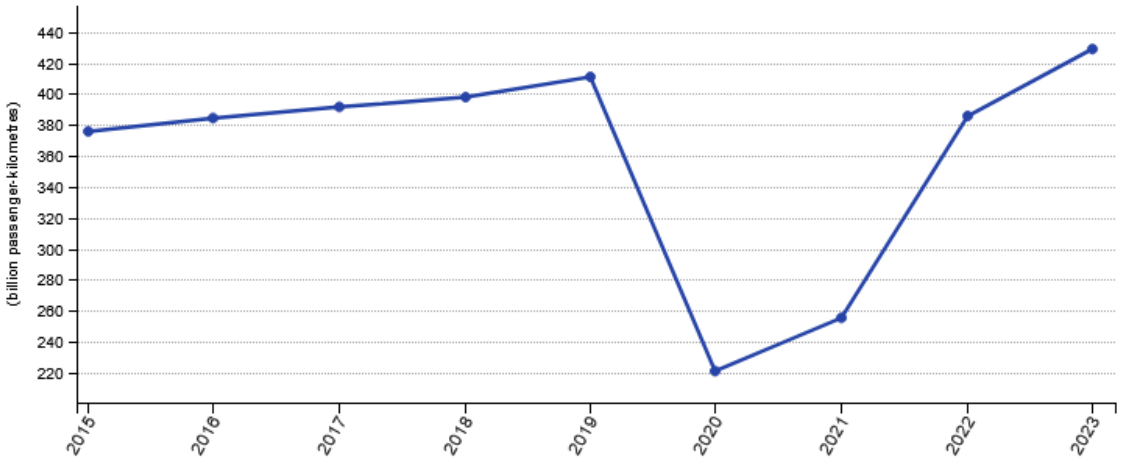

Figure 1. Rail passenger transport for main undertakings, EU, 2015-2023 [7]

Italy reflects these broader European trends, with national rail passenger traffic estimated at 54–58 billion passenger-km in 2023–2024 and the FS Group reporting around 46 billion passenger-km in 2023. Rail freight maintains a share close to 12% in Italy's modal split.

Overall, rail remains one of the most sustainable and safe modes of transport, offering high energy efficiency and low CO_2 emissions, especially when powered by renewable electricity.

Figure 2. Passenger and freight convoys [8]

The UIC Traction Energy and Emission Reporting shows that passenger train energy consumption dropped by 16% from 2005 to 2022, while freight train energy consumption fell by 68% [8].

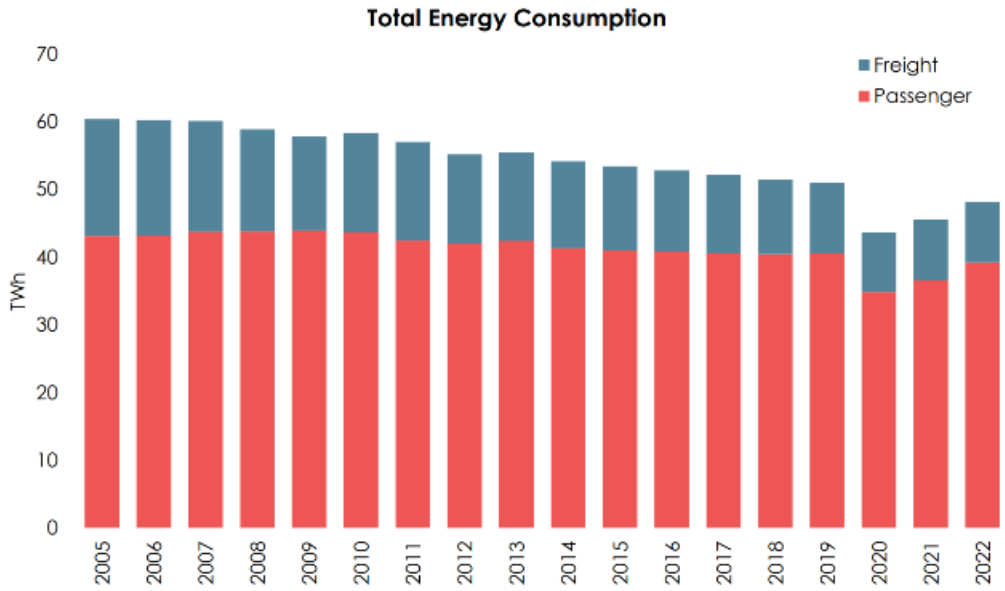

Figure 3. Total Energy Consumption between 2005 and 2022 [8]

Rail transport represents, by far, the fastest and most reliable mode of terrestrial transportation[9].

2.1.2 Rail Transport Maintenance

The importance of railway maintenance lies in its direct impact on safety, reliability, and cost-efficiency of rail transport systems. Proper maintenance ensures the structural integrity of the track and rolling stock, reduces failures and minimizes service disruptions that could affect both passenger and freight operations. In Europe, maintenance activities account for a significant share of total railway expenditure: according to the European Union Agency for Railways, track maintenance costs can represent up to 30–50% of infrastructure managers' annual budgets [10].

The financial relevance of maintenance is particularly evident in high-density networks, such as those of Italy and Germany, where high traffic volumes accelerate track degradation. Consequently, optimizing maintenance strategies—through predictive approaches, advanced monitoring systems, and data-driven decision-making—has become essential to balance operational efficiency, safety, and cost sustainability.

These expenses are typically divided into:

- direct costs: inspection, repair, component replacement
- indirect costs: staff training, transport to a maintenance site, inventory, material order, delays, disruptions, economic losses due to reduced availability of the network.

In railway infrastructure management and maintenance costs could also be distinguished into:

- Ordinary maintenance costs, which refer to routine and recurrent activities required to ensure the safe and efficient operation of the network: inspections, minor repairs, replacement of worn-out components, and ballast cleaning. These interventions are predictable, relatively low in cost, and are typically planned on a regular schedule.
- Extraordinary maintenance costs are associated with major interventions aimed at restoring or significantly extending the service life of infrastructure assets: large-scale track renewal, replacement of switches and crossings, structural rehabilitation of bridges or tunnels, and interventions following unexpected failures or accidents.

While ordinary maintenance is crucial for preventing deterioration and minimizing operational disruptions, extraordinary maintenance represents a substantial financial burden, often requiring significant capital investment and causing temporary service suspensions. The balance between these two categories is a central issue in railway asset management, as

optimizing ordinary maintenance can reduce the frequency and cost intensity of extraordinary interventions.

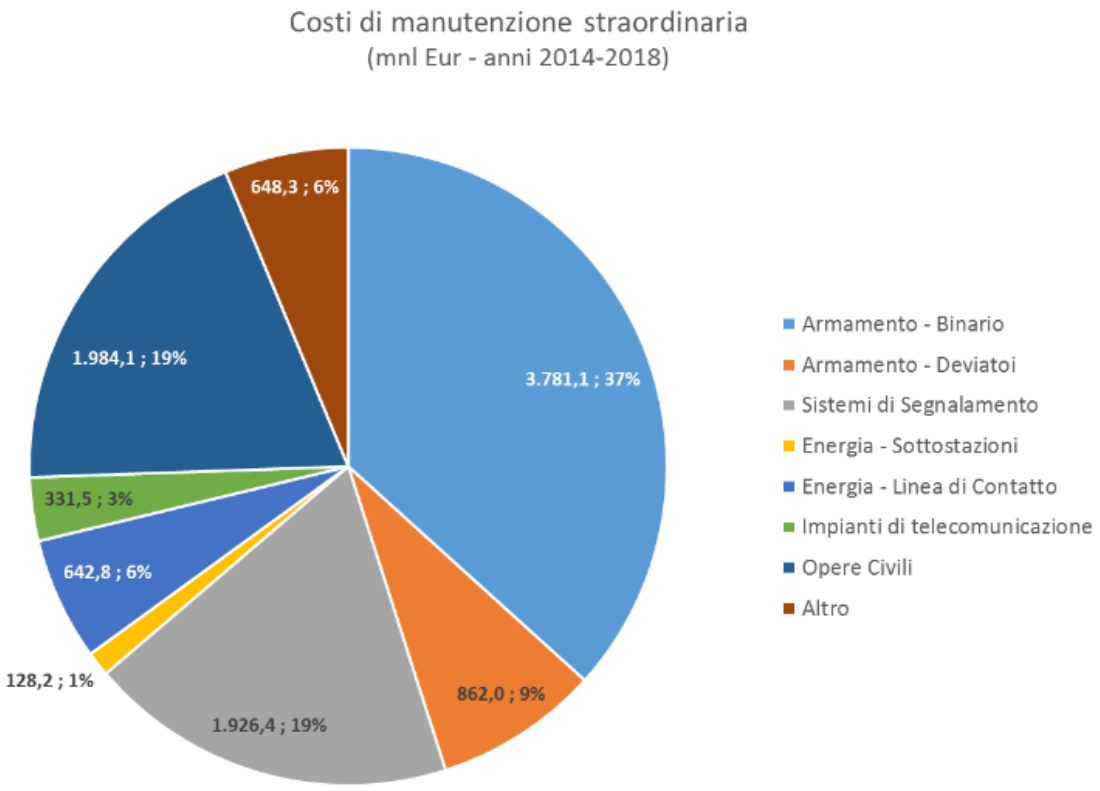

Figure 4. Distribution of extraordinary maintenance costs for the period 2014-2018 by cost category of Rete Ferroviaria Italiana [11]

Figure 4 illustrates the amount and distribution of extraordinary maintenance costs of Rete Ferroviaria Italiana (RFI), broken down into the main categories, for the period 2014–2018. Particular attention should be paid to the percentage of extraordinary costs allocated to track and switches, which accounts for approximately 50% of the total extraordinary costs. Specifically, the insulated rail joint (IRJ) requires frequent maintenance, as it introduces material discontinuity in the track and significantly reduces the service life of that rail section. This represents one of the key issues associated with the use of such complex joint systems: the generation of substantial extraordinary costs [11].

2.2 Structure of the Railway Track

Railway track consists of parallel lines of rails fastened to the sleepers: this system is placed over a stratified ballast bed.

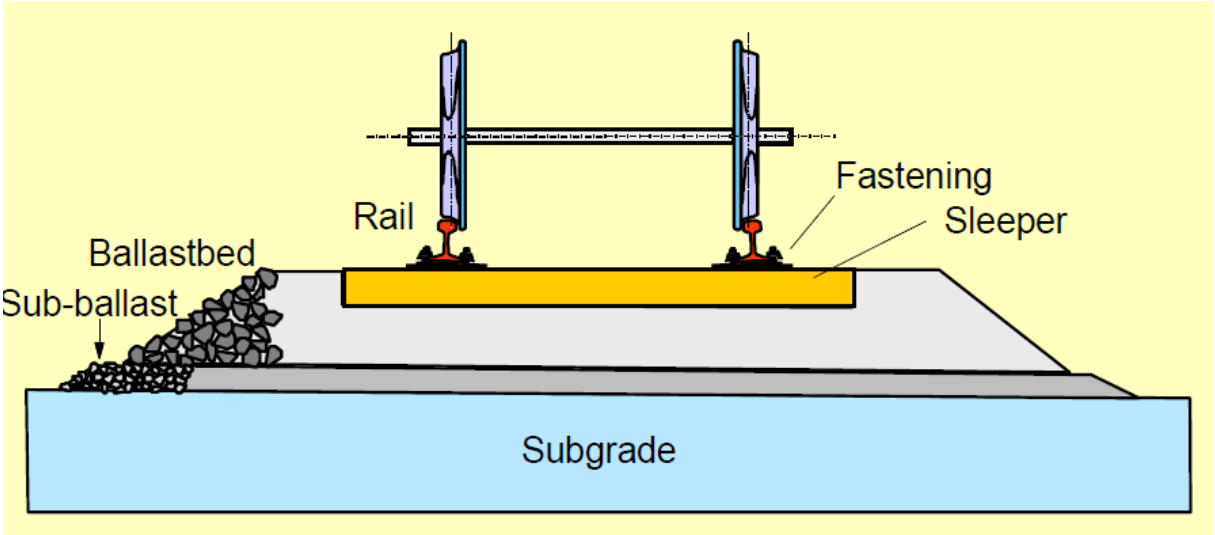

Figure 5. Railway Track Cross Section

2.2.1 Rail

The rail is the most important part of the track, and it is made of steel, for example R260, an unalloyed carbon steel, with a minimum tensile strength of approximately 880 MPa and a hardness of 260 HB.

The main functions of the rail are to:

- Distribute the weight of a train to the sleepers
- Provide a smooth-running surface and assist the wheels in guiding the coaches along the intended direction
- Return the traction current and ensure the transfer of electric signals in track-circuited sections.

There are numerous types of rails, depending on their shape; however, in this work, we will consider exclusively flat-footed ones.

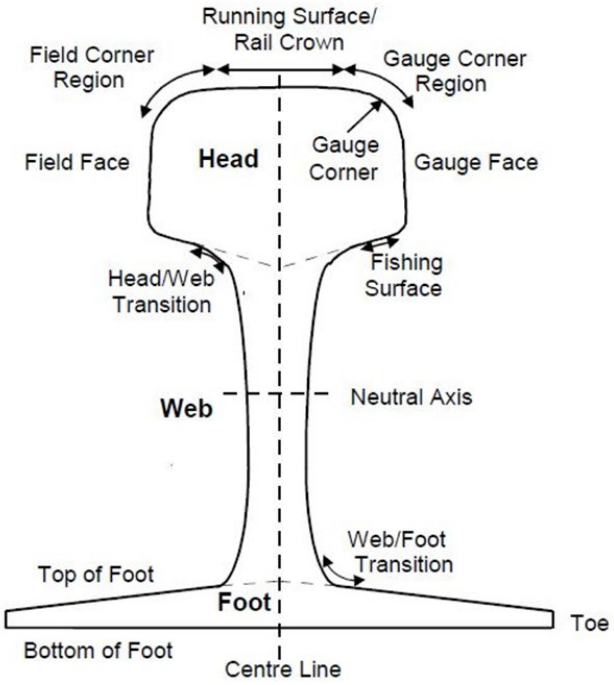

Figure 6. Flat footed rail

The three main sections of a flat-footed rail are:

- The head
- The web
- The foot

The shape of flat-footed rails is a "I" shape (see Figure 6). In the beginning, flat-footed rails were located immediately on the sleeper, but nowadays steel bearing plates have been put between the rail foot and the sleepers due to the increase in loads.

2.2.2 Sleepers

Sleepers are used to transmit the oncoming loads to the track ballast and to maintain the gauge (distance between the inner edges of rail heads, typically 1435 mm in Europe). Nowadays, there are three types of sleepers commonly used:

- Wooden sleepers
- Metal sleepers (cast iron or steel)
- Concrete sleepers

This work will consider only the last type; Sleepers could also have different geometries.

Figure 7. Concrete sleepers

2.2.3 Ballast

Ballast is the layer of crushed stone that forms the lower part of the railway superstructure, located between the track bed and the sleepers. It consists of medium-large, hard, and resistant stones that ensure stability and drainage.

Its functions are to:

- Evenly distribute the loads transmitted by the tracks and trains to the subgrade, preventing deformation and subsidence (with the increasing axle loads and train speeds, the importance of the ballast has risen)
- Ensure effective drainage of rainwater, preventing stagnation that could compromise the stability of the track
- Contribute to the anchoring of the sleepers, maintaining the correct geometry of the tracks

- Facilitate maintenance, as it can be easily cleaned, leveled, or replaced in case of wear or contamination.

In summary, ballast is an essential element in ensuring safety, durability and comfort in railway travel.

2.3 Definition and Role of Insulated Rail Joints

Insulated Rail Joints (IRJs) represent one of the most critical discontinuities within railway tracks. Their primary function is to ensure electrical insulation between adjacent track circuits while simultaneously maintaining mechanical continuity for safe train operations. In essence, an IRJ is a purposely introduced discontinuity in the metallic continuity of the rails, achieved by inserting insulating materials between the cut rail ends and around the fastening system. Unlike conventional rail joints, which serve only structural purposes, IRJs embody a dual role: they must both transmit mechanical loads from one rail to the other and guarantee electrical separation to enable signalling and train detection systems.

The importance of IRJs arises directly from their integration into railway signalling. Modern train detection relies on track circuits, in which electrical current flows through defined sections of the track to detect the presence of a train axle. To ensure that this current remains confined to its intended section, the rail ends must be electrically isolated from neighboring sections. This is precisely the role of IRJs. Without them, it would be impossible to divide a long railway line into discrete blocks for safe signalling and traffic management.

Figure 8. Insulated Rail Joint

From a structural perspective, however, IRJs constitute a weak point in the track. They disrupt the homogeneity of the continuous welded rail (CWR), introducing stress concentrations, stiffness variations, and wear-prone regions.

2.3.1 Historical Background and Development

The origins of insulated rail joints date back to the late nineteenth and early twentieth centuries, coinciding with the rapid development of railway signalling systems. In the earliest railways, train movements were controlled primarily by time intervals and mechanical signalling, without precise train detection along the track. The introduction of track circuits revolutionized railway safety, enabling the automatic detection of trains and thereby reducing the risk of collisions. To make track circuits functional, however, it became necessary to electrically isolate different track sections. This technological shift marked the birth of IRJs.

The first insulated joints were rudimentary in design. Typically, a small insulating element, often made of wood, fiberboard, or basic resin, was inserted between the two rail ends. These early designs provided only limited durability, as the insulating materials degraded rapidly under repeated wheel loads, moisture ingress and temperature fluctuations. Failures were frequent, and maintenance costs were high.

By the mid-twentieth century, with the widespread adoption of continuous welded rail (CWR), the mechanical challenges associated with IRJs became more severe. Whereas conventional fishplated joints were already known to be weak points in the track, the emergence of long stretches of welded rail made the contrast with insulated joints even more evident. As the rest of the track became increasingly continuous and durable, IRJs stood out as localized discontinuities prone to damage. Railways worldwide began to report high maintenance demands associated with IRJs, particularly under conditions of heavy axle loads and increasing train speeds.

To mitigate these issues, many innovations were introduced: the use of advanced polymer composites as insulating materials, hybrid solutions combining adhesives with mechanical fastening and improvements in bolt preload techniques to reduce loss of clamping force. The evolved IRJs, compared to earlier bolted-only joints, demonstrated superior fatigue resistance and longer service lives.

Despite these advancements, IRJs continue to be regarded as one of the weakest elements in railway infrastructure. Numerous studies have highlighted their susceptibility to degradation mechanisms such as cracking, delamination, bolt loosening, and spalling of the insulating material [12], [13]. Field data from European networks consistently show that IRJs require more frequent inspection and replacement compared to other track components, representing a significant share of extraordinary maintenance costs.

In Italy, Rete Ferroviaria Italiana (RFI) has adopted specific standards for IRJ design and testing, reflecting the unique operating conditions of its network. These include not only requirements for static and dynamic strength but also performance under varying climatic conditions, from humid coastal regions to Alpine environments.

Today, the research and development of IRJs continue to focus on two parallel directions:

- Extension of service life: through improved adhesives, more resilient insulating materials and better bolt preload retention.
- Integration with monitoring technologies: IRJs are increasingly seen not only as passive components but also as potential sites for embedded sensors, enabling predictive maintenance strategies.

2.3.2 Function in Railway Signalling and Track Systems

Insulated Rail Joints (IRJs) are special joints used in railway tracks as part of the signalling system. Their main role is to divide the track into separate sections, called blocks, so that the presence of trains can be detected.

Each block works like an electrical circuit: a battery sends a low-voltage current into the rails at one end, and a relay is connected at the other. When no train is on the track (Figure 9), the current flows through the rails and keeps the relay switched on, which tells the signal system that the section is free. When a train enters the block, its wheels and axles connect the two rails together, creating a short circuit (Figure 10). This stops the current from reaching the relay, which then switches off and tells the system that a train is in that section. In this way, IRJs help keep trains moving safely and prevent collisions.

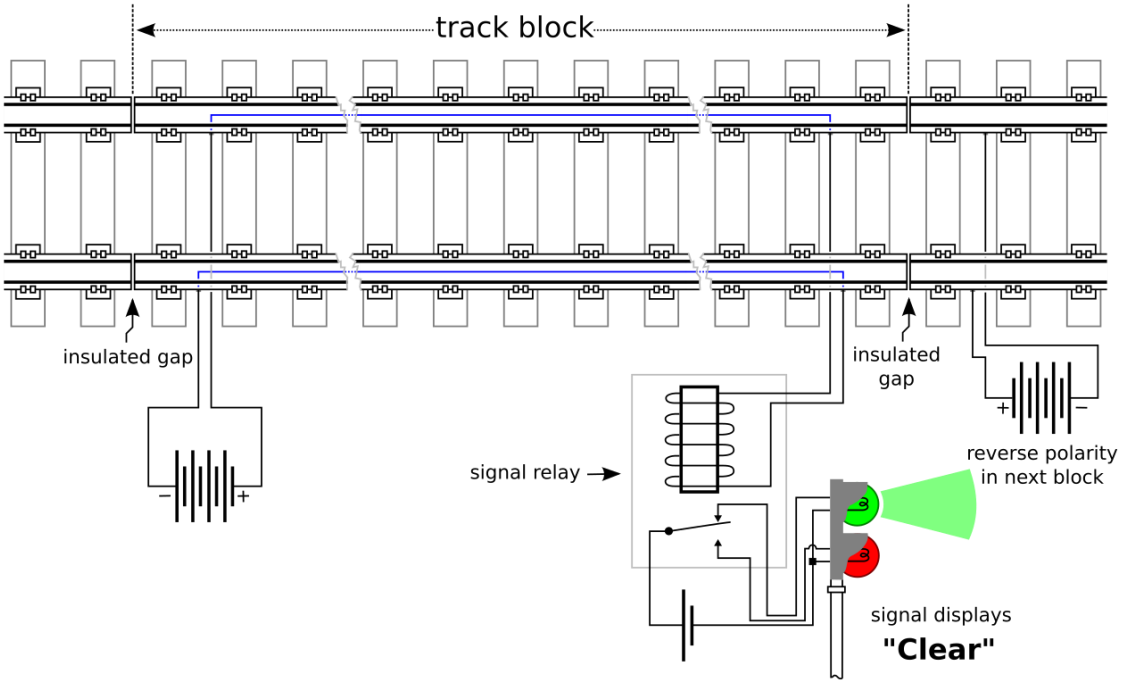

Figure 9. Clear track circuit

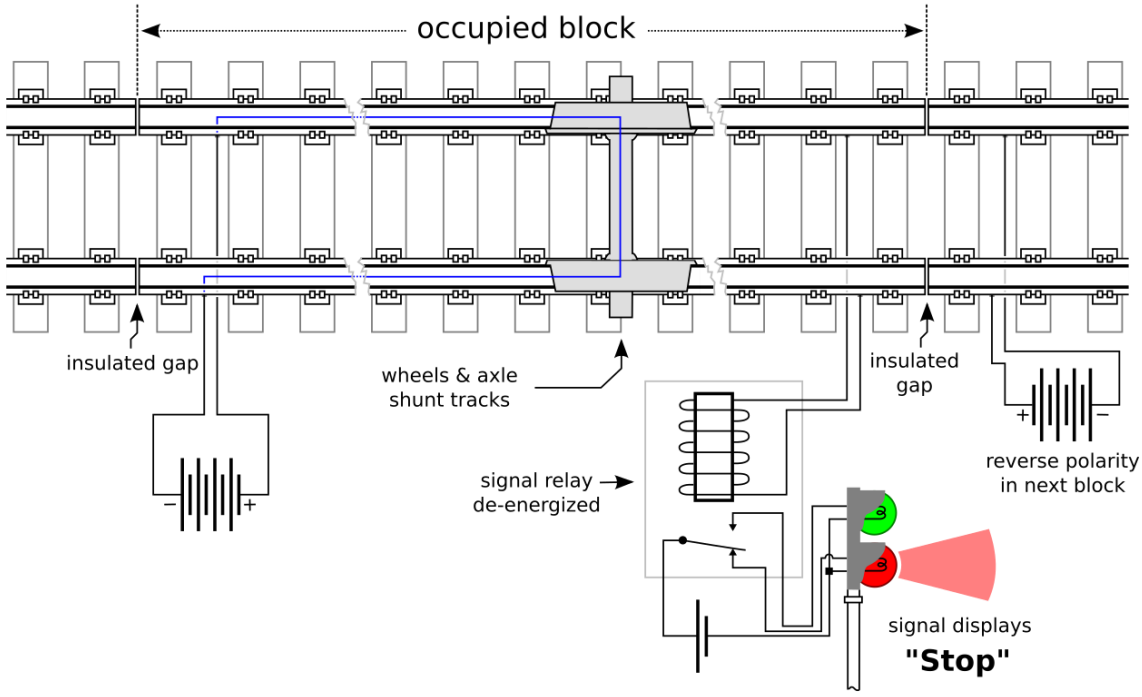

Figure 10. Occupied track circuit

2.4 Structural Characteristics of Insulated Rail Joints

2.4.1 Geometric and Material Aspects

Structurally, IRJs resemble conventional rail joints in their fundamental layout, consisting of two abutting rail ends connected by joint bars (or fishplates) and clamped together by high-strength bolts. However, the critical difference lies in the insertion of insulating components—typically liners, bushes, and end-posts—that prevent metallic contact across the joint. The geometry of the joint must therefore accommodate both mechanical fastening requirements and insulating materials, resulting in a complex and highly stressed discontinuity within the otherwise continuous rail.

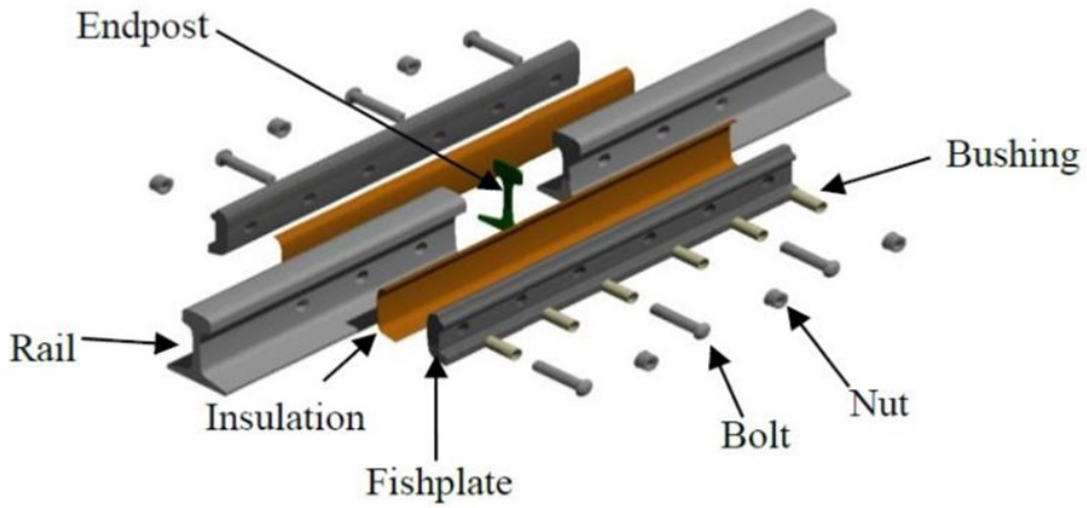

Figure 11. Exploded view of the rail section featuring IRJ

From a geometric perspective, the IRJ comprises three principal regions: the rail ends, the joint bars, and the end-post gap.

The rail ends are precisely machined to ensure a flat and uniform contact surface with the insulating end-post, which is usually 5–10 mm thick depending on national standards.

The joint bars extend along the web and foot of the rail, transferring bending moments and shear forces across the discontinuity. Their length typically ranges between 0.6 and 1.2 meters,

but the optimal geometry is strongly dependent on axle load and line category (conventional, high-speed, or heavy haul). The number and spacing of bolts are equally crucial, as they define both the clamping force distribution and the stiffness of the joint. Excessive spacing may reduce load transfer efficiency, while too close spacing increases stress concentration and accelerates bolt preload loss. Modern designs therefore seek a balance between structural performance and ease of installation.

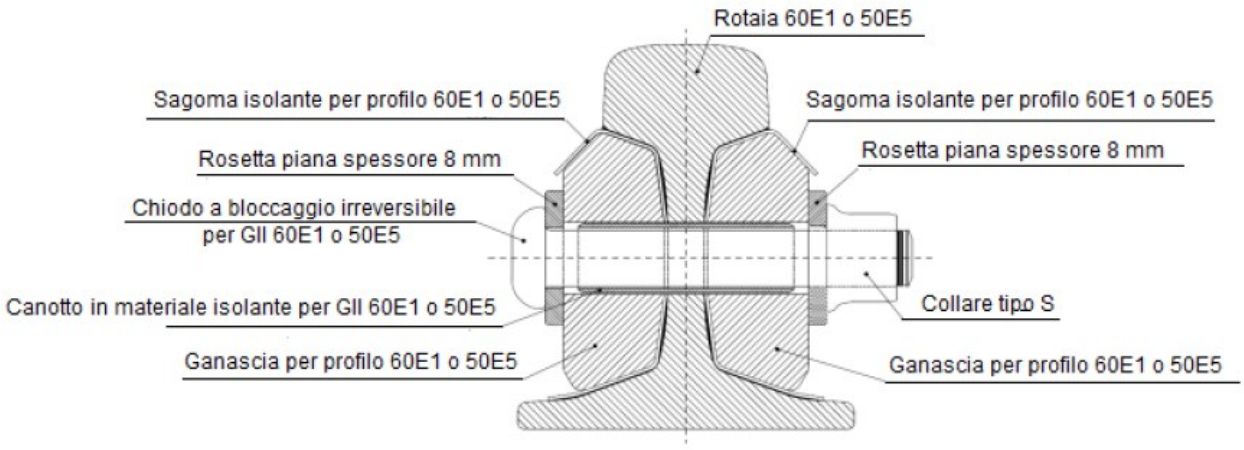

Figure 12. Cross section of IRJ

The insulating elements play a decisive role in IRJ geometry. The end-post, usually made of high-performance epoxy or glass-fiber composites, ensures electrical separation between the rail ends. Its thickness determines the overall joint gap, which, while small, introduces a local discontinuity in wheel-rail contact.

Figure 13. End post

In the most common configuration, the end-post is inserted in the rail gap perpendicular to the longitudinal axis of the track. Alternatively, the insulating element can be installed with an inclination of approximately 15° relative to the rail axis, producing what is known as an inclined IRJ (see Figure 1:15).

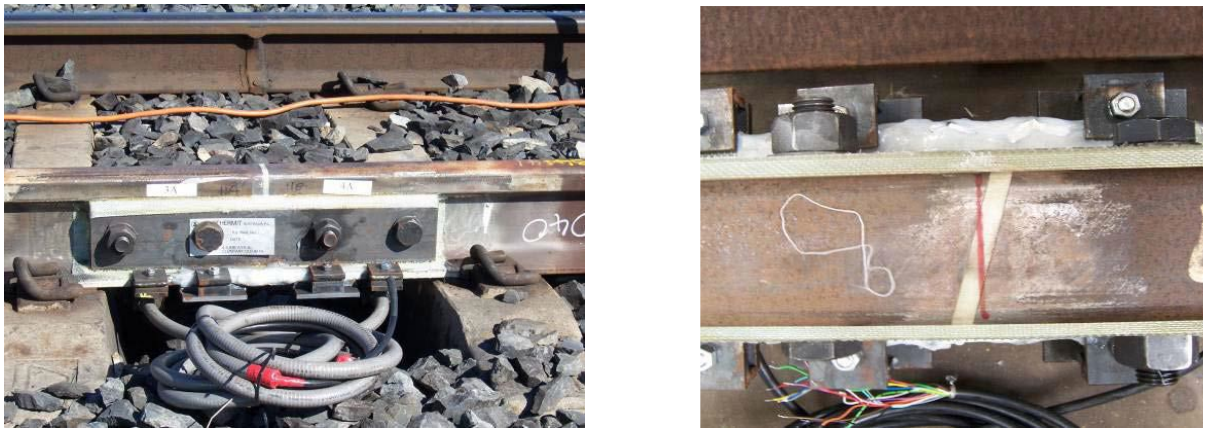

Figure 14. End post configurations

Around the bolts, insulating bushes and washers prevent metallic continuity through the fastening system. Similarly, insulating liners are interposed between the joint bars and the rail web, introducing a layer of non-conductive material that modifies the stiffness distribution across the section. The presence of these components alters the local stress flow within the joint, creating zones of stress concentration that differ significantly from those observed in standard rail sections.

Material selection is equally critical for IRJ performance. The rails themselves are generally manufactured from high-strength pearlitic carbon steels, with typical tensile strengths around 880 MPa and hardness values in the range of 260–300 HB. These materials offer an optimal balance of toughness and wear resistance, but their performance is compromised at the joint due to the introduction of insulating materials with markedly different mechanical properties. Epoxy resins reinforced with glass-fiber, while electrically effective, are comparatively brittle and less resistant to fatigue. This mismatch in stiffness between steel and polymer-based components is one of the principal causes of degradation phenomena such as delamination, cracking, and spalling.

Joint bars are usually made of heat-treated medium-carbon steels, selected for their high yield strength and fatigue endurance.

The bolts used in IRJs are generally high-tensile fasteners (grade 8.8 or higher), preloaded to values that ensure adequate clamping force without inducing excessive crushing of the insulating components. However, the preload is prone to relaxation due to creep in the insulating materials, thermal cycling, and dynamic loading. The loss of bolt preload is a critical factor influencing IRJ mechanical behavior, as it leads to increased impact loading at wheel passage and accelerated degradation of both steel and insulating components.

Overall, the geometric and material characteristics of IRJs highlight the complexity of their structural behavior. The combination of dissimilar materials, geometric discontinuities, and high dynamic loads creates an environment where mechanical performance and durability are difficult to optimize simultaneously.

PART OF IRJ	MATERIAL
Rails	UIC 900A non-alloyed carbon steel
End Post	Nylon or epoxy resin glass fiber reinforced
Fishplates	Medium carbon steel, EN 13674-1 grade R260
Bolts and Nuts	High strength alloy steel, ISO 898-1 grade 10.9
Insulating bushes and layers	Nylon or epoxy resin glass fiber reinforced

Table 1. IRJ parts' materials

2.4.2 IRJ's configurations

Different types of insulated rail joints (IRJs) can be identified, and they are generally classified according to three main criteria:

1. The number of bolts employed: six-bolt joints are typically adopted in heavy haul and high-speed lines, where dynamic forces are more severe, while four-bolt solutions are often sufficient for lighter traffic conditions (Figure 15).

2. Whether the joint is glued or non-glued: in first ones, epoxy resin adhesives are applied, in addition to mechanical fastening, to increase stiffness and reduce relative movement

at the rail interface. This results in improved fatigue life and better electrical insulation performance, making glued joints the preferred solution in modern railway systems. Non-glued IRJs, on the other hand, rely solely on mechanical bolting and insulating components. While they are simpler and less expensive to install, they generally exhibit lower durability and require more frequent maintenance (Figure 16).

3. The relative position of the joint and sleepers: joints can be positioned directly above a sleeper (supported) or between two sleepers (suspended). On-sleeper joints benefit from increased structural support and reduced deflection under train loads, whereas between-sleeper joints are more prone to bending and stress concentration, leading to accelerated degradation. Therefore, modern track design tends to favor on-sleeper placement, although site constraints and track geometry can sometimes dictate alternative solutions (Figure 17).

Figure 15. IRJ with four and six bolts

Figure 16. Glued and non-glued IRJs

Figure 17. Suspended and supported IRJ

2.5 Influencing Factors on IRJ Performance

The mechanical and operational performance of IRJs is influenced by a variety of factors, each of which can significantly affect their durability, reliability, and maintenance requirements.

- The loading conditions: axle loads, train speed and traffic density, which dictate the magnitude and frequency of forces transmitted through the joint.
- Environmental and climatic conditions, such as temperature variations, humidity, and seasonal effects, also play a decisive role, impacting material behavior, thermal expansion, and the long-term performance of insulating components.
- Additionally, the geometry of the track and the quality of installation can either mitigate or exacerbate stress concentrations within the joint, influencing the onset of wear, fatigue, and structural degradation.

Understanding these factors is essential for both the design and the maintenance of IRJs, as it allows engineers to anticipate critical vulnerabilities, optimize inspection schedules, and implement effective mitigation strategies. In the following subsections, each of these influencing factors will be analyzed in detail, highlighting their interaction with the mechanical and operational behavior of the joint under real-world conditions.

2.5.1 Loading Conditions

The loading conditions imposed on IRJ represent one of the most significant factors affecting its mechanical performance and service life. These conditions are primarily determined by three interrelated parameters:

- Axle load
- Train speed
- Traffic density

The axle load transfers both vertical and horizontal loads to the rail, due to the truncated cone geometry of the railway wheel, and directly influences the bending and shear stresses experienced by the joint. Heavier axle loads, as encountered in freight or high-speed rail, amplify bending moments at the rail ends, especially in fishplate and end-post regions, significantly increasing the probability of micro-cracking and stress concentration, accelerating mechanisms of wear, fatigue, and failure [14].

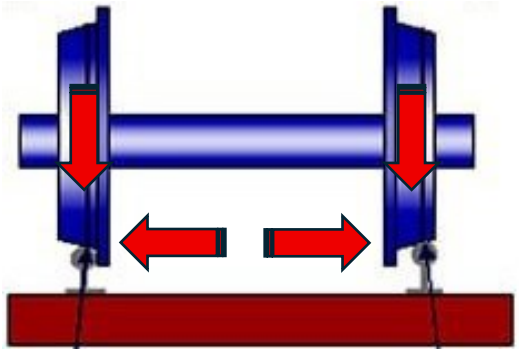

Figure 18. Axle load transmission diagram

Train speed also plays a crucial role, not only in amplifying dynamic forces but also in modifying the frequency and magnitude of cyclic loads. At higher speeds, the IRJ experiences increased impact forces, which can exacerbate wear at the rail-end contact surface and accelerate bolt preload loss, increasing maintenance requirements. Furthermore, the interaction between speed and track irregularities may induce localized vibration modes that can reduce fatigue life [15].

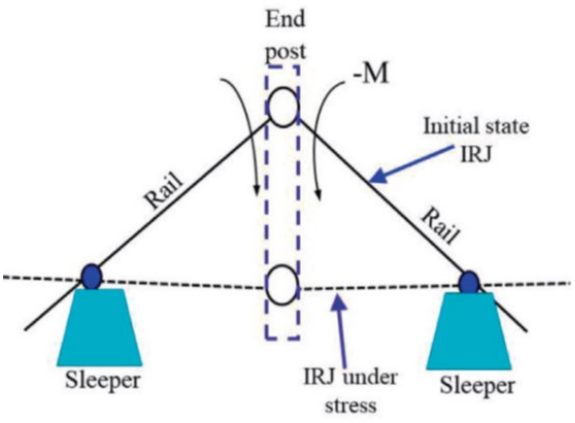

Figure 19. IRJ structural scheme

Traffic density, encompassing the number of train passages over a given period, further complicates the stress scenario. High traffic density leads to more frequent load cycles, increasing cumulative fatigue effects on both metallic and insulating components. In European networks, heavily trafficked lines have been shown to require more frequent inspection and replacement of IRJs compared to lighter lines[16]

The combination of high axle loads, elevated speeds, and dense traffic can synergistically amplify mechanical degradation, highlighting the need for careful consideration during the design phase, as well as for predictive maintenance strategies.

2.5.2 Environmental and climatic conditions

Environmental and climatic conditions are another major set of influencing factors for IRJ performance. Temperature fluctuations induce thermal expansion and contraction of the rails, which can generate differential movement at the joint, particularly at the insulating end post. Unlike continuous welded rail, where thermal stresses are distributed over long lengths, the IRJ represents a local discontinuity that concentrates these forces. Seasonal variations in temperature can therefore cause cyclic compression and tension on the end post and adjacent rail ends, potentially leading to material degradation, microcracking, or adhesive failure in glued joints.

Moisture and precipitation are also critical: high humidity and water ingress can accelerate corrosion of joint bars and bolts, reducing both electrical and mechanical integrity.

In addition, freeze-thaw cycles can affect the ballast and the rail-supporting structure, indirectly influencing the load transfer and dynamic behavior of the IRJ. Europe's alpine regions are characterized by frequent IRJ maintenance due to these environmental stresses, while southern regions face challenges related to high ambient temperatures and UV degradation of polymeric insulating components.

2.5.3 Track Geometry and Installation Quality

Track geometry and installation quality constitute the final major factors influencing IRJ performance. Track irregularities, such as variations in gauge, alignment and cross-level, can induce localized bending, twisting, and lateral forces at the joint, which may accelerate wear and fatigue.

Proper installation practices are therefore critical. This includes ensuring accurate bolt torque and preload, correct placement of insulating components, and precise rail-end geometry. Poor installation not only compromises mechanical performance but also increases the likelihood of electrical failures in signalling circuits.

In heavily trafficked European lines, quality control protocols are strictly enforced to mitigate these risks, including the use of laser-guided measurement systems, torque-calibrated hydraulic tools, and post-installation verification via dynamic testing.

2.6 Mechanical and operational challenges

Insulated rail joints by virtue of being deliberate discontinuities in the otherwise uniform track, are inherently more vulnerable to wear and degradation processes than continuous welded rail. The presence of multiple materials (metals and insulating elements), geometrical discontinuities, localized stress concentrations and repeated dynamic loading make IRJs hotspots for damage initiation and progression. In this section we examine the principal wear and degradation mechanisms in IRJs, their interactions, and how they evolve over time under service conditions.

2.6.1 Wear and degradation mechanisms

As previously discussed, the section of railway superstructure characterized by an insulated rail joint has a significantly reduced service life. In its final stage, the IRJ does not fail abruptly, but rather begins to exhibit early signs of wear, leading to progressive malfunctions.

Two primary categories of failures can be distinguished:

- Electric failures
- Mechanical failures

In the first case, the insulating layers—whose mechanical resistance is relatively low—start to crack and detach. As a result, the metallic parts of the joint come into continuous contact, thereby compromising both the insulating function and the electrical separation of the railway track.

However, mechanical failures have greater relevance to this thesis, as they represent the dominant mode of degradation and the focus of the study.

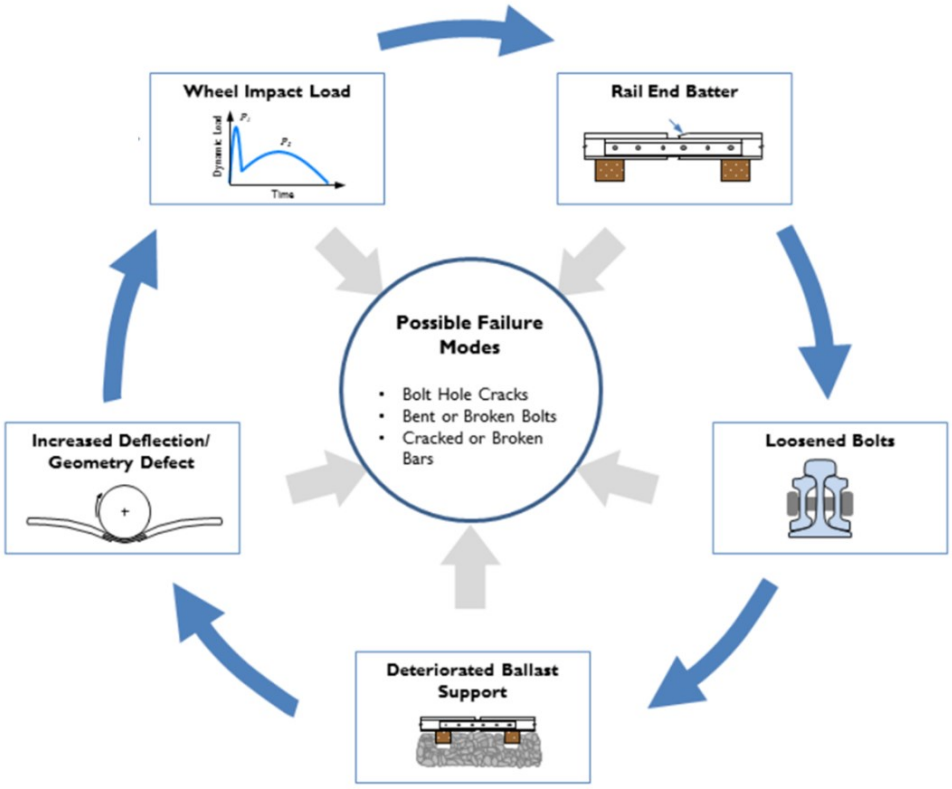

Figure 20. IRJ mechanical degradation cycle

Figure 20 illustrates the progressive degradation cycle that typically occurs in insulated rail joints because of mechanical, structural, and operational stresses. This cycle highlights how minor anomalies at the joint can evolve into severe damage modes, ultimately compromising mechanical integrity.

The dynamic load generated by the repeated passage of trains—varying in weight and speed—together with seasonal thermal cycles and the varying stability of the ballast bed, initiates the first and most fundamental wear mechanism of the joint: the bolt loosening within the joint assembly. Bolts, nuts, and insulating bushes gradually lose their preload due to micro-slippage, wear, and fatigue. Once loosened, bolts allow larger relative displacements between the rail, fishplates, and insulating components, which further amplifies stresses on the insulating end post and adhesive layers. In glued joints, adhesive delamination is often accelerated at this stage, while in mechanically fastened joints, insulating liners or bushes may crack. In the worst-case scenario, the bolts can even come completely out of their seats.

Figure 21. Loss of IRJ bolts

Therefore, due to the excessive play within the joint caused by bolt loosening, the loads generated by train passages become even more severe, exerting significant stress on the fishplates and causing serious damage near the rail ends and the end post. These irregularities disturb the continuity of the running surface and introduce localized discontinuities. When a train passes over such discontinuities, the wheels encounter sudden changes in stiffness and geometry, which generate wheel impact loads. These impact forces are considerably higher than the static wheel loads and are applied repeatedly at the same location, thereby intensifying the stress concentration at the joint.

The area of contact between train wheel and rails (approximately 100 mm^2) is small compared with the overall dimensions of the wheel and rail: from this, it's easy to understand the intensity of the loads concentrated in this area [17]

Figure 22. Battered rail ends and delaminated end post

As a direct consequence, the rail ends experience battering, a form of localized plastic deformation and material flow. The ends of the rails become progressively damaged, leading to mushrooming, cracks, and surface irregularities. This deformation exacerbates the initial anomaly and increases the severity of wheel impacts in subsequent loading cycles.

Another consequence of battering of the rail ends is the end post delamination: this phenomenon consists of the separation of steel layers within the end post, leading to a reduction in mechanical strength and increased susceptibility to crack propagation. This structural weakening can compromise the integrity of the insulation, as displacement of the rail ends or damage to insulating components may occur, potentially causing electrical short-circuits.

Consequently, the reliability of track circuits is reduced, highlighting the critical interplay between mechanical fatigue and electrical performance in IRJs.

The repeated impacts and asymmetric load transfer induce excessive vibrations and settlements beneath the sleepers. This degradation of ballast stiffness causes differential settlement, loss of alignment, and even void formation under sleepers, all of which amplify the dynamic response of the joint.

The deterioration of ballast leads to increased deflection and track geometry defects. Under wheel passage, the rail at the joint deflects more than the surrounding sections, introducing bending stresses in the rail ends and in the joint bars: misalignments worsen and stress concentrations intensify. Such geometric defects not only degrade ride quality but also feed back into the cycle by producing higher impact loads during wheel crossing.

Figure 23. Evident instability of the ballast due to IRJ

Over time, all these factors interact and reinforce each other, fueling and exacerbating the degradation loop of IRJ, illustrated in Figure 20. As previously mentioned, the joint does not fail abruptly; rather, without timely maintenance or replacement, it gradually begins to function improperly, progressively worsening until severe and potentially catastrophic damage occurs:

- Bolt hole cracks, initiated by cyclic stresses around stress concentrators
- Bent or broken bolts, due to fatigue or overload
- Cracked or broken joint bars, which eventually compromise the entire joint assembly
- Rail end fractures, which may develop from battered rail ends or fatigue cracks

From a maintenance perspective, this model highlights the importance of early detection and intervention. Addressing small anomalies such as bolt loosening or minor end battering before

the cycle advances can significantly extend the service life of IRJs and reduce extraordinary maintenance costs.

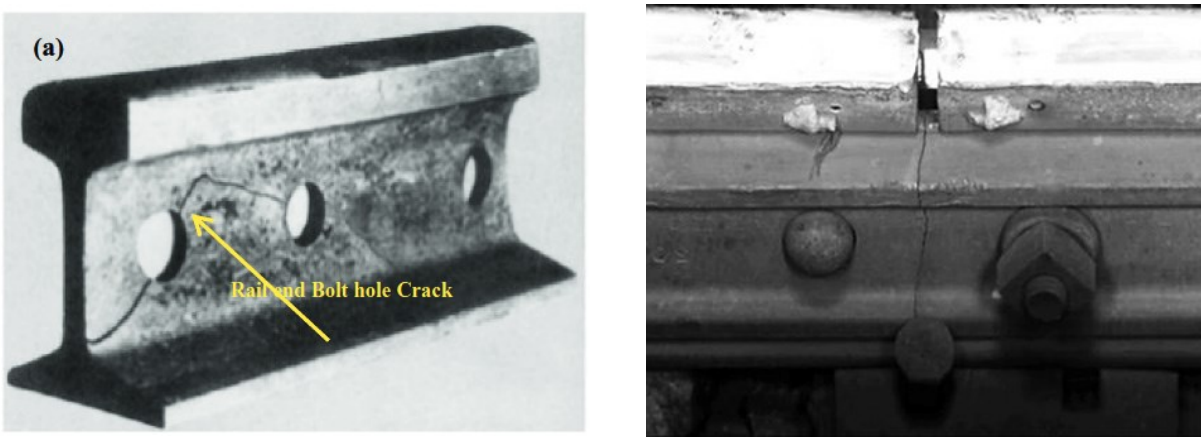

Figure 24. Bolt hole crack and broken fishplate

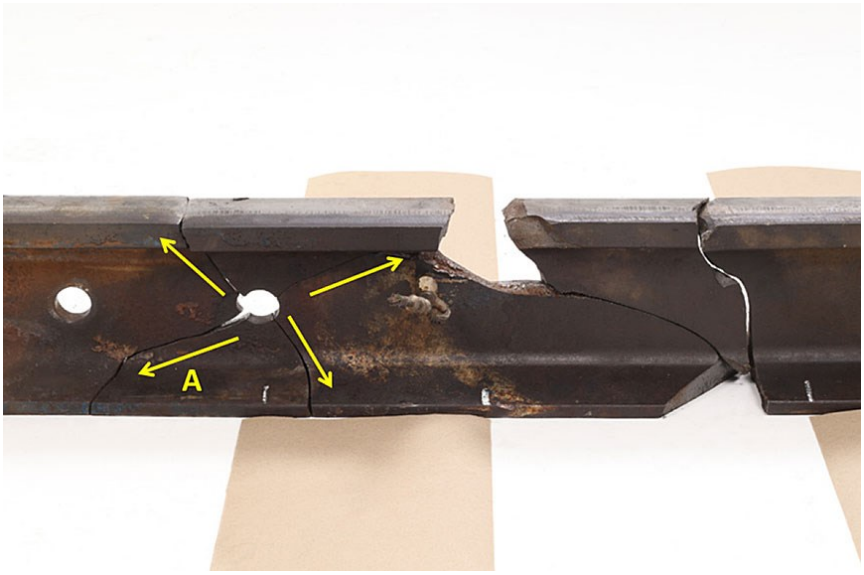

Figure 25. Typical propagation of a crack from the rail hole, which follows the 45° planes and reaches the railhead

Figure 26. Cracked fishplate

2.6.2 Maintenance strategies

Maintaining the durability of insulated rail joints fundamentally depends on well-structured maintenance strategies that address both preventive and corrective measures. Because IRJs combine structural complexity (metallic and non-metallic materials, bolts, adhesive layers, insulating components) with dynamic loading, thermal cycles, and environmental exposures, a proactive maintenance regime is essential for safety, reliability, and cost-effectiveness.

There are three maintenance strategies:

1. Preventive maintenance
2. Condition based and predictive maintenance
3. Corrective maintenance

Preventive maintenance refers to routine actions designed to identify wear or damage before failure occurs. In the context of IRJs, effective preventive strategies include:

- Scheduled visual inspections: regular visual checks allow the early detection of clues such as cracking (in rail ends or insulating layers), loosening of bolts, corrosion signs on fishplates, and surface wear. While visual inspection is limited (many critical defects are hidden under fishplates, end-posts, or insulating layers), it remains a low cost and essential first line of defense.
- Distance/time-based replacement of components: recognizing that components like end-posts, insulating liners, and bushes deteriorate over time even without apparent external damage, many railway infrastructure managers adopt replacement schedules based on elapsed time, traffic volumes, or load cycles. For example, after every certain number of million gross train ton-kilometers (MGTK) or after a fixed number of years of service, insulating parts may be replaced regardless of condition.
- Lubrication and surface treatments: where applicable, applying wear-protective coatings or lubrication at vulnerable surfaces (i.e. rail ends, bolt holes) can reduce friction and delay wear. Corrosion inhibitors on bolts and fishplates also slow down chemical degradation. Thermal expansion cycles are less aggressive to coated surfaces because a smoother surface reduces micro-crack nucleation.
- Monitoring of bolt preload: because loss of preload is a key contributor to many degradation paths in IRJs (bolt hole clearance, uneven load distribution, increased

impacts), measuring and maintaining proper bolt torque is vital. Some organizations conduct torque checks during visual inspections; others use sensors or indicators to monitor bolt torque or movement.

Preventive maintenance is necessary but insufficient for optimizing durability and cost. Condition-based and predictive maintenance strategies offer greater return by focusing efforts where degradation is already underway and forecasting failure risk. Key elements include:

- Non-destructive testing (NDT): techniques such as ultrasonic testing, eddy current, acoustic emission and thermography can detect subsurface or hidden defects (e.g., cracks under the insulating liner, micro-cracks near bolt holes).
- Vibration monitoring and modal analysis: dynamic behavior of IRJs (changes in natural frequencies, increased damping, shifting mode shapes) can act as early warning indicators. Modal testing, impact hammer or shaker excitation schemes, or use of accelerometers installed on or near joints can reveal anomalies like loss of stiffness due to adhesive degradation or bolt loosening before they become visually apparent.
- Data analytics and machine learning: with the accumulation of inspection, monitoring, and operational data, predictive models can forecast when a joint is likely to reach critical wear or failure thresholds. Machine learning algorithms have been used to correlate loading history, environmental data, bolt preload history, and early damage indicators to predict lifespan of IRJs (e.g. Neural Network-based fatigue life prediction models).

When degradation has advanced sufficiently, corrective actions become necessary to restore joint functionality. Such strategies include:

- Repair vs replacement decisions: determining whether a joint component (fishplate, bolt set, insulating liner) can be repaired (e.g. grinding, filling cracks, replacing bolts) or needs full replacement. Cost-benefit analyses are essential here because frequent small repairs may cumulatively cost more than scheduled replacements.
- Reinforcement techniques: in some cases, particularly under heavy loads or in high-speed lines, reinforcing joints with supplemental plates, external stiffeners, or upgraded bolt patterns can extend life. Modifications might involve thicker fishplates, larger or more bolts, or external clamps to reduce flexing.

- Adhesive re-bonding: glued IRJs may suffer bond deterioration; in such cases, removal of fishplates, surface preparation, reapplication of adhesive, and reassembly under strict curing and preload control can restore the joint's adhesive functionality.

Figure 27. IRJ's end post repair operation

2.7 Safety concerns and accident case studies

The reliability and safety of railway infrastructure are fundamental to ensuring efficient, continuous, and secure operations across modern transport networks. Within this complex system, IRJs represent one of the most critical yet vulnerable components. While their electrical insulating properties make them indispensable for track-circuit-based signalling systems, their intrinsic structural discontinuity introduces localized weaknesses that may evolve into safety hazards over time.

Over the past decades, both European and international railway authorities have recorded numerous cases where degradation or malfunction of IRJs has contributed to operational incidents. These range from minor service disruptions to catastrophic accidents with fatalities, underscoring the importance of rigorous maintenance, inspection, and design improvement.

The complexity of their composite structure—combining metallic rails, insulating materials, adhesive layers, and bolted connections—means that deterioration can manifest electrically (loss of insulation) or mechanically (cracking, bolt loosening, material delamination). Both

failure paths threaten the safe operation of railways, as they may compromise the track circuit's ability to detect trains or reduce the structural integrity of the running surface.

For these reasons, the analysis of accidents involving IRJs provides essential guidance for improving design standards, maintenance protocols, and monitoring strategies. By examining documented failures and learning from real-world case studies—such as the Pioltello derailment in Italy and similar incidents across Europe—it becomes possible to identify the recurring patterns that lead to joint degradation and to develop mitigation strategies aimed at preventing future occurrences.

2.7.1 Documented failures and incidents

Among the numerous degradation mechanisms affecting Insulated Rail Joints, the most severe consequence is undoubtedly the loss of mechanical integrity leading to track failure and train derailment.

One of the most tragic and well-documented cases is the Pioltello accident, which occurred on 25 January 2018, close to Milan, Italy. The accident involved a regional passenger train (Trenord 10452) travelling from Cremona to Milan Porta Garibaldi. At approximately 6:57 a.m., while running at a speed of around 130 km/h, the train derailed, causing the death of three passengers and injuring over forty others.

Figure 28. Pioltello rail accident

The investigation conducted by the Italian National Agency for Railway Safety (ANSFISA) and the Public Prosecutor's Office of Milan identified the fracture of an Insulated Rail Joint as the primary cause of the derailment. The joint, located between two continuous welded rail (CWR) sections, exhibited a fatigue crack originating from the bolt-hole edge on one of the rail ends. The crack had propagated progressively over time, eventually leading to the detachment of a 20 cm long piece of rail head. The fracture created discontinuity in the running surface, which caused the first bogie of the train to lose contact and subsequently derail.

Figure 29. IRJ collapsed: a bolt is missing, and material has completely detached from the rail head

Microscopic and metallographic analyses revealed that the crack had initiated from stress concentrations around the bolt hole due to repeated cyclic loading, worsened by progressive bolt preload loss and corrosion fatigue. The damage pattern was consistent with vibration-induced fatigue and local material embrittlement, typically in heavily trafficked lines where IRJs are subjected to high dynamic loads.

In addition, inspection records demonstrated that the joint had not been replaced according to the prescribed maintenance intervals, suggesting deficiencies in preventive inspection protocols and the difficulty of detecting sub-surface damage through routine visual examination.

The Pioltello incident emphasized the inherent vulnerability of IRJs and highlighted the need for more advanced Structural Health Monitoring (SHM) systems capable of detecting early-stage damage.

Following the accident, Rete Ferroviaria Italiana (RFI) implemented a series of measures, including stricter inspection schedules, ultrasonic testing campaigns on joints, and an acceleration of the IRJ replacement plan across high-traffic lines.

Beyond the Pioltello accident, several other European railway incidents have been linked, directly or indirectly, to IRJ degradation or failure. In the United Kingdom, Network Rail documented multiple cases of cracked or fractured insulated joints between 2012 and 2020, particularly on high-speed routes such as the East Coast Main Line and the West Coast Main Line. In one notable case (2016, Lincolnshire), a track inspection revealed a fully separated glued insulated joint, which, had it not been detected in time, could have caused a derailment. Metallurgical examination attributed the failure to adhesive layer delamination and improper curing of the epoxy bond, resulting in load redistribution to the bolts and accelerated fatigue.

Similarly, the Swedish Transport Administration (Trafikverket) reported in 2019 that IRJs in cold regions were experiencing premature cracking due to extreme thermal cycling and frost heave effects, leading to a phenomenon comparable to “rail breathing.” In these cases, the repetitive contraction and expansion of the rail section surrounding the joint caused local stress reversals and degradation of the adhesive interface.

In Germany, Deutsche Bahn’s 2020 Infrastructure Reliability Report identified IRJs as among the top five contributors to extraordinary maintenance costs in conventional and high-speed networks. Several non-fatal derailments were traced back to loosened joint bolts or fishplate deformation, especially under high axle loads exceeding 22.5 tonnes. The observed mechanism often combined bolt-hole elongation, end-post crushing, and uneven vertical stiffness between the joint and the adjacent rail, resulting in impact loading and microcrack propagation.

These cases collectively illustrate that IRJ-related incidents are not isolated or geographically constrained, but rather a systemic issue affecting diverse climatic and operational environments across Europe. They underscore the urgent need for harmonized inspection standards, predictive maintenance models, and improved material technologies to extend the service life of insulated joints.

3 Methodological approaches in IRJ studies

The complexity of the Insulated Rail Joint system, characterized by its combined mechanical and electrical functions, necessitates a multidisciplinary approach for its study. Understanding the behavior and failure mechanisms of IRJs cannot rely on a single experimental or analytical method. Instead, a combination of numerical simulations, laboratory testing, and field measurements is required to capture the interplay between materials, geometry, and operational conditions.

This chapter provides an overview of the main methodologies adopted in IRJ research, describing their evolution, relevance, and complementarity. The goal is not only to present the individual techniques but also to highlight how their integration contributes to a more accurate representation of joint performance under realistic service conditions.

In recent decades, advances in Finite Element Modeling (FEM), experimental testing procedures, and data-driven monitoring strategies have transformed the way railway components are analyzed. These methods allow for deeper insight into stress distribution, load transfer mechanisms, dynamic responses, and degradation phenomena that were previously inaccessible. Each of these approaches, however, comes with specific assumptions, advantages, and limitations that must be properly understood when interpreting results or comparing different studies.

Accordingly, this chapter is organized as follows:

- Sections 3.1: numerical approaches, deepening the FEM fundamentals
- Section 3.2: experimental approach, from static to dynamic tests
- Section 3.3: Measurement set up
- Section 3.4: Data processing and analysis

Together, these methodologies establish the scientific foundation for the subsequent experimental and numerical work carried out in this thesis.

3.1 Numerical Approaches

Finite Element Method (FEM) is a powerful engineering analysis tool and has been widely used in engineering since it was introduced in the 1950s. This paragraph presents the fundamental concepts and simple applications of FEM along with common terminology.

3.1.1 Finite Element Method fundamentals

The Finite Element Method (FEM) is a powerful computational technique that has been extensively used in engineering analysis since its introduction in the 1950s. It provides a systematic numerical framework for solving complex physical problems that cannot be addressed through analytical solutions.

From a mathematical standpoint, FEM transforms the governing differential equations—typically expressed as partial (PDEs) or ordinary differential equations (ODEs)—into a set of algebraic equations that can be solved numerically. In engineering applications, FEM approximates continuous field variables (such as displacements, temperatures, or stresses) by discrete values defined at a finite number of nodes within the domain.

The process of applying FEM to real-world problems is generally referred to as Finite Element Analysis (FEA). This approach enables engineers to model systems with complex geometries, boundary conditions, and material behaviors with high accuracy and flexibility. Over the decades, FEM has become one of the most essential tools in modern engineering practice, forming the foundation of numerous commercial software packages used for structural, thermal, and multiphysics simulations.

A clear understanding of the fundamental terminology used in the Finite Element Method (FEM) is essential for correctly formulating and interpreting engineering models. Each concept—ranging from the mathematical definition of the domain to the physical meaning of nodes and elements—plays a critical role in the process of discretizing a continuous system into a solvable numerical model. The following terms summarize the core vocabulary commonly employed in Finite Element Analysis (FEA).

- Domain: in mathematics, the domain represents the set of independent variables over which a function is defined. In the context of finite element analysis, the domain refers to the physical region or system governed by the laws of physics. In structural engineering, this may correspond to a beam, a frame, or an entire building structure, while in mechanical or thermal analysis, the domain could represent a mechanical component or a region with a temperature field.
- Governing Equations: these are the fundamental equations derived from the physical principles governing the behavior of a system—such as equilibrium, conservation of energy, or constitutive relations. The governing equations define the essential characteristics and response of the system under given conditions and typically take the form of differential equations.
- Boundary Conditions: boundary conditions specify the known values of a field variable at the limits of the domain. They represent the physical constraints—such as prescribed displacements, temperatures, or loads—imposed on the system. Proper definition of boundary conditions is essential for obtaining a unique and physically meaningful solution to the governing equations.
- Element: an element represents a discrete subregion of the problem domain. It is typically defined by simple geometric shapes such as triangles or quadrilaterals in two dimensions, and tetrahedra or hexahedra in three dimensions. Each element carries its own interpolation functions to approximate the variation of the field variable within its boundaries.
- Node: a node is a specific point within the discretized domain, commonly located at the vertices of elements. Nodes serve as connection points between adjacent elements, and they are the locations where the primary unknowns—such as displacements, temperatures, or potentials—are computed.
- Mesh: the mesh is the complete collection of nodes and elements which defines the discretized representation of the continuous domain. It constitutes the central data structure of finite element analysis and determines the accuracy and efficiency of the numerical solution. A finer mesh generally leads to higher accuracy but also increases computational cost. Most modern Finite Element Analysis (FEA) software packages incorporate automatic mesh generation capabilities that create refined grids to enhance solution accuracy. In large-scale or geometrically complex analyses, the automatic generation of the finite element mesh becomes essential, as manual discretization would be impractical and time-consuming. Numerous sophisticated algorithms have been

developed for automatic mesh generation, each designed to optimize element quality, maintain geometric fidelity, and balance computational efficiency with numerical precision.

Furthermore, there are two types of FEA analysis:

1. Linear Finite Element Analysis: it's founded on a series of simplifying assumptions that make the governing equations linear and computationally efficient to solve. Specifically, it assumes:
   a. Static conditions, where inertial and damping effects are neglected
   b. Infinitesimally small displacements and strains, ensuring that geometric relations remain linear
   c. Linear elastic material behavior, meaning that the stress–strain relationship follows Hooke's law and is independent of the load magnitude.

2. Nonlinear Finite Element Analysis: In contrast, nonlinear analysis accounts for deviations from these assumptions. Nonlinearity may arise from material behavior (e.g., plasticity, hyper elasticity, or viscoelasticity) and/or geometric effects (such as large deformations and rotations). The latter is commonly referred to as geometric nonlinearity or large deformation analysis. Nonlinear FEA provides a more realistic representation of physical behavior but requires iterative solution procedures and higher computational effort.

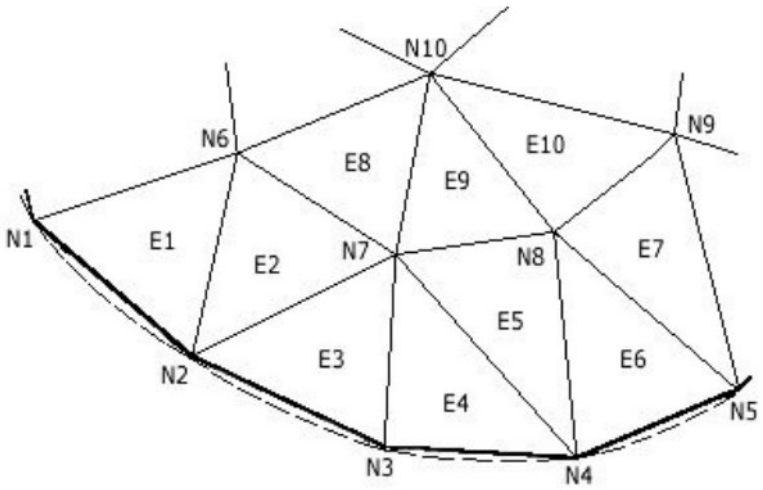

Figure 30. Triangulation of surface domain

From a mathematical standpoint, many engineering phenomena can be described by a set of governing equations and corresponding boundary conditions that define the system's physical behavior. These relationships originate from fundamental principles such as equilibrium, conservation, and constitutive laws.

$$G(\varphi) + f = 0 \qquad \text{Eq. 1}$$

$$B(\varphi) + h = 0 \qquad \text{Eq. 2}$$

Equation (1) represents the governing equation valid within the domain, while Equation (2) expresses the boundary conditions along the edges or surfaces of that domain. In many engineering problems, the governing equations take the form of differential equations that can be reformulated in algebraic matrix form through the Finite Element Method:

$$Ku = f \qquad \text{Eq. 3}$$

$$u = K^{-1}f \qquad \text{Eq. 4}$$

Here, K represents the property matrix that characterizes the physical parameters of the system (such as stiffness, conductivity, or viscosity), u is the unknown vector describing the system's response (such as displacement, temperature, or velocity), and f represents the applied external actions or loads.

Problem Type	**Property (K)**	**Behavior (u)**	**Action (f)**
Elastic Problem	Stiffness	Displacement	Force
Thermal Problem	Conductivity	Temperature	Heat Source
Electrostatic Problem	Dielectric Permittivity	Electric Potential	Charge
Fluid Problem	Viscosity	Velocity	Body Force

Table 2. Summary of Property, Behavior and Action in FEM

To analyze an engineering problem using FEM, the continuous physical domain is discretized into a finite number of small, simple subregions known as elements. Within each element, the field variable is approximated by a polynomial interpolation function. Adjacent elements share common degrees of freedom at their connecting nodes, ensuring continuity and compatibility across the domain.

By assembling these discrete elements, the field variable becomes piecewise continuous across the structure. This discretization process leads to a set of simultaneous algebraic equations defined at nodal points. Solving these equations provides the primary unknown field variables, from which secondary quantities such as stresses, strains, or heat fluxes can be computed.

The Finite Element Analysis (FEA) process generally follows a well-defined sequence of operations to transform a physical problem into a solvable numerical model. The main steps are summarized below:

1. Select the element type: this determines the modeling flexibility and the expected accuracy of the results. Depending on the problem domain, elements may be one-, two-, or three-dimensional, and may employ linear or higher-order shape functions.
2. Discretize the domain: the continuous structure or problem domain is subdivided into a finite number of smaller, simpler subregions called elements. This process converts the continuous field into a discrete model composed of interconnected nodes.
3. Derive element governing equations: for each element, governing matrix equations are derived from the underlying physical laws using methods such as the principle of minimum potential energy, the virtual work principle, or Galerkin's approach.
4. Assemble the global system of equations: the element matrices are assembled into a single global matrix equation, typically expressed as

$$Ku = f \qquad \text{Eq. 3}$$

where K is the global stiffness (or property) matrix, u the nodal displacement (or field) vector, and f the load (or action) vector.

For example, for a 2-D beam element, with two nodes "i" and "j", Equation 3 becomes:

$$\begin{bmatrix} \frac{EA}{L} & 0 & 0 & -\frac{EA}{L} & 0 & 0 \\ 0 & \frac{12EI}{L^3} & \frac{6EI}{L^2} & 0 & -\frac{12EI}{L^3} & \frac{6EI}{L^2} \\ 0 & \frac{6EI}{L^2} & \frac{4EI}{L} & 0 & -\frac{6EI}{L^2} & \frac{2EI}{L} \\ -\frac{EA}{L} & 0 & 0 & \frac{EA}{L} & 0 & 0 \\ 0 & -\frac{12EI}{L^3} & -\frac{6EI}{L^2} & 0 & \frac{12EI}{L^3} & -\frac{6EI}{L^2} \\ 0 & \frac{6EI}{L^2} & \frac{2EI}{L} & 0 & -\frac{6EI}{L^2} & \frac{4EI}{L} \end{bmatrix} \begin{pmatrix} u_i \\ v_i \\ \vartheta_i \\ u_j \\ v_j \\ \vartheta_j \end{pmatrix} = \begin{pmatrix} a_i \\ p_i \\ m_i \\ a_j \\ p_j \\ m_j \end{pmatrix}$$

in which E=Elastic modulus, A=Area, I=Moment of Inertia, L=Length of the beam, u=Longitudinal displacement, v=Transverse displacement, θ=Rotation, a=Axial force, p=Shear force, m=Internal moment, u=Displacement vector, and f=Force vector. The field variables with subscripts "i" and "j" represent the values at the left and right end of the element, respectively.

5. Apply boundary conditions: they define known values for specific degrees of freedom or field variables. Applying these constraints modifies the global system to ensure that the physical limitations of the problem are accurately represented.
6. Solve for the primary unknowns: the modified global system of equations is solved for the primary unknowns, typically the nodal values of the field variables. This step produces the numerical approximation of the system's behavior.
7. Compute derived quantities: based on the nodal solutions, derived quantities such as stresses, strains, reaction forces, or heat fluxes are computed using constitutive relationships and interpolation functions within each element.
8. Verify and interpret the results: the results obtained must be critically examined to ensure physical consistency and accuracy. Any unrealistic or unexpected outcomes may require mesh refinement, improved boundary definitions, or re-analysis to enhance model reliability.

Referring to point one, there are several common finite elements used for structural problems:

- Line elements (truss or beam)
- Surface elements (triangular or quadrilateral)

- Solid Element (tetrahedral or hexahedral)

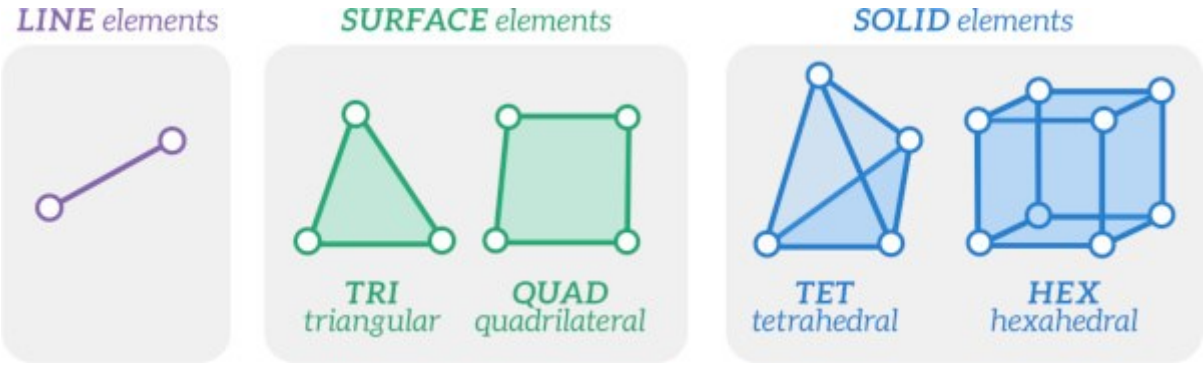

Figure 31. Types of Finite Elements

Each of these elements can be defined as either linear or quadratic, depending on the desired accuracy of the numerical approximation. Linear elements use linear polynomials and are commonly employed in most engineering applications due to their simplicity, while quadratic elements use quadratic polynomials for higher accuracy.

The main difference between a truss element and a beam element lies in the degrees of freedom at the nodes. A 3-D truss element has only three translational degrees of freedom per node, whereas a 3-D beam element includes three rotational degrees of freedom in addition to the three translational degrees of freedom at each node.

The standard Finite Element Equation 3 applies only to static problems; for dynamic problems, the equation of motion is expressed as:

$$M\ddot{u} + C\dot{u} + Ku = f \qquad \text{Eq. 4}$$

where:

- M is the mass matrix
- C is the damping matrix
- K is the stiffness matrix
- $\ddot{u}$ is the acceleration vector
- $\dot{u}$ is the velocity vector

- u is the displacement vector, and
- f is the force vector

This equation represents the general equilibrium condition for any physical system. In the case of a static problem, where acceleration $\ddot{u}$ and velocity $\dot{u}$ are zero, the equation simplifies to the familiar static form:

$$Ku = f \qquad \text{Eq. 3}$$

Dynamic or forced-vibration problems are time-dependent, meaning the time domain must also be discretized to obtain Finite Element solutions.

If damping and external forces are neglected, the equation reduces to:

$$M\ddot{u} + Ku = 0 \qquad \text{Eq. 5}$$

This represents a free vibration or undamped dynamic problem, which from a mathematical perspective is an eigenvalue problem. The solution of this eigenvalue problem yields the natural frequencies of the structure.

3.1.2 Fem applications to IRJ modelling

Finite Element Method studies of insulated rail joints have concentrated on a set of complementary problems that together characterize the joint's mechanical and tribological behavior under wheel passage. Early work examined how a free rail end alters the local elastic–plastic contact stress distribution, demonstrating that proximity effects significantly increase peak stresses near the gap [18].

Subsequent dynamic and structural FEM investigations focused on impact loading at rail ends and how impact forces vary with geometry, load and gap size [19][20], while three-dimensional and dynamic FEM simulations have elucidated the plastic flow and mechanical response of

rails under rolling wheel action [21]and have specifically modelled contact–impact stress fields within the joint region [22].

FEM has also been used to study the influence of IRJs on wheel–rail contact under partial slip conditions, showing modified stress and slip distributions that may accelerate wear [23].

More integrated vehicle–track interaction models have predicted how IRJs amplify dynamic loads and contribute to progressive material deterioration [24].

Finally, sensitivity analyses using FEM have quantified the role of end-post material properties in joint performance, identifying which material parameters most strongly affect stress concentrations and deformation [25].

Using the ABAQUS/CAE software, it has been examined the stress distribution within joint bars of three different sizes under wheel loading conditions. The study focused on evaluating the longitudinal stresses developed at the top and bottom surfaces of the joint bars, taking into account the bending moments induced by the passing train loads on the IRJ assembly [26].

Although these computational studies have been valuable in isolating mechanisms such as contact stress amplification, impact concentration, gap-dependent loading, and material sensitivity, the current FEM literature on insulated rail joints remains limited by the lack of investigations into bolt pre-tension and its influence on the mechanical response of the joint. In particular, few models explicitly incorporate the initial clamping force and its evolution under cyclic wheel loading, despite its critical role in governing stress redistribution, joint stiffness, and long-term degradation. This gap highlights the need for advanced FEM frameworks that couple realistic bolt pre-load modelling with contact and material nonlinearity, enabling more accurate predictions of stress transfer, wear evolution, and potential failure modes in IRJs.

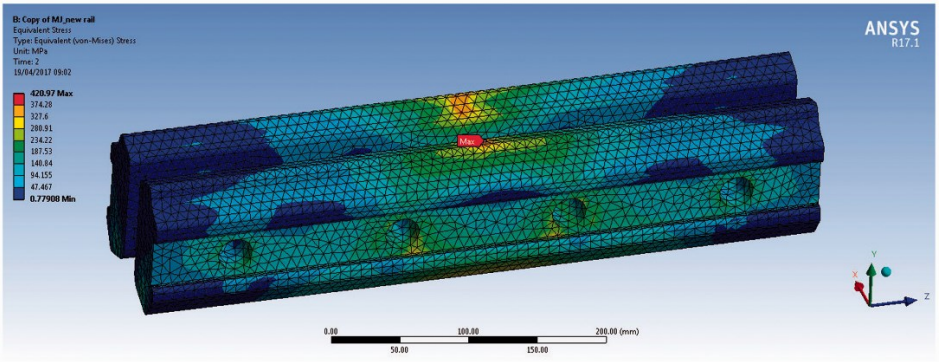

Figure 32. FEM model of IRJ's fishplates[4]

3.1.3 Strengths and limitations of FEM in railway studies

The Finite Element Method offers a powerful and versatile framework for analyzing the complex mechanical behavior of railway systems, particularly in understanding localized phenomena such as stress concentration, fatigue initiation, and contact mechanics in components like Insulated Rail Joints, wheel–rail interfaces, and track substructures.

One of its principal strengths lies in its ability to model geometrically intricate assemblies composed of heterogeneous materials under diverse boundary conditions. FEM enables detailed visualization of stress and strain fields, facilitates parametric studies on design variables such as bolt preload or material stiffness, and supports the virtual testing of alternative configurations prior to experimental validation. This makes it invaluable for assessing the structural integrity, fatigue life, and durability of railway components, as well as for optimizing maintenance schedules and improving overall safety.

Moreover, FEM's adaptability allows it to incorporate nonlinear material behavior, contact interactions, and dynamic or thermal effects that are characteristic of railway environments. In the context of IRJs, FEM enables coupling between thermal expansion, mechanical load transfer, and adhesive layer degradation, providing insights into the long-term performance of glued joints under operational stresses. When integrated with field measurements—such as strain, acceleration, or displacement data—FEM also forms the foundation for digital twin systems, offering predictive monitoring capabilities and supporting condition-based maintenance strategies.

However, despite these advantages, FEM has inherent limitations that must be carefully considered. The accuracy of simulation results depends strongly on the quality of input data, such as precise material properties, contact friction coefficients, and realistic boundary conditions, which are often difficult to obtain for large-scale railway systems. The computational cost of high-fidelity 3D models can also be significant, especially for dynamic simulations involving moving loads or nonlinear contact phenomena. Furthermore, FEM is sensitive to meshing strategies: inadequate discretization or inappropriate element types may lead to numerical instabilities or artificial stress concentrations. Another limitation lies in the challenge of capturing degradation processes—such as wear, crack propagation, or ballast settlement—over long time periods, since these require advanced multiphysics coupling and damage mechanics formulations that remain computationally expensive.

3.2 Experimental Approaches

The experimental investigation of Insulated Rail Joints plays a fundamental role in understanding their mechanical behavior, durability, and failure mechanisms under realistic service conditions. While analytical and numerical modelling offer valuable insights into stress distributions and global dynamic responses, experimental testing remains indispensable for validating models, capturing nonlinearities, and revealing degradation processes that are difficult to predict theoretically—such as adhesive debonding, bolt relaxation, and wear at the rail ends.

IRJs represent a mechanical and electrical discontinuity in otherwise continuous welded rail systems. This discontinuity induces localized stress concentrations, abrupt changes in stiffness, and complex interactions between metallic and polymeric materials. The mechanical integrity of the joint directly affects track safety, ride quality, and signalling reliability. For these reasons, a wide variety of experimental approaches have been developed to evaluate IRJ performance across different spatial and temporal scales—from laboratory coupons and component-level tests to full-scale track investigations.

Experimental studies on IRJs can broadly be divided into static and dynamic testing approaches:

- Static testing focuses on the quasi-static load–deformation behavior of the joint under controlled loading. It provides key parameters such as vertical stiffness, bond strength, and residual capacity, as well as insights into structural integrity under service-level and ultimate loads. Static tests form the foundation for validating finite element (FE) models and for understanding the influence of design parameters (fishplate geometry, adhesive type, bolt pretension, and insulation layer thickness) on overall stiffness and stress distribution.
- Dynamic testing, on the other hand, addresses the effects of transient, cyclic, and impact loads associated with wheel–rail interaction. Such tests allow the identification of resonance frequencies, damping characteristics, and fatigue mechanisms, which ultimately govern the long-term performance and failure of IRJs in service.

A comprehensive experimental program on IRJs typically combines both approaches. Laboratory-based static and dynamic tests enable precise control of variables and facilitate detailed instrumentation, whereas full-scale field tests provide realistic boundary conditions and capture environmental and operational influences. Together, these methods provide a multi-

scale understanding of joint behavior—bridging material-level phenomena (adhesive bond degradation, microcracking) and system-level effects (track stiffness transition, noise and vibration generation).

The following sections present an overview of the main experimental methodologies adopted in the literature for IRJ assessment, structured into static and dynamic testing categories. Section 3.2.1 discusses laboratory and full-scale static tests, while 3.2.2 focuses on dynamic investigations including vibration-based, impact/fatigue, and in-track measurements.

3.2.1 Static testing

Static testing of IRJs aims to characterize their load–deformation behavior and ultimate strength under quasi-static loading, to detect stiffness changes due to assembly type (bolted vs bonded), to evaluate the integrity of adhesive bonds (for bonded IRJs), and to provide calibrated parameters for numerical models.

In the literature static tests appear at two scales:

- controlled laboratory component tests (specimens, joint assemblies)
- full-scale static tests performed in track or on complete joint assemblies under field conditions

3.2.1.1 Laboratory-based static tests

Laboratory static tests are mainly designed to obtain the load–displacement curve of the joint in the vertical and/or transverse directions. Furthermore, they are also used to characterize stiffness and contact behavior between fishplate and rail web/head.

The typical specimen a glued IRJ: polymer/epoxy adhesive fills the end post gap and bonds polymer or steel fishplates to the rail. Several studies explicitly test both virgin and intentionally degraded (debonded) specimens to reproduce field failure modes. Preparation often follows manufacturers or AREMA recommended surface preparation and curing regimes; specimens may include insulation inserts or end posts.

Figure 33. Laboratory three point bending test on IRJ [27]

The most common tests are:

- Three-point bending (vertical static deflection): the most common arrangement used to quantify flexural stiffness and vertical deflection at the rail head over the joint gap. Support span and load application position (at/near the joint) are varied: load is applied quasi-statically to record load vs midspan (or joint) deflection, while typical support spans emulate sleeper spacing.
- Four-point bending: occasionally used to apply a region of constant bending moment across the joint region to measure bending stiffness without local contact effects.
- Axial tensile tests: used for bonded joints to measure bond strength and the progression of epoxy debonding (pull-out or pull-apart tests).
- Quasi-static transverse/lateral loading: to determine lateral stiffness and to evaluate gauge-widening behavior. Less common but used in studies addressing track geometry effects.

The measuring instrumentation used includes:

- Strain gauges: bonded to rail web/head and fishplates to measure local bending and axial strains
- Load cells: calibrated to record applied force (vertical, axial or lateral)
- Visual / ultrasonic inspection: to detect adhesive debonding and crack initiation

Laboratory static testing offers several key advantages for the study of insulated rail joints. First, it provides controlled boundary conditions and high repeatability, enabling parametric investigations of variables such as bolt pretension, adhesive type, and fishplate geometry. Second, laboratory tests facilitate precise instrumentation and high-resolution measurement of localized strains and deflections, which is critical for the calibration of finite element contact

and bond models. Finally, laboratory experiments allow researchers to deliberately introduce and examine specific damage states—such as loss of bolts' preload or crack initiation—under well-defined load histories.

Despite these benefits, several limitations and concerns must be acknowledged. Laboratory specimens cannot fully reproduce the complex support conditions of in-track rails, including ballast, sleeper compliance, and the continuity of long welded rails. The selection of loading span and boundary constraints strongly influences the measured stiffness and may bias results if not carefully controlled; therefore, static laboratory tests alone are generally insufficient to predict in-service performance under realistic wheel–rail interactions and must be complemented by dynamic and field testing. Additionally static testing does not capture high-frequency impact stress spikes caused by wheel passages or rail discontinuities, which are critical drivers of fatigue. Consequently, laboratory static testing should be integrated with dynamic testing to provide a complete understanding of IRJ behavior and durability.

3.2.1.2 Full-scale field static tests

Full-scale static tests are performed either on installed IRJs on track or on large full-assembly rigs designed to reproduce in-track boundary conditions. The goal is to observe joint behavior under realistic support conditions (sleeper/ballast interaction, continuous rail restraint, rail fastening stiffness), measure deflection and bending moment distributions in actual track, and validate whether laboratory-derived parameters produce correct global behavior in models. Field static testing also enables the detection of damage modes caused by environmental factors and cumulative loading not reproducible in laboratories.

Figure 34. IRJ field test[28]

The most common tests are:

- Static loading using hydraulic jacks applied at rail head (or to wheelset simulators) while the joint remains installed; LVDTs and strain gauges measure displacements and strains on rails, sleepers and fishplates
- Instrumented train or wheelset static loading where a slow moving or stationary heavy axle load is put over the joint while measuring deflections and track response
- In-situ pull axial on repaired or replaced bonded joints to verify residual bond capacity in real environmental conditions

The measuring instrumentation used includes:

- vertical deflection at rail head across the joint (via LVDTs or geophones)
- rail bending strains (strain gauges) at rail ends and fishplates
- bolt strains and tensions (where accessible)
- sleeper and ballast pressure (pressure cells)
- visual inspection and non-destructive evaluation (ultrasound, thermography) for bond state

Full-scale field static testing of insulated rail joints presents several notable limitations and challenges. Instrumentation and access in track environments are logistically demanding; the installation of strain gauges and LVDTs is more difficult, and variability in sleeper and ballast conditions introduces measurement scatter, complicating repeatability. Controlling boundary conditions is also challenging, as even with hydraulic jacks it is difficult to isolate the joint's response from that of the surrounding track. Load paths through the ballast cause the apparent stiffness of the joint to depend on large-scale track properties, potentially obscuring localized behaviors. Additionally, field static tests require track possession and strict adherence to safety procedures, which limit the number of tests that can be conducted and constrain sample size, reducing statistical robustness.

3.2.2 Dynamic testing

Dynamic testing of Insulated Rail Joints is essential to understand the response of joints under time-dependent loads typical of real railway operation, including wheel–rail impact, vibrations, and cyclic fatigue. While static tests provide information on ultimate strength and stiffness,

dynamic experiments capture transient phenomena, high-frequency stress peaks, resonance effects, and the long-term fatigue behavior of joints, which are crucial for service life assessment and maintenance planning. Dynamic studies can be conducted at laboratory scale, using controlled vibration and impact setups, or at full-scale, in track, under operational or simulated loading conditions.

Dynamic testing is broadly categorized into:

- vibration-based experiments
- impact and fatigue tests
- full-scale track dynamic investigations

3.2.2.1 Vibration-based experiments

Vibration-based experiments aim to characterize the dynamic properties of IRJs—namely natural frequencies, damping ratios, and mode shapes—that are directly linked to the mechanical integrity of the joint and can serve as indicators of early-stage damage. In the laboratory, modal testing is typically performed using instrumented impact hammers or electrodynamic shakers to excite either scaled specimens or full-size joint assemblies.

Figure 35. IRJ excited by shaker

The dynamic response is recorded through accelerometers or laser doppler vibrometers, from which frequency response functions are computed to identify the fundamental modes of vibration. These measurements enable the estimation of dynamic stiffness and allow the identification of abnormal vibrational signatures that may signal bond degradation, loosening of bolts, or local cracking.

In these studies, accelerometers are usually mounted on the rail head, web, and fishplates, while laser vibrometers provide non-contact measurements of displacement or velocity. High-frequency data acquisition systems—operating at sampling rates in the kilohertz range—are employed to capture both low- and high-frequency components of the response. It has been demonstrated that the dynamic frequency response of IRJs typically lies within 50–1200 Hz, and that changes in natural frequency and damping are correlated with the health of the joint [29].

The main advantage of vibration-based experiments lies in their non-destructive nature: they allow continuous monitoring of IRJ integrity and facilitate early detection of subtle damage, such as bolt loosening or micro-cracking, which might not be visible under static loading. Furthermore, vibration tests provide critical input parameters—mass, damping, and stiffness—for dynamic finite element models used in predictive simulations. However, some limitations must be acknowledged. Laboratory configurations cannot reproduce the complex boundary conditions of real track structures, where ballast and sleeper compliance significantly affect the dynamic response. Moreover, the frequency content obtained from controlled excitations may differ from that induced by actual train operations due to scale effects and simplified loading conditions.

3.2.2.2 Impact and fatigue tests

While vibration-based experiments provide frequency-domain information, impact and fatigue tests focus on the time-domain response of IRJs to repetitive or transient loads that simulate the passage of train wheels and the resulting dynamic stress cycles. These tests are designed to assess the degradation of stiffness, the accumulation of damage, and the fatigue life of both bolted joints. In the laboratory, cyclic loading is commonly applied using hydraulic actuators that replicate wheel–rail contact forces, while drop-weight impact devices are employed to simulate the sudden force peaks caused by wheel flats or rail discontinuities.

Figure 36. IRJ bending test

The vertical and longitudinal deflections of the joint are typically measured using LVDTs or laser displacement sensors, while strain gauges mounted on the rail ends, fishplates, and fasteners capture the evolution of local stresses throughout the test. High-frequency data acquisition systems record force, displacement, and strain histories to enable fatigue analysis.

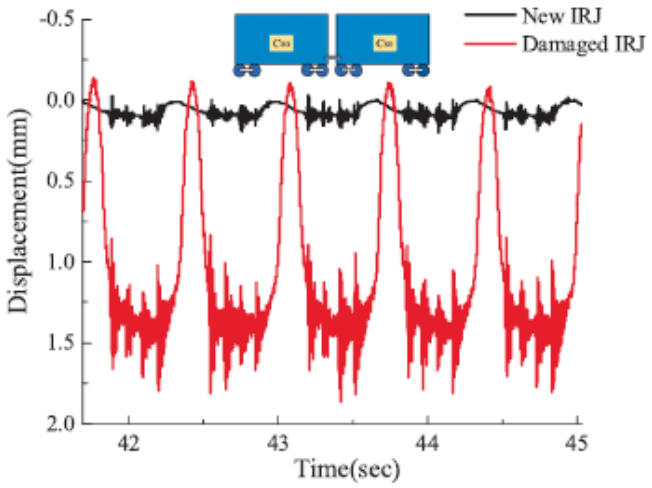

Figure 37. Typical trend of the vertical displacement of the section affected by the joint during the passage of a train [30]

Studies reported that wheel–rail impacts in the joint region generate high-frequency stress fluctuations in fastening clips and fishplates, accelerating fatigue damage and drastically

reducing service life. Furthermore, it has been developed a probabilistic approach to fatigue reliability assessment that incorporated uncertainties in load spectra and wheel–rail interactions, showing that joint failure is highly sensitive to variations in dynamic load amplitude and frequency. These studies collectively highlight that fatigue at IRJs is not merely a function of the number of load cycles, but also of the spectral composition of dynamic loads and the local stiffness discontinuity introduced by the joint.

Impact and fatigue testing provides a direct means to quantify residual strength and predict fatigue life under controlled laboratory conditions, making it invaluable for developing maintenance strategies and replacement schedules. However, such experiments are inherently time-consuming, expensive and often require large, high-capacity rigs to accommodate full-scale specimens. Additionally, the controlled environment of the laboratory cannot fully reproduce field conditions—such as temperature variations, moisture ingress, and ballast settlement—which significantly influence degradation in service. Consequently, laboratory fatigue data should be interpreted as indicative rather than absolute, and it is generally recommended to complement these results with field-based validation.

3.2.2.3 Full-scale track dynamic investigations

Full-scale dynamic investigations aim to capture the in-situ behavior of IRJs under actual operating conditions, providing the most realistic assessment of their dynamic performance and validating laboratory and numerical findings. These studies are typically conducted using instrumented train passages, track-side impact tests, or long-term monitoring campaigns. In the case of instrumented trains, accelerometers, strain gauges, and displacement transducers are mounted directly on the rail, sleepers, and fishplates to record dynamic responses as trains pass over the joints. Track-side excitations using shakers or impact hammers are also employed to characterize the local dynamic stiffness of the track system, while long-term installations use permanently embedded sensors to monitor vibration levels, stresses, and degradation trends over time.

Field data frequently show higher stress peaks than those predicted by laboratory models, due to the combined effects of train speed, wheel irregularities, and non-uniform support conditions. These observations confirm that in-situ measurements are indispensable for capturing the full spectrum of dynamic phenomena affecting IRJ performance.

Despite their importance, full-scale dynamic investigations face several practical challenges. Installing instrumentation on active railway lines requires possession of the track and strict adherence to safety regulations, limiting the number of repeatable measurements. Environmental variability—such as changes in temperature, humidity, and ballast conditions—introduces scatter into the results, making it difficult to isolate the contribution of the joint itself. Moreover, these experiments are often costly and generate large volumes of high-frequency data that require sophisticated processing and interpretation.

3.3 Measurement strategies and data analysis

3.3.1 Measurement strategies and instrumentation

Strain gauges, LVDTs and discrete displacement sensors remain the backbone of IRJ experimental campaigns. Strain gauges provide local, high-resolution measures of bending and axial strain at rail toes, fishplates and bolts; they are inexpensive, mature and directly related to stress through elastic relations. LVDTs and contact displacement sensors quantify vertical and lateral deflection across the joint with good resolution and linearity, which is essential for load–deflection curves and stiffness estimation.

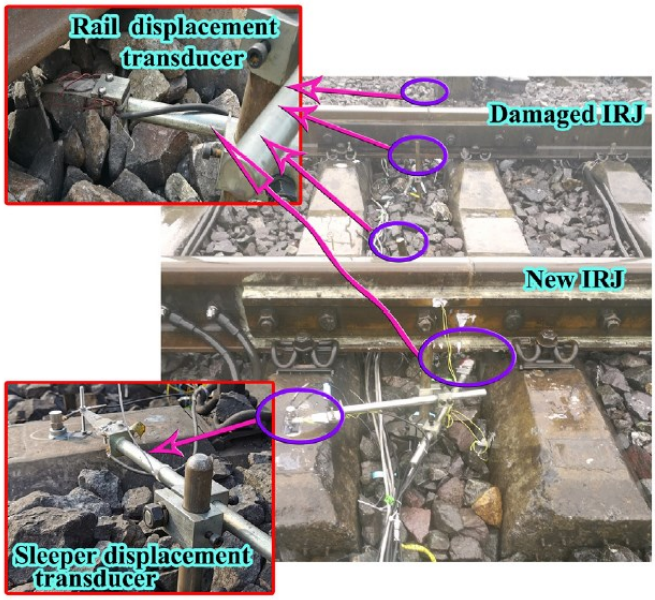

Figure 38. Field instrument installation[30]

The limitations are:

- the need for careful surface preparation and adhesive installation for strain gauges
- the susceptibility to damage in field conditions,
- the limited spatial coverage: each sensor gives a single point measurement, so dense instrumentation is required to map fields
- for field work, ruggedized housing and thermal compensation are necessary to maintain data quality over time

In addition to the aforementioned measuring instruments, advanced sensing technologies should also be included. Among these, fiber-optic sensors (FBG arrays), acoustic emission sensors and vision-based methods expand capability beyond point sensors. FBGs provide distributed or multiplexed strain/temperature sensing with electromagnetic immunity and long-term stability; they are excellent for continuous monitoring over several meters and for capturing gradients near the joint. AE sensors are sensitive to brittle events (crack initiation, rapid debonding) and are useful for detecting the onset of damage rather than quasi-static degradation. Vision-based approaches (digital image correlation, stereo cameras, photogrammetry) yield full-field displacement and strain maps in laboratory tests and can non-intrusively monitor deflection patterns in controlled field setups.

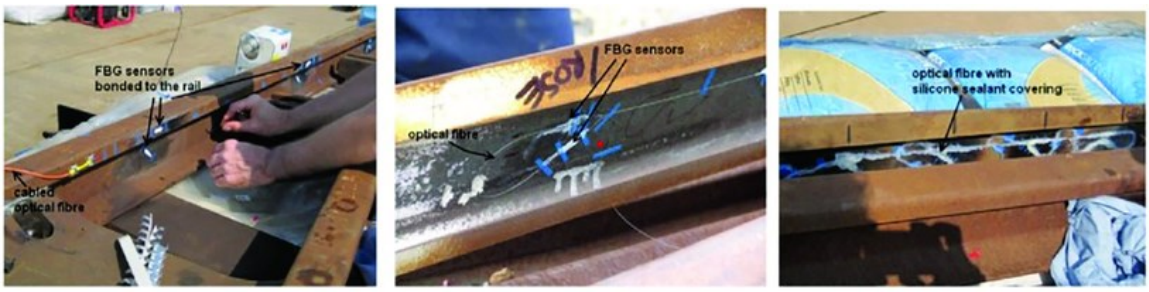

Figure 39. FBG sensors bonded to the rail

It's important to choose sampling rates to capture the highest relevant frequencies: vibration-based phenomena for IRJs may extend from tens of Hz into the kHz range (impacts and high-frequency noise), so accelerometers and AE channels typically require kHz sampling; strain and displacement channels can be sampled at lower rates but must still resolve dynamic transients. The key strategy is implementing anti-aliasing filters and verifying sensor bandwidths against expected signal content.

3.3.2 Data analysis

Frequency-domain analysis and modal identification form the cornerstone of dynamic data interpretation in the study of insulated rail joints. By transforming time-domain signals into the frequency domain—typically through Fast Fourier Transform (FFT)—it becomes possible to identify dominant vibration bands, resonance peaks, and the energy distribution associated with impact events. These spectral features reveal how the joint and surrounding track system respond to different loading frequencies, enabling the detection of stiffness discontinuities or degradation-induced shifts in dynamic behavior.

Building upon this foundation, modal analysis provides a more detailed characterization of the system's structural dynamics by extracting natural frequencies, damping ratios, and mode shapes. In the laboratory, Experimental Modal Analysis (EMA) relies on controlled excitations—usually via impact hammers or electrodynamic shakers—and simultaneous measurement of input and output responses to construct accurate frequency response functions. Conversely, Operational Modal Analysis (OMA) is used in the field to estimate modal parameters from ambient or operational excitations such as train passages, where direct input measurements are not feasible. Although OMA requires high signal-to-noise ratios and advanced output-only identification techniques (e.g., stochastic subspace identification), it enables continuous in-service monitoring without disrupting railway operations.

Modal parameters are highly sensitive to local stiffness and boundary conditions, making their evolution over time an effective indicator of joint health. Tracking variations in natural frequencies or changes in mode shapes allows the identification of progressive damage, debonding, or bolt loosening long before visible failure occurs. Consequently, combining EMA-derived laboratory baselines with OMA-based field measurements provides a powerful framework for structural health monitoring and model validation. For reliable application, modal parameters should always be accompanied by quantified uncertainties—confidence intervals or covariance estimates—to account for environmental and operational variability.

4 Finite element analysis of IRJ

The insulated rail joint (IRJ) represents a critical component of the railway track due to its intrinsic geometry and mechanical characteristics, which make it particularly susceptible to degradation under repeated traffic loading. Accurate recognition and analysis of its deterioration mechanisms are therefore essential to ensure track reliability and long-term performance.

In this thesis, a detailed finite element (FEM) analysis was carried out to investigate the mechanical behavior of insulated four-hole rail joints subjected to loads induced by train passages.

The study compares two typical installation configurations:

1. suspended joints, where the rail gap is located midway between two sleepers
2. supported joints, where the joint is positioned directly above a single or double sleeper.

For both configurations, two operating conditions were simulated:

A. the optimal installation condition, characterized by the nominal bolt preload applied during assembly
B. a progressive deterioration condition, represented by a partial reduction in bolt preload to reproduce the effects of service-induced loosening (P_b value has been set to 10% of the initial value to simulate low conditions)

The primary objective of this analysis is to assess and compare the mechanical response of IRJ under both support conditions as bolt preload decreases, with particular attention to stress distribution and vertical displacements in the critical areas of the joint.

A distinctive contribution of this study lies in addressing a notable gap in existing literature: while numerous works have examined IRJ performance under static and dynamic loading [31] [32], [33], [34], few—if any—have explicitly analyzed the impact of bolt preload loss on the mechanical behavior of both suspended and supported joints during train passage. This research therefore provides new insights into the relationship between bolt preload degradation, joint support configuration, and overall structural integrity, offering valuable guidance for the design, maintenance, and monitoring of insulated rail joints in service conditions.

The chapter is structured as follows: Section 4.1 describes the model development, including geometry, materials, boundary conditions, loading scenarios, the mesh generation and convergence study; Section 4.2 presents the main numerical results and, finally, Section 4.3 the conclusions.

4.1 Model development

In the present case study, the Insulated Rail Joint was modelled using the commercial finite element software Abaqus/CAE.

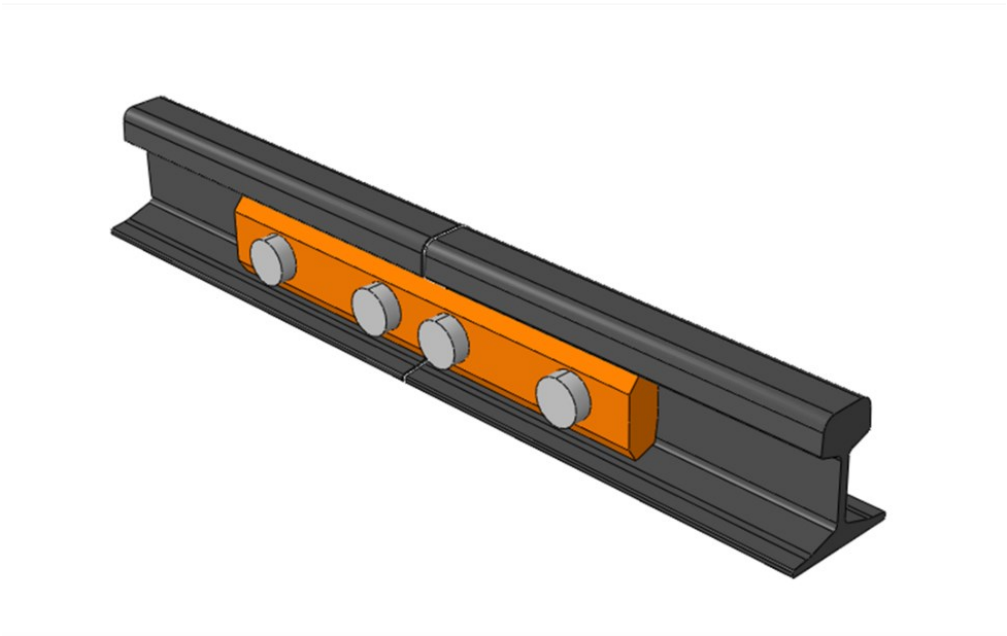

Figure 40. Example of final IRJ FEM model

Before reproducing the exact geometry of the joint in accordance with RFI standards, intermediate and simplified models were developed in order to correctly identify the parameters governing the complex interactions between the various components of the joint.

Initially, a pin-lug model was developed, which included:

- Rail: a plate with dimensions of 300 × 150 mm^2 and a thickness of 11 mm
- Fishplates: two plates with dimensions of 150 × 90 mm^2 and a thickness of 40 mm

- Bolt: a cylinder with a diameter of 32 mm, perfectly fitting into the holes of the rail and the fishplates

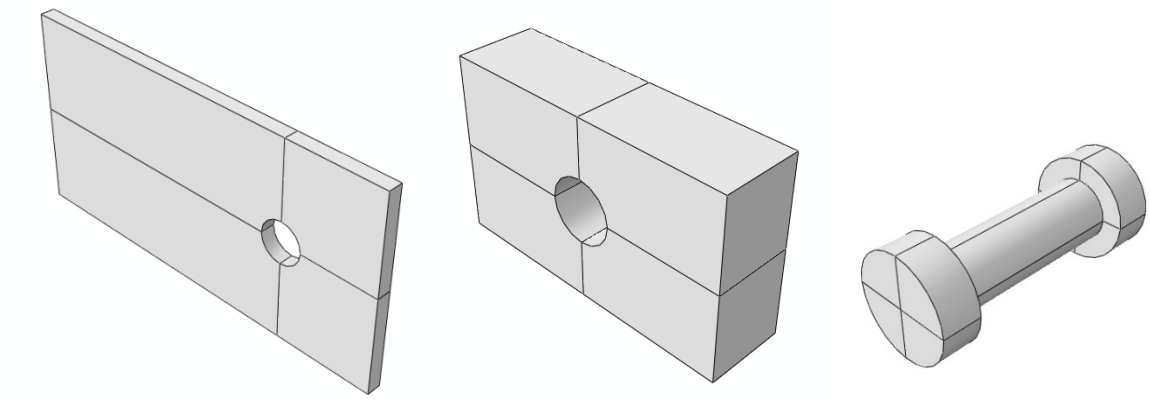

Figure 41. Pin-lug model's components

The purpose of this simplified model was to verify the accuracy of the parameters defining the interactions among the different components of the joint. In ABAQUS, as in other finite element solvers, one of the main challenges concerns the achievement of numerical convergence. Computational failure frequently arises from an improper definition of contact interactions between the various parts of the assembly. In this context, particular attention was devoted to the modelling of the contact behavior between the bolt, the rail, and the fishplates, as this represents one of the most critical aspects affecting the stability and reliability of the numerical solution.

The properties of contact interaction between two surfaces are governed by two main components:

- normal behavior
- tangential behavior.

Normal behavior defines how the contacting surfaces react when they come into or out of contact. It typically controls the transmission of compressive stresses perpendicular to the interface and prevents interpenetration between the parts.

The formulation that proved to be effective in this simplified model, and was therefore extended to the subsequent ones, is the one based on “hard contact”: surfaces can separate freely but cannot penetrate each other.

Tangential behavior, on the other hand, defines the relative motion between the surfaces in the plane of contact and is used to model frictional effects. In Abaqus, this behavior can be described using a Coulomb friction model, where a friction coefficient (μ) limits the tangential force that can be transmitted before sliding occurs.

The solver allows the definition of different friction laws—such as isotropic, anisotropic, or velocity-dependent models—to capture realistic sliding phenomena.

In this case, the model that provided the most reliable results was the isotropic friction model: the resistance to sliding is the same in all tangential directions at the contact interface. The frictional response is governed by a single coefficient of friction (μ), following the classical Coulomb's law:

$$\tau = \mu p \qquad \text{Eq.6}$$

where:

- τ is the limiting tangential stress (shear traction)
- p is the contact pressure.

Once the contact interaction properties between the parts have been defined, it is necessary to specify how the various components transfer forces.

Abaqus allows the definition of different interaction types, such as surface to surface, node to surface, edge to surface or general contact.

In this model, as well as in the subsequent ones, surface-to-surface contact interactions were employed. In the surface-to-surface contact formulation, one surface is defined as the master and the other as the slave. Abaqus enforces contact constraints between these surfaces, preventing any penetration of the slave surface into the master.

This approach is particularly suitable for assemblies with large contact areas or when one component is significantly stiffer than the other, as it provides a more accurate representation of the contact behavior compared to simpler node-to-surface methods. Moreover, it helps

reduce numerical instabilities during the simulation. Typical applications include contacts between bolts and holes, as in the case of IRJ.

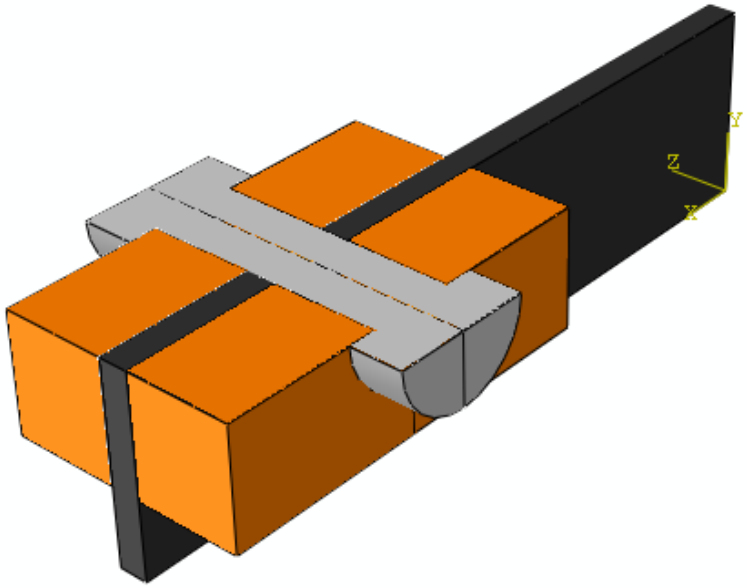

Figure 42. Section of pin-lug assembly

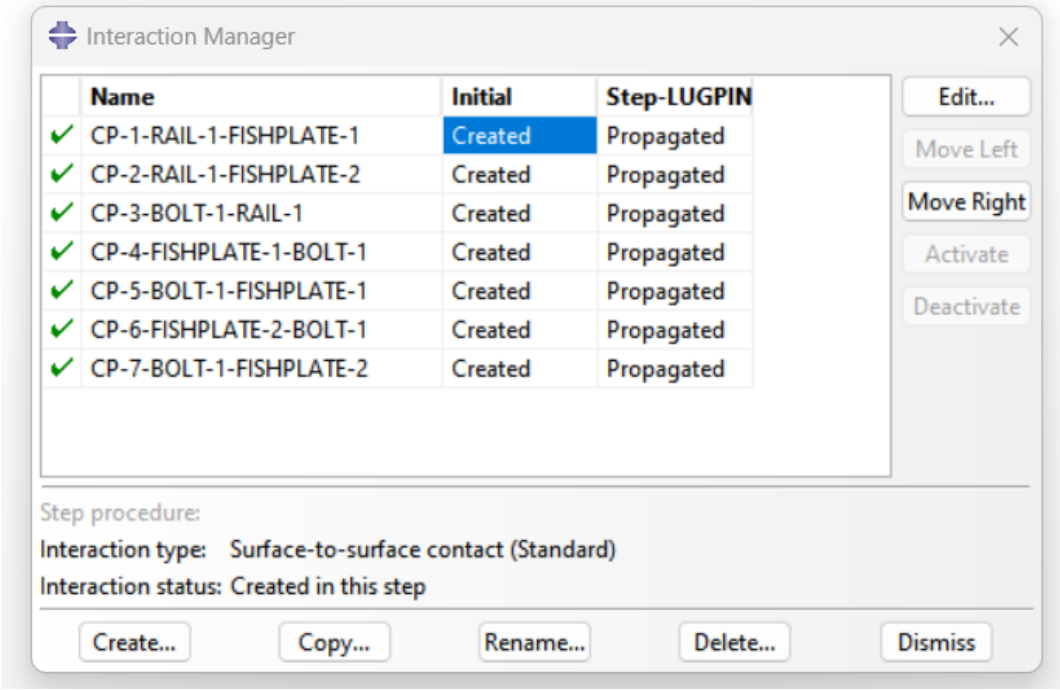

Figure 43. Pin-lug model's interactions

Subsequently, the model was further developed by modifying the geometry of the rails and introducing the first electrically insulating components:

- Rail: double T beam
- Fishplates: two plates with dimensions of 150 × 90 mm^2 and a thickness of 40 mm
- Bolt: a cylinder with a diameter of 26 mm
- Insulating layer between the fishplate and the rail
- Bolt insulating sleeve

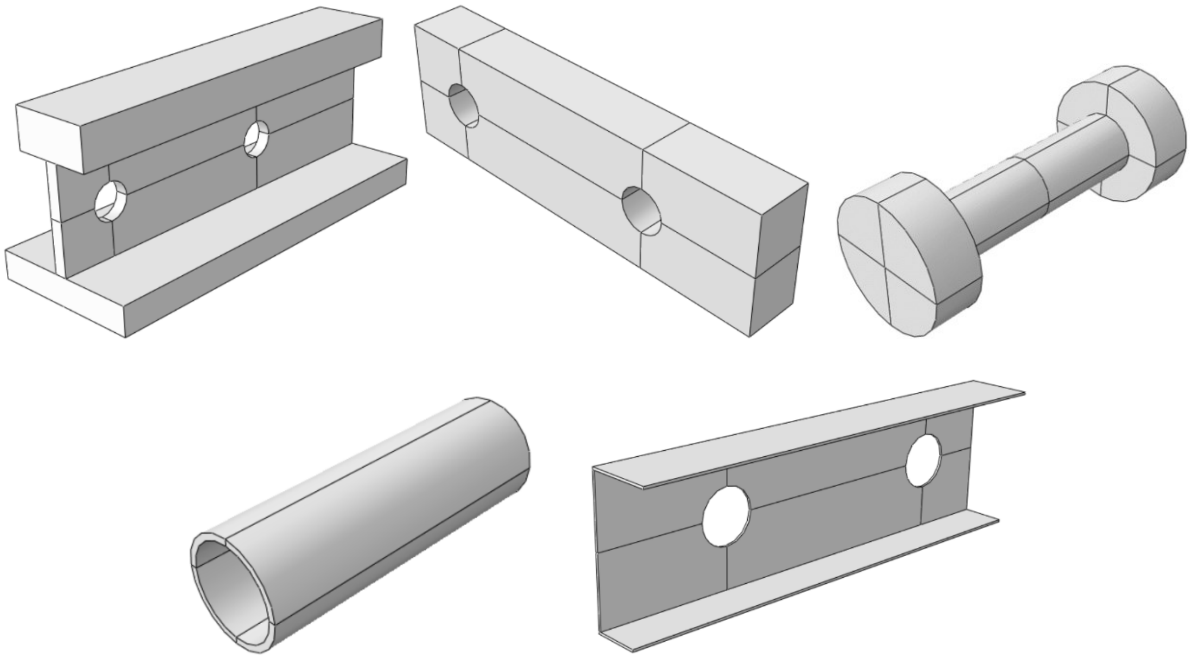

Figure 44. Evolved FEM model with insulating layer and bolt sleeve

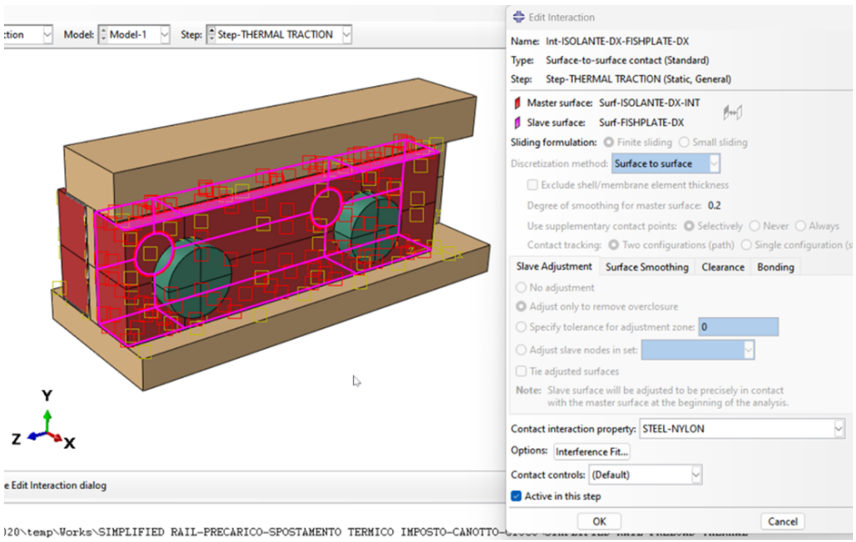

Figure 45. Evolved assembly view with highlighted master/slave surfaces

The management of this model proved to be particularly challenging. The presence of the insulating layer and the insulating sleeve around the bolt introduced significant mathematical complexity to the analysis. Since these components are made of a nylon-like polymer and have a negligible thickness compared to the overall dimensions of their contact surfaces, they caused severe numerical instabilities that hindered the convergence of the simulation.

It is important to emphasize, however, that the main objective of this study is to investigate the mechanical response of the insulated rail joint under loading conditions. The insulating material, by its very nature, exhibits very low mechanical strength compared with the metallic components of the assembly, as its primary function is electrical insulation rather than load bearing.

For these reasons and considering the computational challenges associated with accurately modelling these thin layers, their presence was intentionally neglected in the subsequent simulations to ensure numerical stability and focus the analysis on the mechanical behavior of the joint.

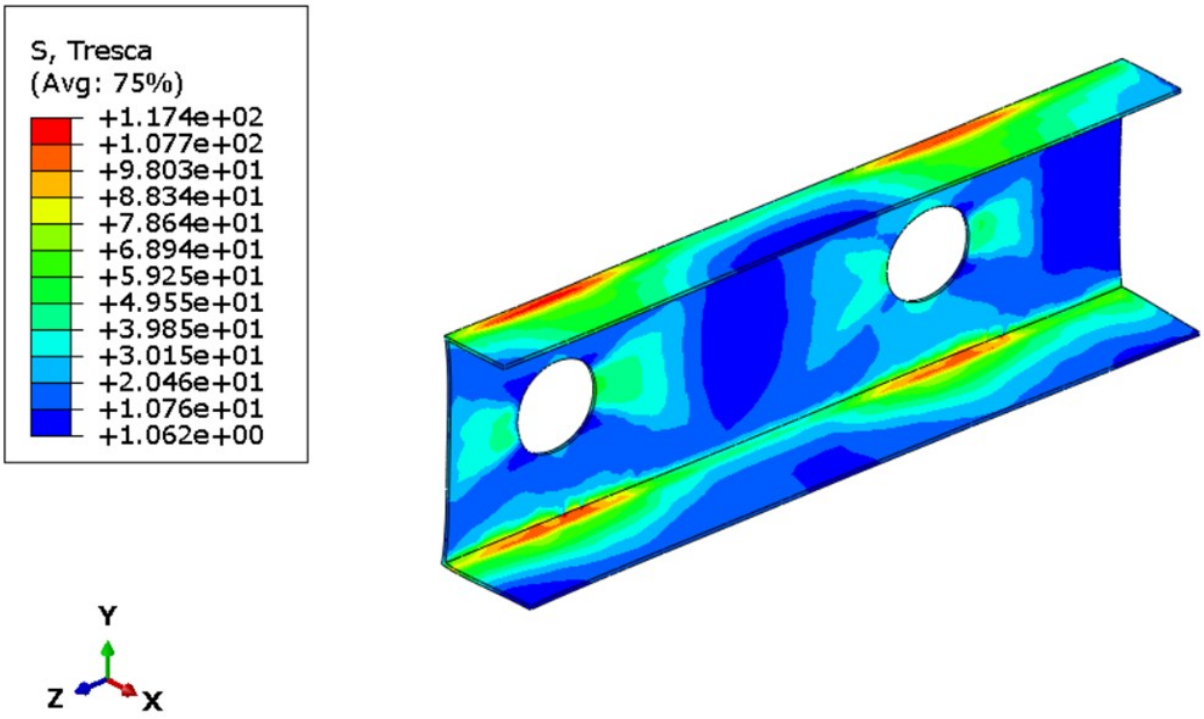

Figure 46. Trend of the internal stresses within the insulating layer between the fishplate and the rail, in the case of a simple axial load (z-direction) and bolt preload

4.1.1 Geometry of IRJ

The intermediate stages described in the introduction to Section 4.1 represent only the preliminary steps necessary for developing the final model geometry and ensuring numerical stability. The selection and calibration of all other parameters used in the more significant simulations will be discussed and justified in detail in the following sections.

This part, instead, focuses on presenting the final geometry of the model, which was defined after completing the previously described development steps.

In this case study, the model reproduces the exact geometry of all joint components in accordance with the R.F.I. (Rete Ferroviaria Italiana) standards (1967, 2003), corresponding to the 50 UNI rail profile.

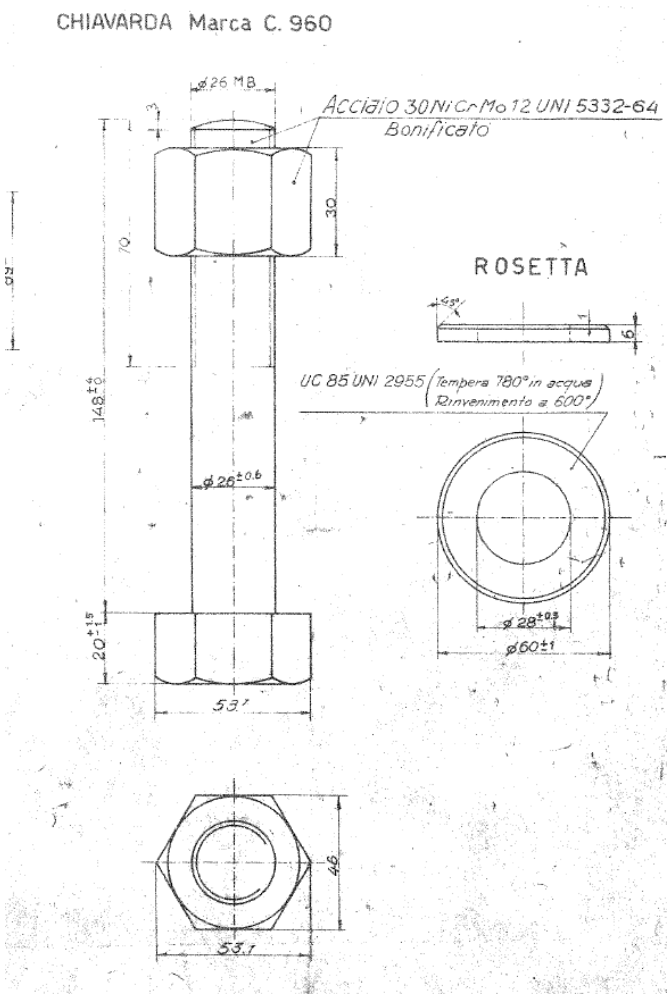

Figure 47. RFI bolt for IRJ, 50 UNI rail profile

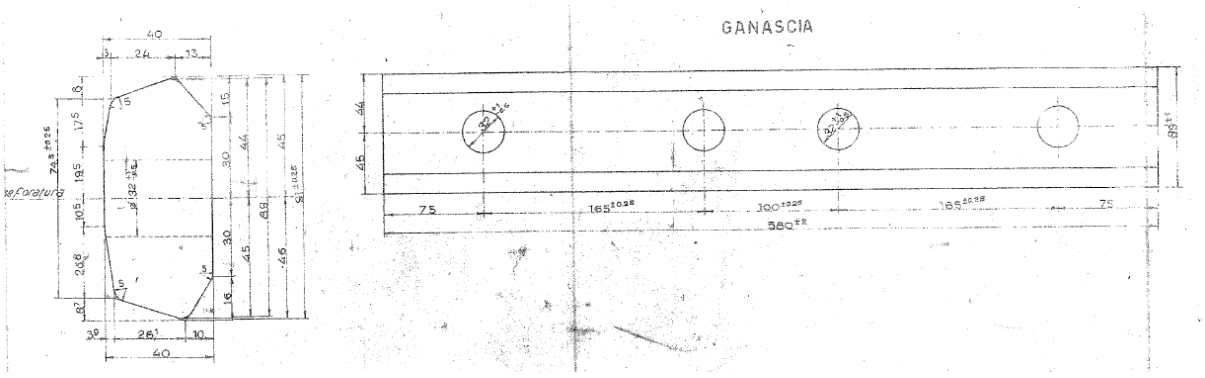

Figure 48. RFI fishplate for IRJ, 50 UNI rail profile

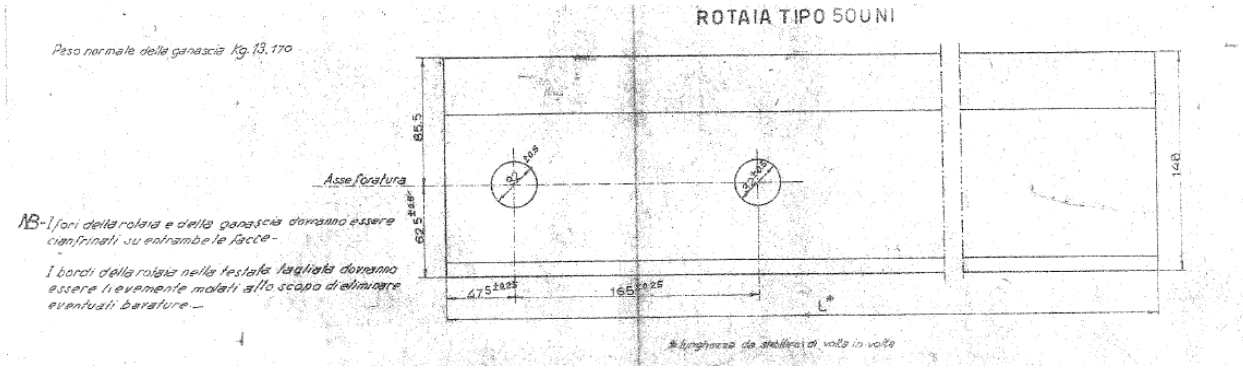

Figure 49. RFI 50 UNI rail for IRJ

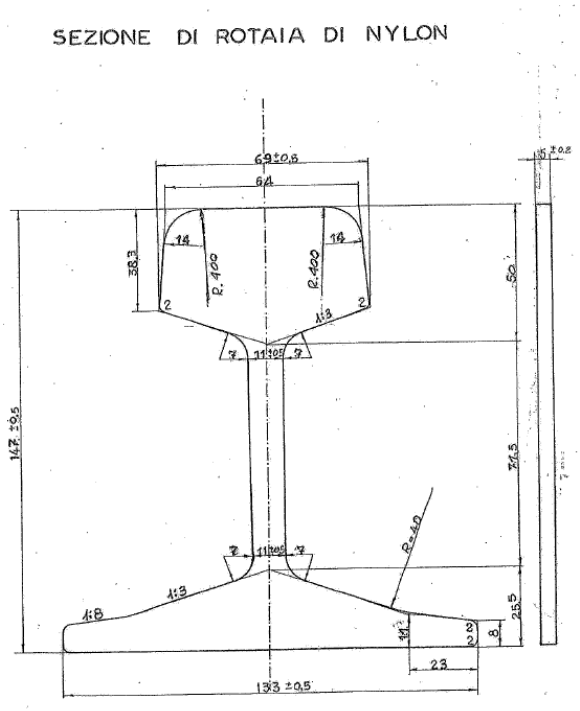

Figure 50. RFI end post for IRJ, 50 UNI rail profile

The assembly consists of two rail segments joined by a pair of fishplates and fastened with four bolts. As said, for simplification purposes, insulating components, such as the bolt insulating sleeves and the insulating layer between the fishplate and the rail, were not included in the model.

The two rail segments are 6-meter long and connected by an Insulated Rail Joint: the modelled system is subjected to the dynamic load of a single axle wheel with an external diameter of 920 millimeters. This rail length was selected in accordance with previous studies [2] [35], as it is sufficient to dissipate the dynamic effects generated by the wheel passage while avoiding boundary influences on the joint behavior.

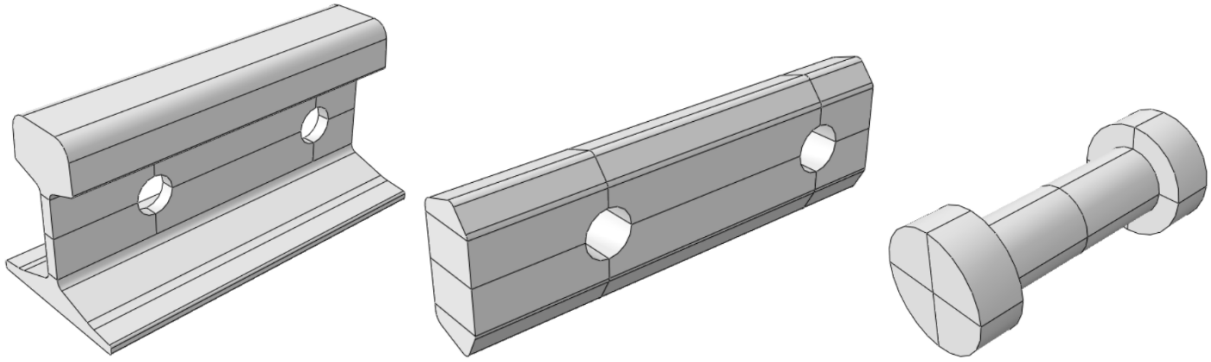

Figure 51. Components of the FEM model of the real IRJ, 50 UNI rail profile

The models shown in Figure 51 were created using the CAD software SolidWorks and subsequently imported into Abaqus/CAE as STEP files. The components were modelled in CAD using the RFI drawings shown in Figures 47 through 50.

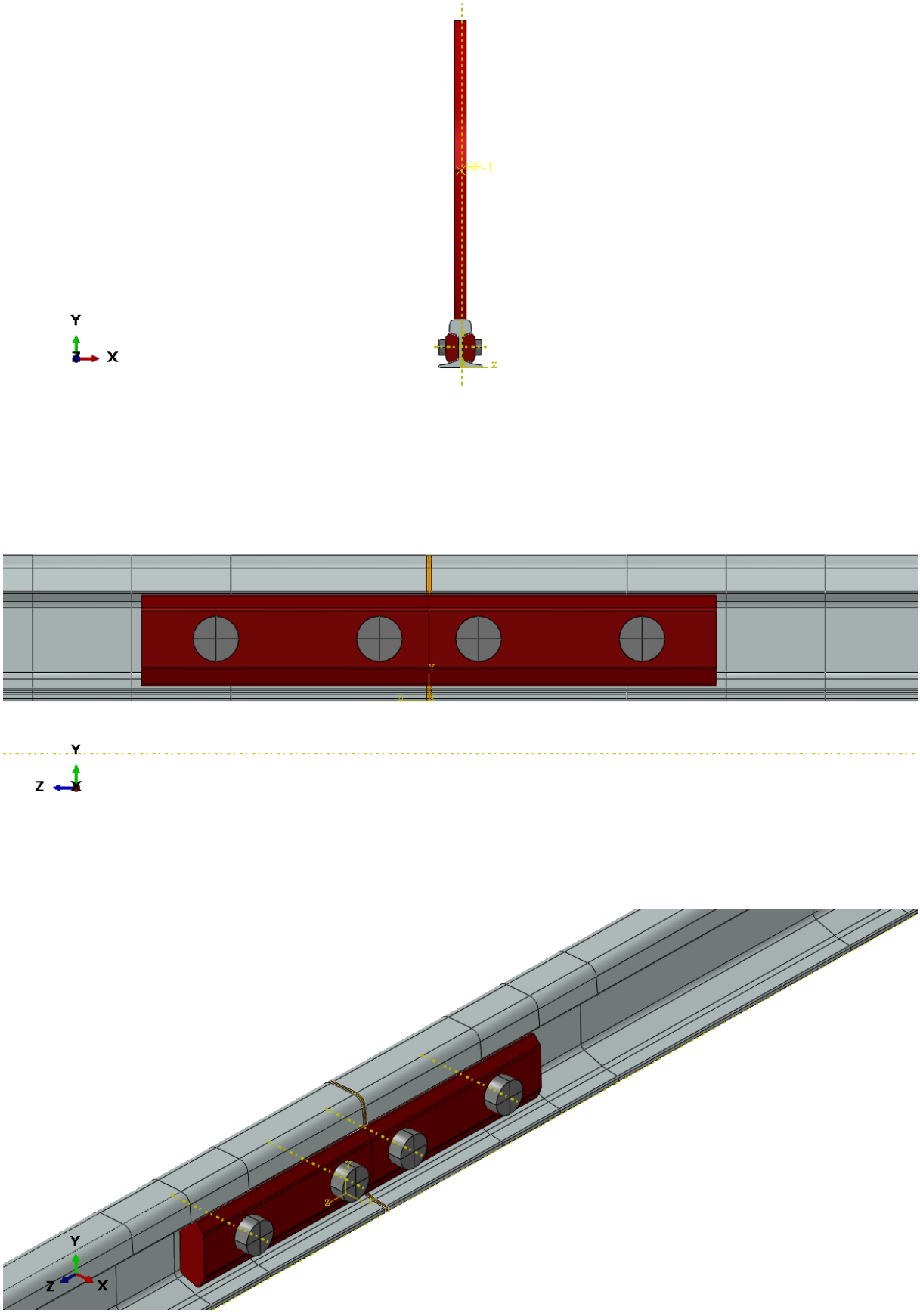

Figure 52. FEM model views

As can be observed, the final model includes exclusively:

- Two 6-meter rails (bolt holes have a diameter of 26 mm)
- Two fishplates (bolt holes have a diameter of 26 mm)
- Four bolts (diameter of 26 mm)
- Insulating End Post
- Axle wheel (the geometry is simplified to a basic disc, with the horizontal component of the load transmitted from the wheel to the rail neglected, and only the vertical component considered)

As can be observed, the various modelled components display lines dividing them into multiple sections. This technique is intentional and is referred to as partitioning and it is a fundamental tool in Abaqus to enhance model accuracy, simulation stability, and computational efficiency.

Partitioning is useful for:

- Mesh control: partitioning allows the user to define different mesh densities in different regions, improving accuracy in critical areas while reducing computational costs in less important regions.
- Application of boundary conditions and loads: specific loads, constraints, or interactions can be applied more precisely to selected regions of the part.
- Contact definition: partitions help define contact surfaces or edges more clearly, making it easier to manage interactions between different components.
- Geometric features and refinements: partitioning enables the creation of local geometric features, such as fillets, holes, or slots, without modifying the overall part geometry.

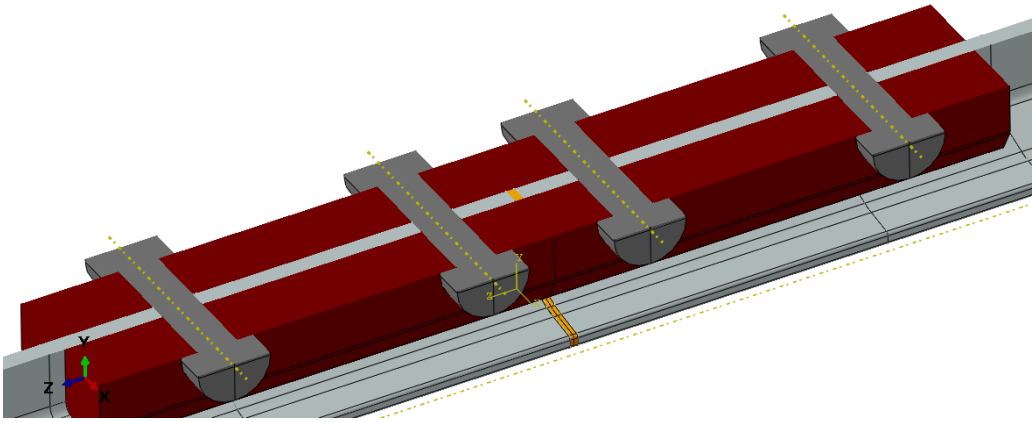

Figure 53. Section of real IRJ model

Two final remarks:

1. The origin of the coordinate system is positioned at the midsection of the end post, at the level of the bottom surface of the rail foot
2. The clearance between the bolts and the holes has been neglected, as in reality this gap is filled with insulating material and adhesive.

4.1.2 Material properties

This short section describes the material properties adopted for the components of the Insulated Rail Joint (IRJ).

Two materials were used:

1. Generic steel for the rails, bolts, fishplates, and axle wheel;
2. Nylon 99 for the end post.

Since the purpose of these simulations is to investigate the mechanical response of the joint under the loads generated by train passages throughout its service life, the analysis was limited to the elastic domain. Plastic behavior was intentionally excluded, as plastic deformation is a condition that must be avoided in real applications and falls outside the scope of this numerical study.

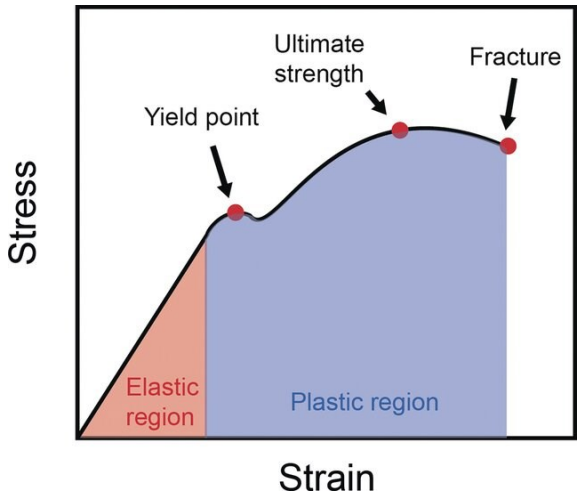

Figure 54. Generic stress-strain curve

GENERIC STEEL	NYLON 99
E: Young Modulus = 210000 MPa	E: Young Modulus = 1590 MPa
ν: Poisson's ratio = 0.3	ν: Poisson's ratio = 0.39
ρ: Density = 7.85E-009 tonn/mm³	ρ: Density = 1.14E-009 tonn/mm³

Table 3. Materials parameters

Some considerations:

- The unit system adopted in Abaqus is MM–TON–S, where length is measured in millimeters, mass in tonnes, force in Newtons and time in seconds.
- The materials are assumed to have isotropic elastic properties and the density is considered uniform throughout each component.
- Any additional parameters that were not relevant to the simulation were omitted in order to reduce computational cost.

4.1.2 Simulation steps: quasi-static approach for low-speed wheel passage

The low-speed passage of a railway wheel can be effectively represented in Abaqus using a static general step, rather than a fully dynamic analysis.

This assumption relies on the fact that, at low velocities, the inertial and damping effects associated with the wheel–rail interaction are negligible compared to the quasi-static mechanical response of the joint.

In such conditions, the load transmitted by the wheel can be considered to move slowly enough that the structure reaches an equilibrium configuration for each load position. Therefore, the static general step in Abaqus is suitable to reproduce the gradual transfer of vertical load along the rail while maintaining computational efficiency.

This approach allows the investigation of the stress and displacement distribution within the IRJ under realistic service loads, without the complexity and computational cost of an explicit dynamic simulation, which would be necessary only for high-speed or impact-type loading conditions.

The simulation was divided into two main steps:

1. Step 1: Application of the bolt preload
2. Step 2: Simulation of the wheel passage.

Before specifying the parameters used in the analysis and their corresponding values, it is necessary to introduce some fundamental concepts related to the numerical formulation and computational procedures adopted in Abaqus:

- Automatic stabilization enhances numerical stability, particularly during the initial increments, when contact interactions and nonlinearities can cause convergence difficulties. In Abaqus, this technique introduces a small amount of artificial damping that dissipates energy from unstable modes without significantly affecting the overall mechanical response. The dissipated energy fraction defines the maximum portion of strain energy that can be removed through this damping mechanism, ensuring that stabilization remains minimal and physically acceptable. The adaptive stabilization option allows Abaqus to automatically adjust the stabilization energy throughout the analysis, up to a prescribed maximum ratio between stabilization and strain energy, thus maintaining both stability and accuracy of the solution.

- The Nlgeom (nonlinear geometry) option in Abaqus is used to include the effects of geometric nonlinearity in a finite element analysis. When this feature is activated (Nlgeom = ON), the solver continuously updates the model geometry as the structure deforms, ensuring that equilibrium equations are satisfied with respect to the current, deformed configuration rather than the initial one. This allows the analysis to accurately capture large displacements, rotations, and changes in contact conditions, which can significantly influence the overall response of the system. Activating Nlgeom is essential in problems where deformations alter the load path or contact states such as in bolted assemblies or rail joints—because neglecting these effects (Nlgeom = OFF) would lead to an overly simplified linear approximation, ignoring important nonlinear behaviors and resulting in less accurate or even unrealistic predictions.

- The equation solver settled to the direct method, with the default matrix storage option, ensures robustness in solving large, complex systems of equations.

- The solution technique adopted was Full Newton, which recalculates the stiffness matrix at each iteration, providing higher accuracy in nonlinear analyses.

- The load variation with time was defined as linear ramping throughout the step, allowing a smooth and gradual application of the load.

- Finally, linear extrapolation of the previous state was applied at the beginning of each increment to improve convergence and computational efficiency.

PARAMETERS	STEP 1	STEP 2
Procedure	Static, General	Static, General
Step time	0.1 seconds	0.75 seconds
Nlgeom	ON	ON
Automatic stabilization: dissipated energy fraction	0.0002	0.0002
Maximum ratio of stabilization to strain energy	0.05	0.05
Maximum number of increments	1000	4000
Initial increment size	0.1	0.1
Minimum increment size	1E-10	1E-10
Minimum increment size	0.1	0.1
Equation solver method	Direct	Direct
Matrix storage	Default	Default
Solution technique	Full Newton	Full Newton
Load variation with time	Ramp	Ramp
Extrapolation of previous state	Linear	Linear

Table 4. Steps parameters

The table above summarizes all the parameters selected to define the simulation steps: the values adopted result from extensive optimization and calibration efforts, carried out through multiple iterative tests aimed at ensuring numerical stability and accurate convergence of the solution.

4.1.3 Interactions and constraints

First of all, it is necessary to define the interactions between the different components of the assembly. As extensively discussed in the introduction to Section 4.1, a surface-to-surface contact interaction was adopted, featuring:

- normal behavior: hard contact, allowing separation after contact;
- tangential behavior: friction coefficient of 0.2

In surface-to-surface contact definitions in Abaqus, one surface must be assigned as the master and the other as the slave. The criterium for assigning master and slave surfaces is critical for numerical accuracy and convergence: in this study, the surface with the larger area is usually designated as the master, while the smaller surface becomes the slave. This helps avoid excessive penetration of the slave nodes into the master surface and improves stability.

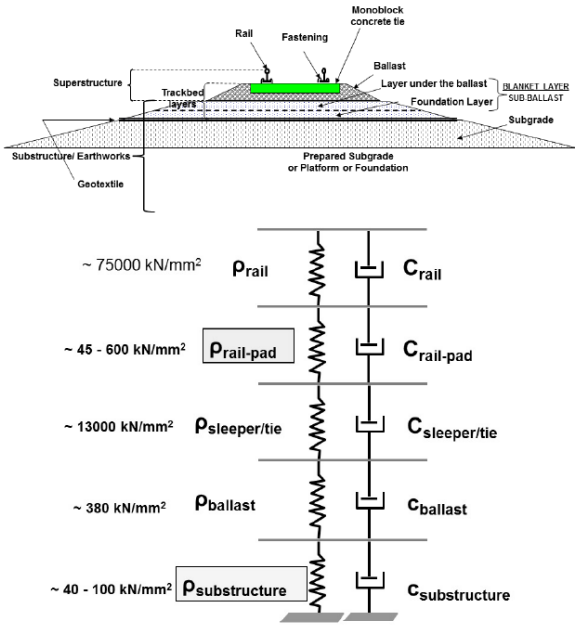

Figure 55. Railway superstructure modelling using Spring-Damper Elements [36]

Since the purpose of this finite element model is to evaluate the mechanical response of the joint under a quasi-static load—representing the weight of half a railway axle—both under progressive bolt preload loss and when either supported by the sleepers or suspended between them, it was also necessary to model the elastically-damped effect of the railway ballast beneath the sleepers.

It was therefore necessary to introduce a new type of interaction, referred to as an elastic foundation.

In Abaqus, an elastic foundation is a type of interaction used to simulate the elastic support provided by an underlying material, such as soil or railway ballast, without explicitly modeling the entire support medium. This interaction allows the structure to respond realistically to distributed support reactions, making it particularly suitable for applications such as railway tracks, pavements, or slabs resting on an elastic substrate.

The key parameter defining an elastic foundation is its stiffness, which represents the resistance offered by the supporting medium and is expressed in terms of force per unit volume, in this case N/mm³.

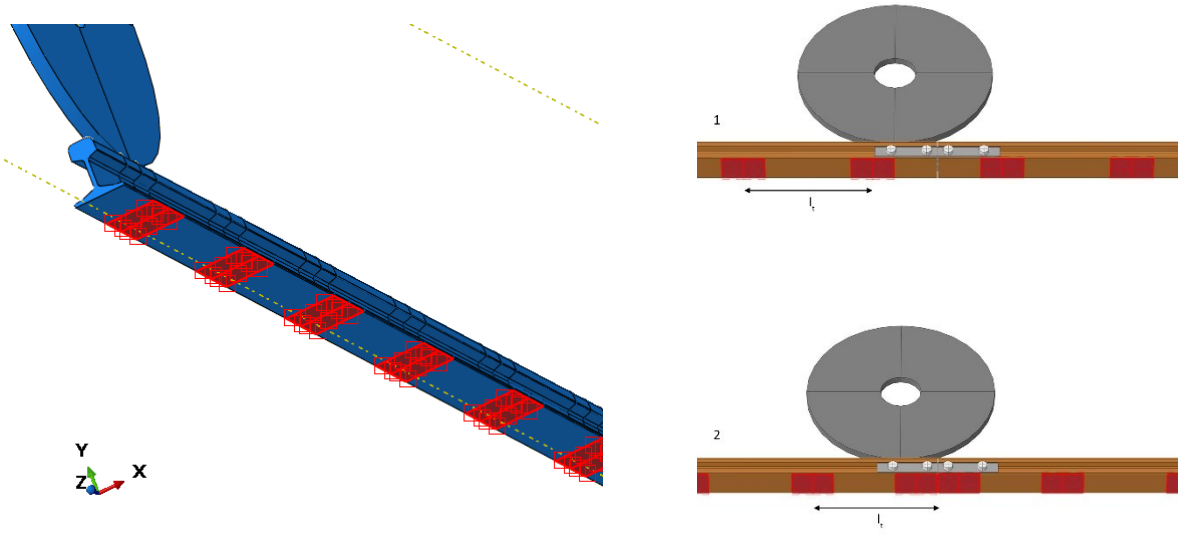

Figure 56. Rail partitions for elastic foundation

In the present model, the rail foot was subsequently partitioned into areas measuring 200 mm in length and a depth equivalent to the rail thickness, each assigned an elastic foundation with a stiffness of 0.2 N/mm³ [37]. The chosen length corresponds to the dimensions of standard gauge monoblock sleepers. These partitioned surfaces were repeated at 600 mm intervals, consistent with typical sleeper spacing. In the supported scenario, the use of special joint

sleepers was also considered, which effectively double the contact area while maintaining the original distance between sleepers.

These regions, highlighted in Figure 56, allowed the localized application of the elastic foundation simulating the elastically-damped response of the ballast beneath the sleepers. This approach enables a realistic simulation of the support conditions, distributing the elastic reaction along the length and thickness of the rail without the need to explicitly model the granular ballast.

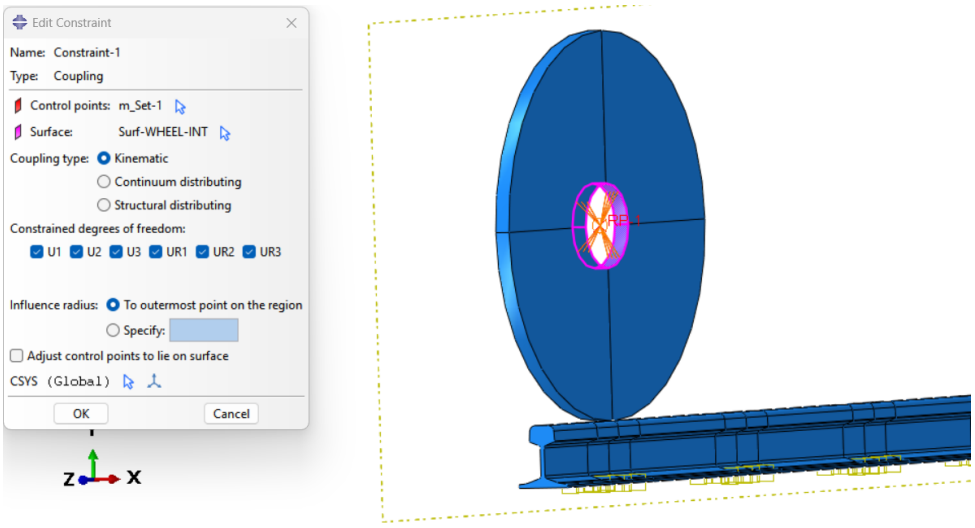

Figure 57. Coupling constraint used in the model

Finaly, two constraints have been introduced:

- A coupling constraint: used to kinematically link a set of nodes or a surface (referred to as the slave) to a single reference point (the master), ensuring that the motion of the slave nodes follows that of the master according to the specified degrees of freedom. This type of constraint has been particularly useful for simplifying the application of loads or boundary conditions on complex geometries, as it allows the user to control the motion of an entire surface through a single point. In the present study, a coupling constraint was employed to connect all nodes on the wheel surface (slave) to a reference point (master), to which the axle load was subsequently applied. This approach ensures that the load is uniformly transmitted to the wheel surface while maintaining computational efficiency and simplifying the load application process.

- A tie constraint: used to create a rigid connection between two surfaces, ensuring that the slave surface follows the motion of the master surface without any relative displacement. This type of constraint has been particularly useful for modeling perfect bonding between different components, such as welded or glued connections, where relative motion at the interface can be neglected. In the present study, a tie constraint was employed to connect the end post to the rails, ensuring a complete transfer of forces and moments between the components and accurately representing their structural interaction.

4.1.4 Loads and boundary conditions

This section presents all the loads applied to the system as well as the necessary boundary conditions, such as structural constraints.

The first load applied corresponds to Step 1, namely the bolt preload. To apply this type of load, Abaqus requires a specific partition of the affected part: the red section shown in Figure 58 illustrates the result of this partitioning.

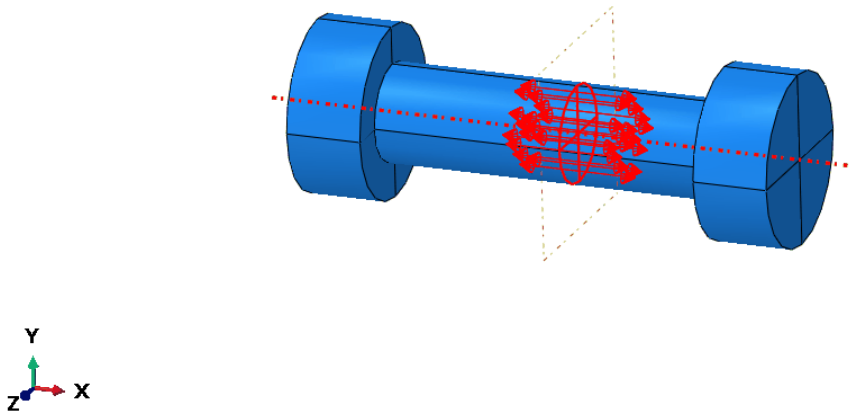

Figure 58. Bolt preload application

Abaqus applies a tensile load to this section, which simulates the effect of tightening the bolt: specifically, in this model, a preload of P_b = 200'000 N was applied to each bolt.

This value is derived from the application of Equation 7:

$$P_b = \frac{T}{Dk_b} \qquad \text{Eq. 7}$$

where P_b represents the preload applied to each bolt, T is the bolt torque specified by the manufacturer (set to 1'050'000 Nmm), k_b is the bolt torque coefficient (assumed as 0.2), and D is the bolt diameter (26 mm in this case).

The second load applied to the system corresponds to half the weight of a D_2-category railway axle, according to EN 15528: since the maximum axle load is 22.5 tonnes, a vertical load of 11 tonnes was applied in the model to the reference point located at the center of the wheel.

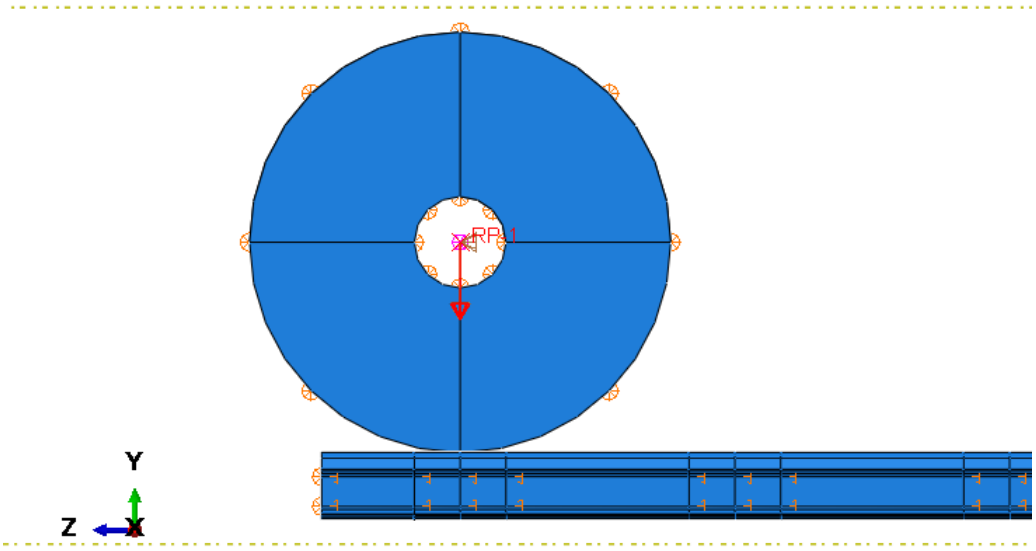

Figure 59. Axle load application

The vertical load was applied by running the wheel at a constant speed of 16 m/s.

The assembled model is constrained at the first face of the left rail, restricting displacement in the two directions perpendicular to the rail axis (x and z directions).

Additionally, a boundary condition is applied to ensure that the wheel remains properly aligned with the track during motion.

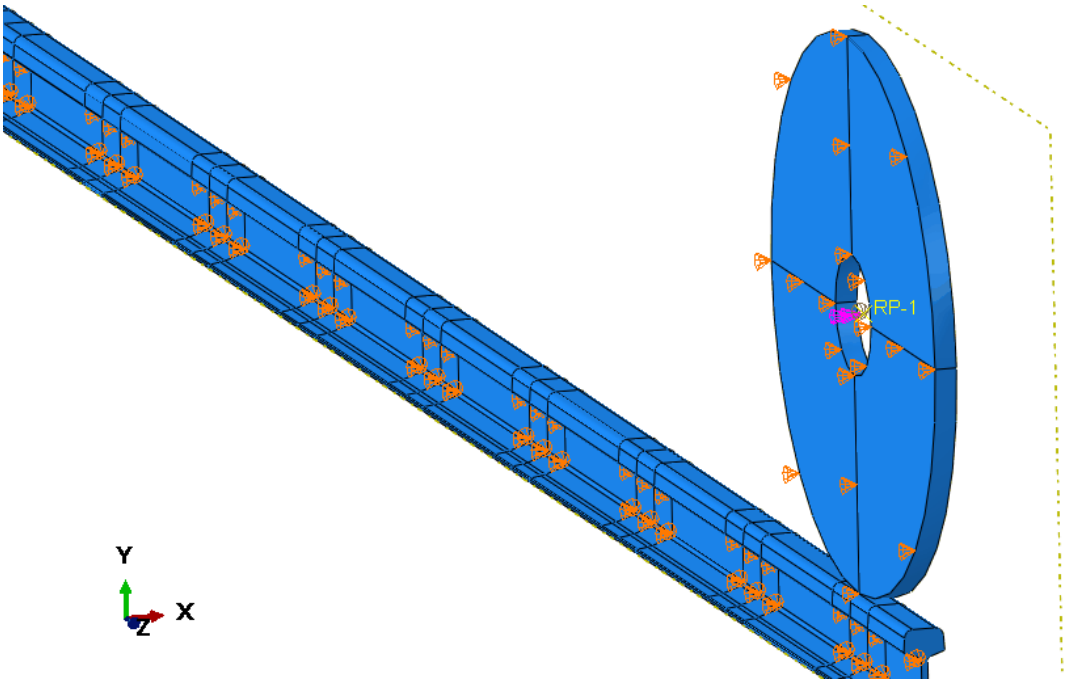

Figure 60. Model boundary conditions

4.1.5 Mesh

Figure 61 shows the mesh of the solid model, highlighting the complexity of the system's geometry.

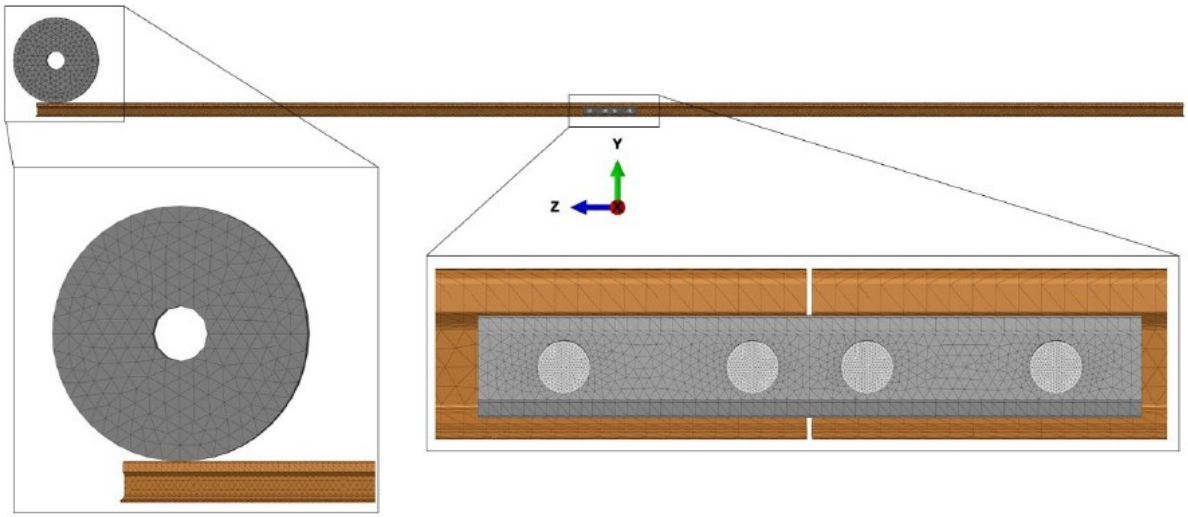

Figure 61. FEM model mesh with IRJ and wheel details [38]

Thanks to the partitions, it was possible to apply a finer mesh in the most critical and relevant areas, including:

- The bolt head and shank
- The fishplates
- The rail material adjacent to the bolt holes

In less critical areas, such as the rail material far from the joint section or the wheel, a coarser mesh was used to reduce the computational cost, which was already significant due to the complexity of the model.

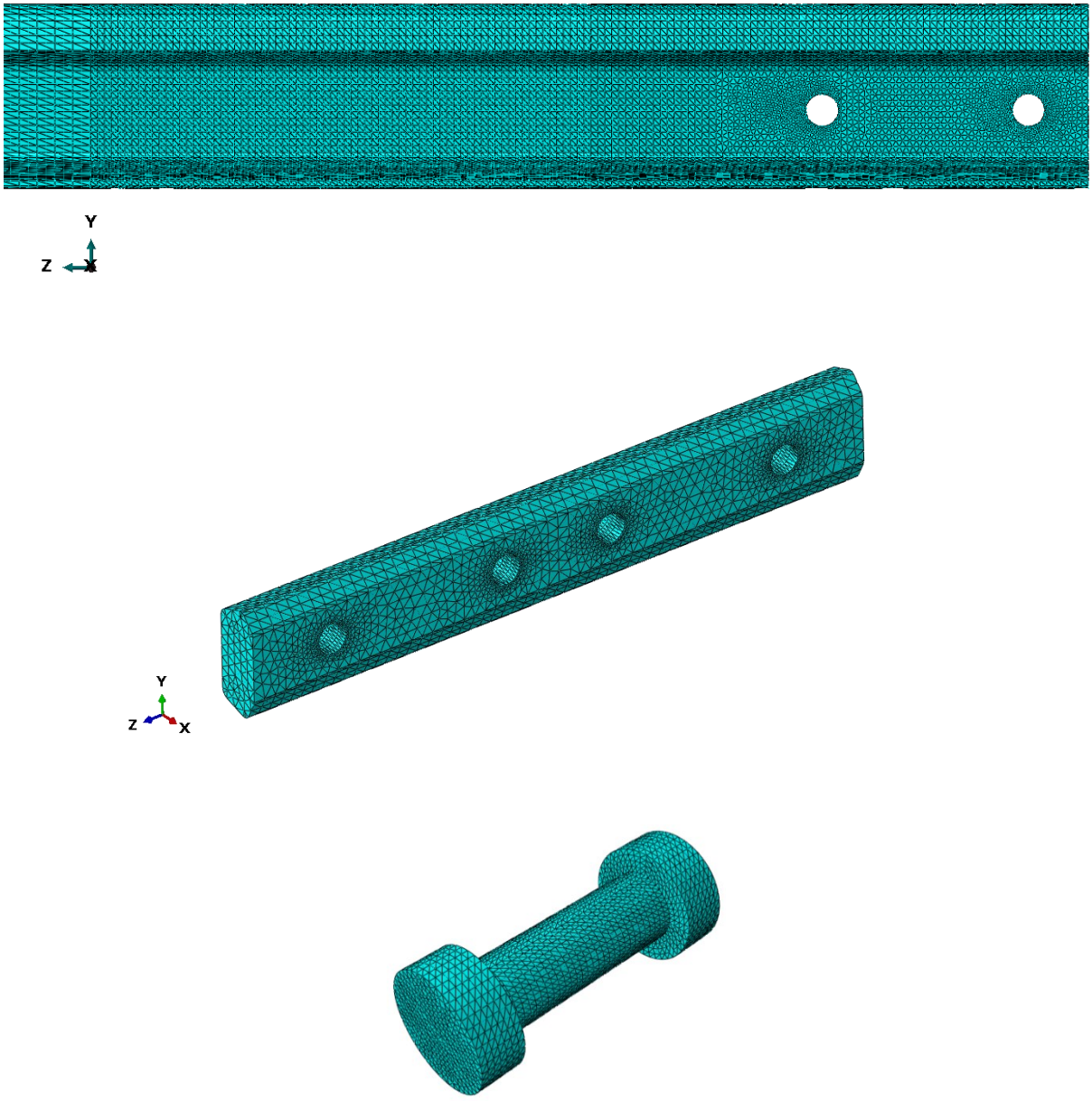

Figure 62. Model parts mesh, refined in the most critical areas

The mesh consists of two types of elements, whose selection was not straightforward and resulted from a dedicated mesh convergence study.

The element types used are as follows:

- Linear tetrahedral elements (C3D4) for the bolts, end post, and plates
- Quadratic tetrahedral elements (C3D10) for the rails.

In Abaqus, both C3D4 and C3D10 are three-dimensional tetrahedral solid elements, but they differ significantly in formulation and accuracy.

The C3D4 element is a linear tetrahedral element with four nodes, each possessing three translational degrees of freedom. Its shape functions are linear, meaning that it can only represent constant strain within each element. As a result, C3D4 elements are computationally efficient and suitable for regions with simple stress distributions or where geometric complexity makes meshing more challenging, but they may lead to lower accuracy and higher stiffness (a phenomenon known as numerical locking) in regions with significant stress gradients.

The C3D10 element, on the other hand, is a quadratic tetrahedral element with ten nodes, allowing for quadratic interpolation of the displacement field. This enables it to capture stress and strain variations more accurately and to represent curved geometries more effectively. Although C3D10 elements are more computationally expensive, they provide improved convergence and more realistic stress distributions, particularly in areas with high stress concentrations or complex loading conditions: it's important to remember that the most critical areas are the ones near the rail holes.

For these reasons, C3D10 elements were chosen for the rail, where accurate stress evaluation and smooth representation of the curved rail geometry are essential.

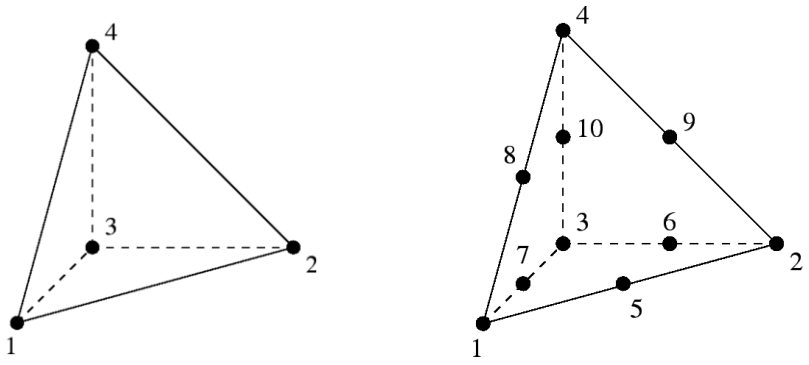

Figure 63. C3D4 and C3D10 elements

The mesh convergence study was carried out by comparing the contact pressures caused by bolt preload, obtained from a simplified analytical model with those extracted from a numerical simulation performed in Abaqus, which incorporated the actual geometric configuration of the system.

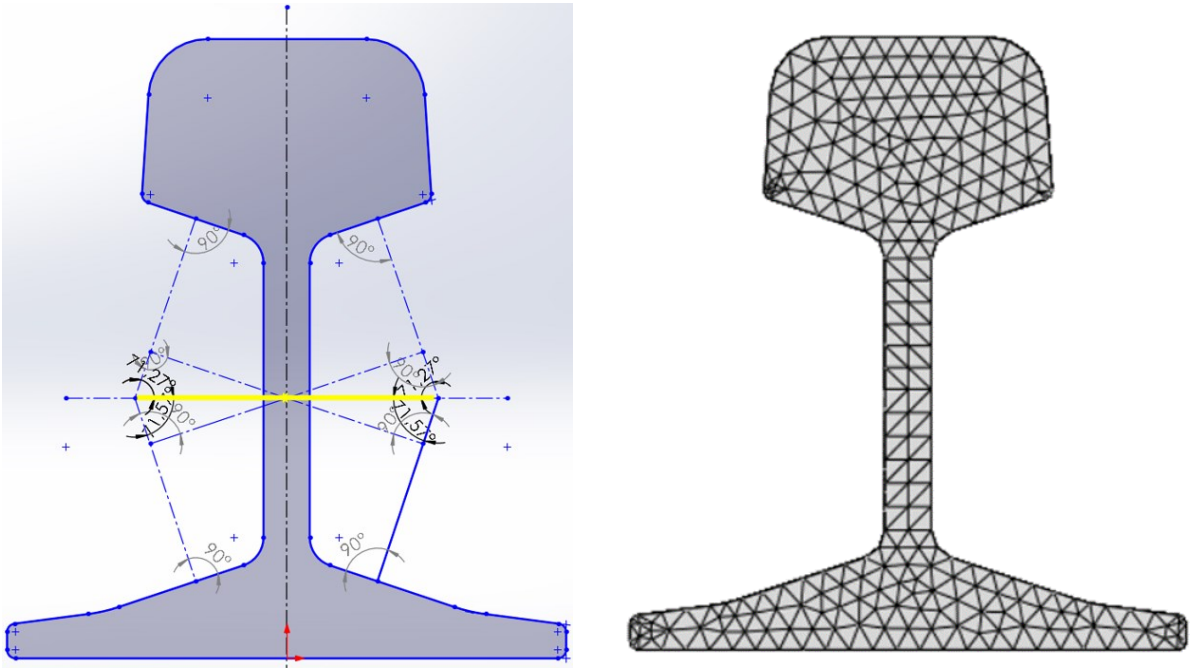

Figure 64. CAD model and its STEP file meshed in CAE

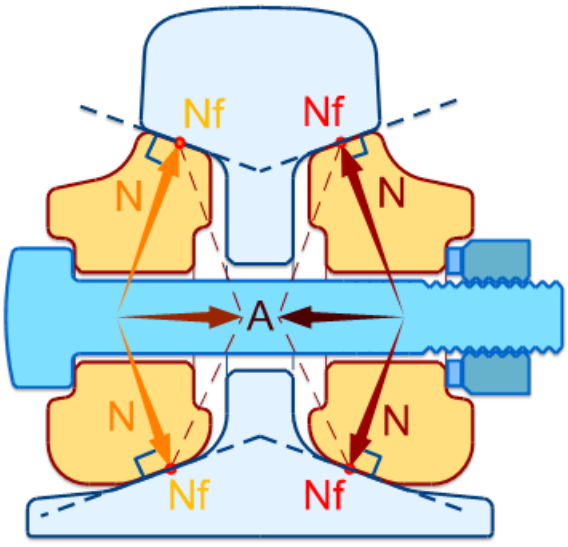

Figure 65. Contact force scheme

The contact force transmitted beneath the head and on the foot of the rail, resulting from the bolt preload, can be easily calculated using the following equation:

$$F_c = 2\left(\frac{P}{2}\cos\vartheta\right) \qquad \text{Eq. 8}$$

Where, referring to the left image of Figure 64:

- F_c is the contact force [N]
- P is the divided value of bolt preload: 100'000 [N] (there are two yellow arrows, each one represents a half of total bolt preload)
- θ is projection angle

In this way, four contact forces (F_c) are obtained, grouped in pairs of equal values: two corresponding to the rail feet and two to the regions beneath the rail head. By dividing these forces by their respective contact areas (calculated by CAD software), the resulting contact pressures can be compared with the average CPRESS values obtained from Abaqus.

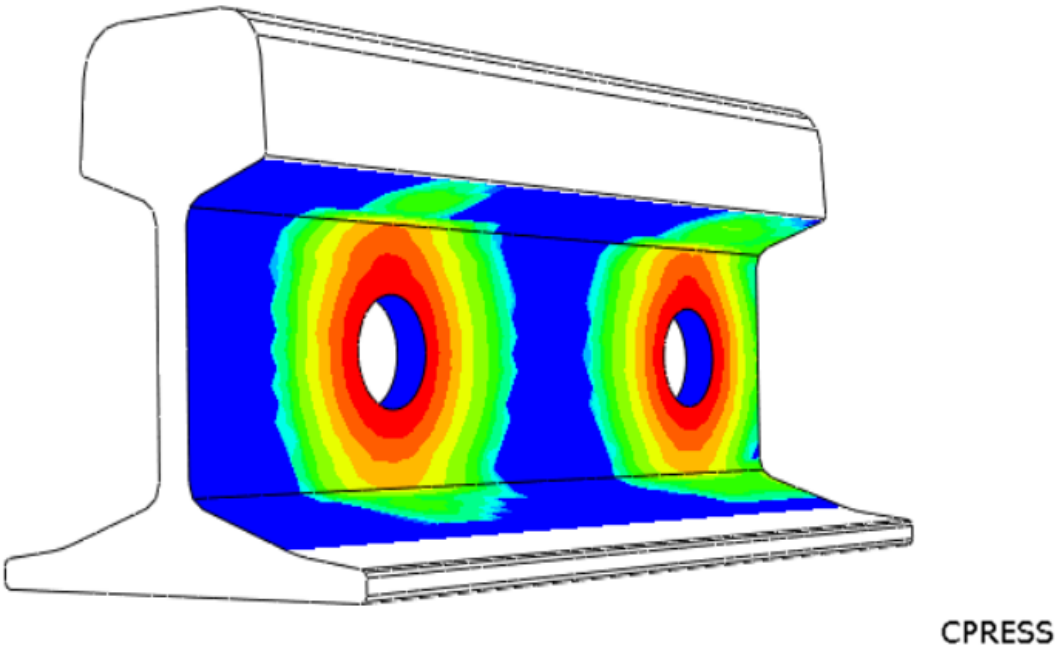

Figure 66. Distribution of contact pressures obtained from the FEM model in Abaqus

The results are shown in the table below:

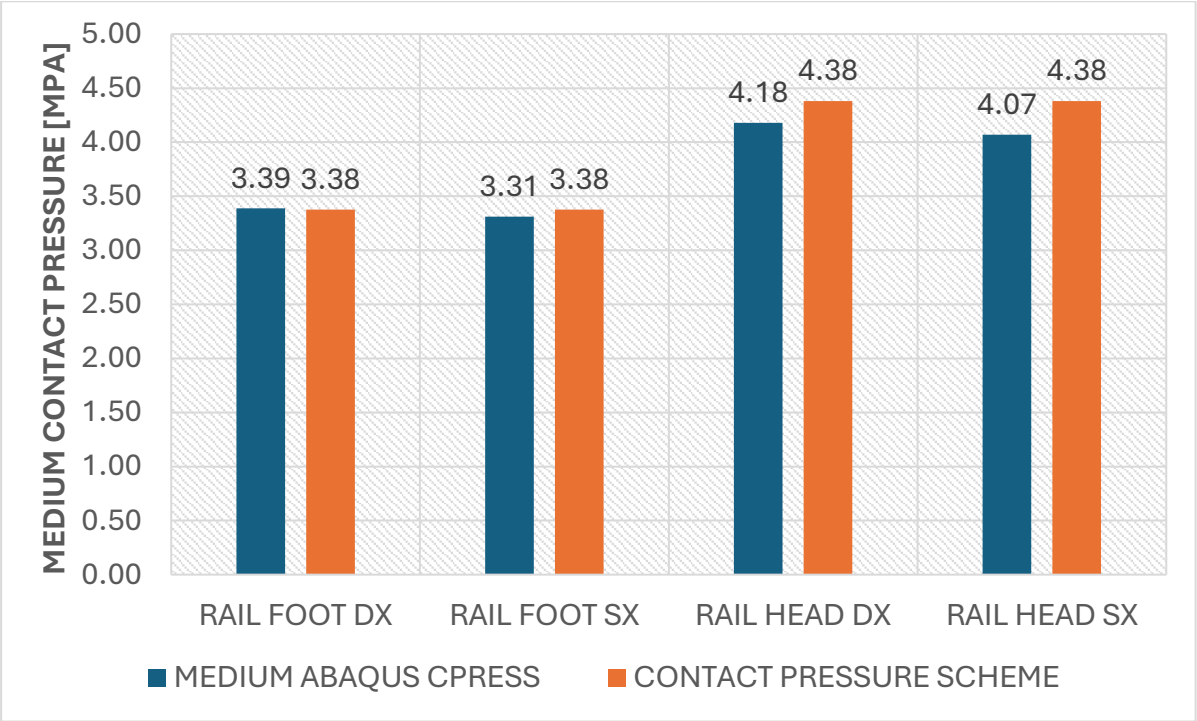

	MEDIUM ABAQUS CPRESS [MPA]	CONTACT FORCE SCHEME [N]	AREA [MM^2]	CONTACT PRESSURE SCHEME [MPA]
RAIL FOOT DX	3.39	31564.88	9347.22	3.38
RAIL FOOT SX	3.31	31564.88	9347.22	3.38
RAIL HEAD DX	4.18	31622.78	7220.97	4.38
RAIL HEAD SX	4.07	31622.78	7220.97	4.38
TOTAL	14.95	126375.31	33136.38	15.51

Table 5. Comparison between analytical and numerical contact pressure results

The results are clear, and, disregarding the natural asymmetry of the mesh, an almost perfect agreement between the analytical and numerical results is observed. This indicates that the chosen element types and their sizes in the regions of interest were appropriately selected, following numerous optimization attempts.

Thus, the element sizes were carefully selected: as previously mentioned, a finer mesh was used in the rail web where the joint holes are located. The resulting mesh achieves an optimal balance between result accuracy and acceptable computational cost. The quality of the mesh is further confirmed by the aspect ratio, which is below 10 for approximately 95% of the elements.

4.2 FEM study results

It is useful to remember that the objective of this study is to compare the two possible sleeper configurations in the presence of an insulated rail joint (IRJ).

Accordingly, the following configurations are considered:

1. Suspended joint
2. Supported joint

For each configuration, two loading conditions have been analyzed:

A. Full preload, representing the optimal operating condition.
B. Partial preload, simulating the progressive loss of bolt tension over the service life of the joint. In this case, the preload value (Pb) was reduced to 10% of its initial value to represent a degraded condition.

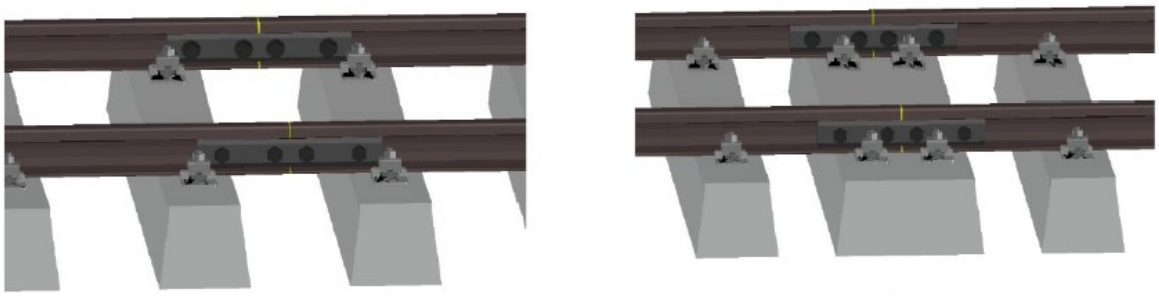

Figure 67. Sleeper support joint: on the left the suspended configuration, on the right the supported one

The bending stiffness of an insulated rail joint (IRJ) is generally lower than that of the continuous rail. Consequently, wheel passages induce greater local deformations in the joint region [13]. These deformations are further amplified by any geometric or contact irregularities at the joint interface, resulting in a dynamic increase in stress levels and, consequently, accelerated degradation of both the IRJ and the adjacent rail.

Among the available configurations, the supported joint solution is widely adopted, as it offers improved stability and continuity between adjacent rail sections. However, this configuration can also lead to higher impact forces and post-impact vibrations generated by train passages compared to the suspended joint. Furthermore, modern alternatives such as special joint

sleepers, designed with a widened rail foot support, must ensure compatibility with standard mechanized maintenance procedures, particularly ballast tamping.

This section discusses the results of numerical simulations, analyzing the mechanical response of the IRJ in the four configurations investigated.

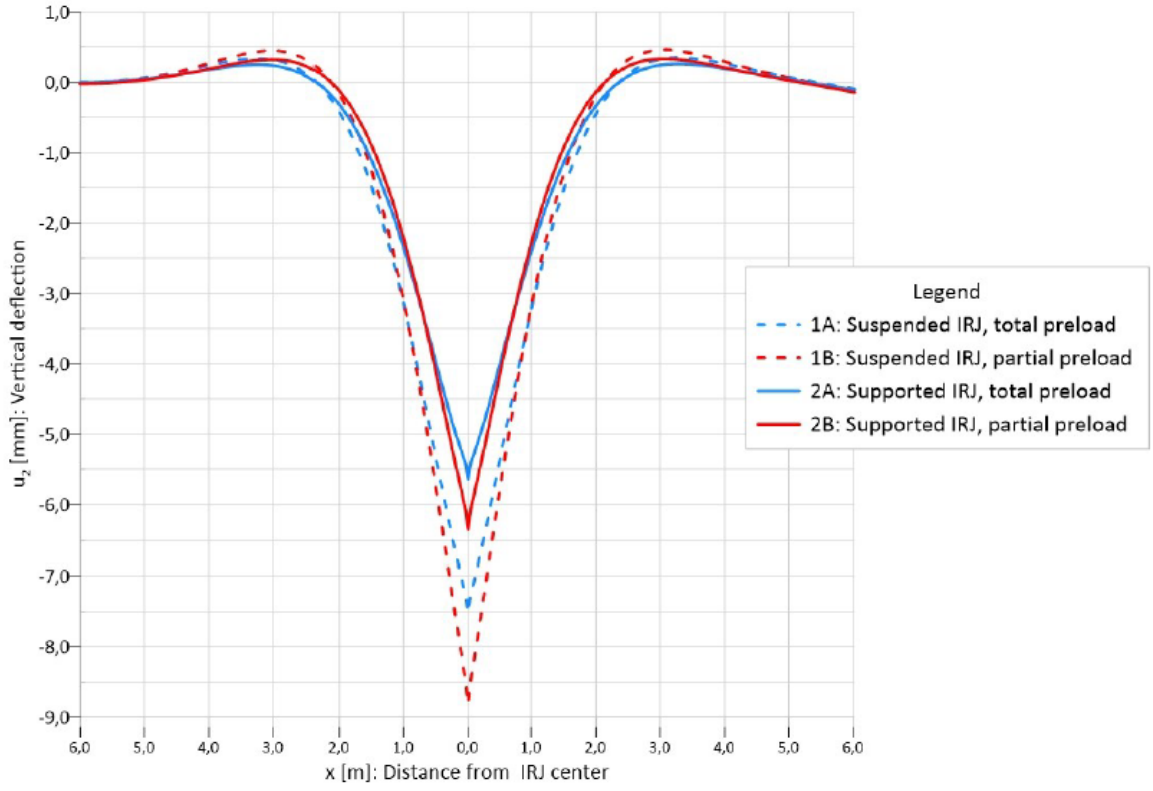

Figure 68. Vertical deflection: suspended and supported IRJ [38]

Figure 68 presents the vertical deflection (u_2, with reference to the coordinate system in Figure 61) of the running surface at the joint, captured when the wheel is positioned midway between the two connected rail sections.

As expected, the supported configuration provides greater stiffness and stability across the discontinuity between the two rail ends. Under full operational conditions, with a maximum bolt preload of 200'000 N, the minimum vertical deflection is –7.51 mm for the suspended configuration and –5.63 mm for the supported one, corresponding to a 33% reduction in deflection.

In the partial preload condition (20’000 N) the minimum deflection reaches –8.81 mm in the suspended configuration and –6.35 mm in the supported one, indicating a 38% reduction in the latter. The loss of 90% of the bolt preload results in a 17% increase in deflection for the suspended configuration and a 12% increase for the supported configuration.

Case	Minimum vertical deflection [mm]	Rail hole maximum Von Mises stress [MPa]
1A: Suspended joint, full preload	-7.51	150
1B: Suspended joint, partial preload	-8.81	250
2A: Supported joint, full preload	-5.63	120
2B: Supported joint, partial preload	-6.35	160

Table 6. Model output: suspended and supported IRJ

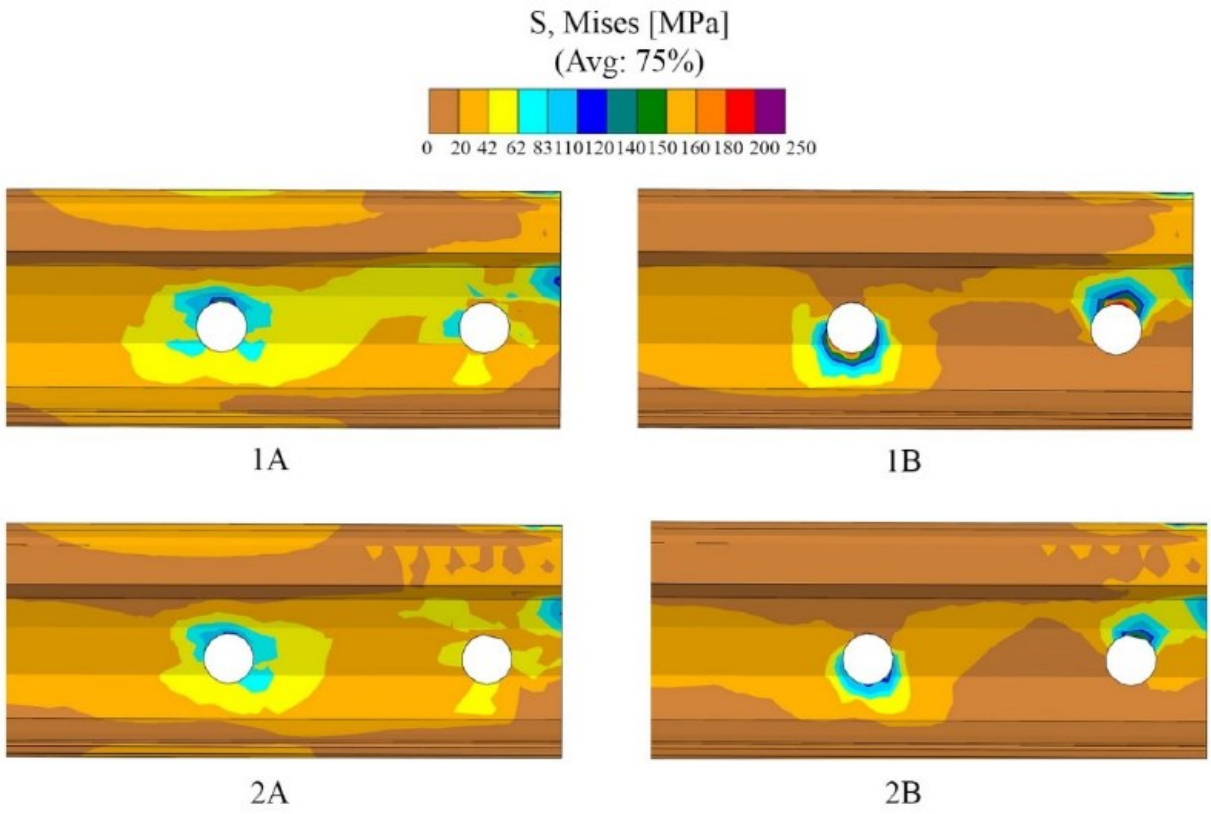

Figure 69. Von Mises stress of the IRJ in the suspended and supported cases [38]

These findings are corroborated by the analysis of the Von Mises stresses, as illustrated in Figure 69, which focuses on the rail-hole region—a critical area prone to crack initiation. Higher stress concentrations are observed in the suspended IRJ compared to the supported configuration, with the most critical condition occurring in configuration 1B, characterized by a suspended IRJ with partial bolt preload. In this case, the stresses in the rail holes exceed those of the supported case by more than 35%, suggesting a higher likelihood of fatigue damage and crack propagation.

The main results obtained from the numerical simulations are summarized in Table 6.

4.3 FEM study discussion

In this research, a digital twin of a four-hole bonded insulated rail joint (IRJ) was developed to analyze the mechanical behavior of the joint under different configurations and preload conditions. A 12-meters rail segment was modelled to evaluate vertical deflections and stress distribution during the passage of a train wheel in both supported and suspended configurations. The results demonstrated that both the support condition and the bolt preload significantly influence the structural performance of the IRJ. Specifically, the supported configuration exhibited lower vertical deflections—by 33% under full preload and 38% under partial preload. Conversely, preload loss had a greater effect on the suspended configuration, leading to a 17% increase in deflection. These findings indicate that the supported configuration provides better mechanical stability and reduced stress concentration near the rail holes, thereby mitigating crack initiation risks. However, its increased stiffness may lead to higher wheel–rail impact forces and must be assessed for compatibility with automated ballast maintenance.

5 Static tests on IRJ

The insulated rail joint represents one of the most particular components of the railway track, where complex stress states arise at the discontinuity between adjacent rail sections. While numerical simulations can effectively reproduce the mechanical behavior of the joint under various loading and boundary conditions, experimental validation remains essential to verify model accuracy and understand the actual physical response of the system under static loading.

In this thesis, the static tests presented in this chapter were therefore designed to investigate the mechanical response of IRJs under different bolt preload conditions, with the primary objective of assessing how this parameter influences the joint's stiffness and deformation characteristics and to compare laboratory results directly against the FEM outcomes discussed in Chapter 4. A key motivation for this research lies in the need to validate or refine the numerical model and to provide a deeper understanding of the influence of bolt preload loss, a degradation mechanism often observed in service but rarely quantified through laboratory testing.

Several studies have experimentally investigated insulated rail joints, focusing primarily on aspects such as the flexural behavior of the joint or of individual joint components (e.g., fishplates) [39], [40]. However, these works were generally conducted under nominal conditions, without examining the phenomenon of bolt preload loss. Other works concentrated on the plastic deformation occurring in the jointed rail section under wheel passage [41], while others analyzed the variation in global track stiffness resulting from the presence of the joint [27].

The originality of this work therefore lies in conducting controlled static tests on IRJ specimens with systematically varied bolt preloads, thereby bridging a significant gap in the literature and offering new insight into the relationship between bolt preload degradation, joint support configuration, and structural integrity.

The tests were carried out on a real IRJ specimen, excluding the effects of ballast support in order to evaluate the intrinsic stiffness of the joint assembly alone. This approach allows the observed deformations—typically of the order of tenths of a millimeter—to be attributed solely to the structural compliance of the joint components. Consequently, when compared with the millimetric vertical displacements predicted by the FEM simulations (which include the

deformability of the elastic foundation representing the ballast), it can be inferred that a substantial portion of the total deflection in the numerical model originates from ballast compression rather than from the joint itself.

This important distinction, as well as the potential discrepancies between the experimental observations and the numerical predictions, will be examined in detail in the concluding discussion of this chapter.

The experimental activity followed the procedures outlined by the standards of Rete Ferroviaria Italiana (RFI), with specific adaptations introduced to account for the particular test setup and instrumentation required to assess the effect of preload variation. The IRJ specimen was instrumented to measure local displacements and strains, enabling a detailed evaluation of its static response under a four-point bending configuration.

The chapter is structured as follows: Section 5.1 presents the reference standards and testing guidelines, including any deviations adopted for this experimental program. Section 5.2 describes the preparation of the test specimen, the applied modifications, and the instrumentation layout. Section 5.3 details the testing procedure, including load application, sequence, and data acquisition strategy. Section 5.4 reports and analyses the experimental results, focusing on displacement–time and load–displacement responses and the influence of bolt preload. Finally, section 5.5 provides a critical discussion of the findings, addressing implications for joint performance, design, and maintenance, as well as limitations of the experimental approach.

5.1 Test standards and guidelines

The static bending tests were performed in accordance with the specifications defined by Rete Ferroviaria Italiana (RFI) in document TCAR SF AR 03 003 F and RFI TCAR SF AR 07 008 A, which aligns with the principles of UNI EN 13230-4. This standard provides the official reference procedure for the four-point bending test, used to determine the flexural stiffness and cracking behavior of sleepers and similar structural elements under quasi-static loading.

According to the RFI specification, the specimen is supported on two bearing devices designed to reproduce realistic boundary conditions. The left bearing is a rigid (not deformable) support, while the right bearing is an articulated support, allowing free rotation of the beam under load.

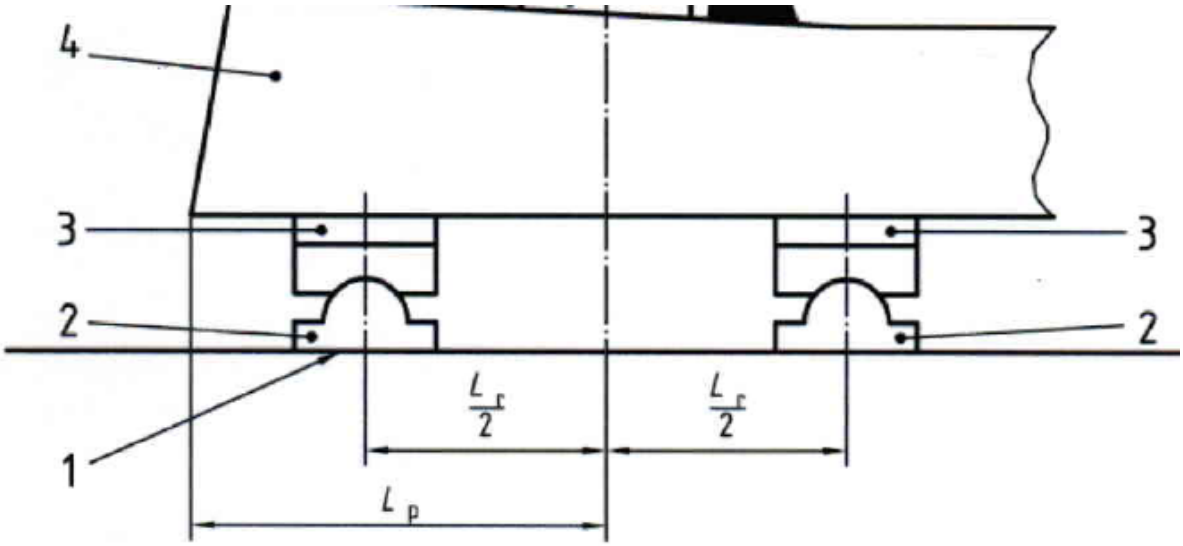

Legenda:

1. Appoggio indeformabile
2. Appoggio articolato (vedere allegato A per i dettagli)
3. Suola elastica (vedere allegato A per i dettagli)
4. Traversa

Figure 70. Specimen supports in four points bending test [42], [43]

Both supports are made of hardened steel (minimum hardness HBW 240) and are installed on an alignment base with a maximum flatness deviation of ±0.1 mm. Between the supports and the specimen, elastomeric pads are interposed to reproduce the rail-seat conditions; their static stiffness must range between 1 N/mm³ and 4 N/mm³, and their length must exceed the rail-seat width by at least 20 mm to ensure uniform contact pressure distribution.

The load is applied through two cylindrical steel rollers, positioned symmetrically with respect to the mid-span of the specimen to generate a constant bending moment in the central region. The rollers are mounted on transverse distribution beams to guarantee uniform force transmission across the rail seat. The geometry of the test rig is defined by the total bearing span L_p and the half-reaction span $L_r/2$, ensuring equal lever arms between load and support points, as illustrated in Figure 70.

Loading is applied quasi-statically by means of hydraulic jacks operating under displacement-controlled or load-controlled mode, with a maximum load-increase rate of 120 kN/min, as prescribed by the standard.

This setup ensures controlled and reproducible test conditions, accurately reproducing the support and load transfer mechanisms encountered in service, while maintaining compliance with national railway standards for static flexural testing.

5.1.1 Adaptations and deviations from standard procedures

Due to the availability of only one specimen, it was decided to carry out non-destructive static tests. Although the procedure followed the RFI standards described above almost in their entirety, certain adaptations and deviations from the standard protocol were necessary to meet the specific objectives of this research.

The author wishes to express their gratitude to the P&P Laboratory in Seriate (Bergamo), which has long-standing expertise in the execution of specialized mechanical tests for the railway, naval, and automotive sectors. As a certified RFI testing facility, P&P ensured that all tests were performed with the highest precision and attention to detail, drawing upon years of experience and collaboration with the national railway authority.

In agreement with the P&P technical staff, the following modifications to the standard RFI procedure were therefore implemented to accommodate the experimental requirements and research objectives of this study and to suit the physical constraints of the available specimen.

Figure 71. IRJ specimen

Unlike the RFI procedure — designed for full-scale structures — this study focused on a cut-out section of an insulated rail joint (IRJ) extracted directly from an in-service track. Consequently, the test configuration was proportionally scaled and modified while maintaining the fundamental principles of the four-point bending setup.

The main deviations from the standard procedure are summarized below:

- Specimen length: the RFI standard specifies a full sleeper length of approximately 2600 mm, whereas in this study the specimen measured 1180 mm. This reduced size resulted from the extraction of an IRJ segment directly from the field, isolating the joint area for detailed examination. The total mass of the specimen was approximately 150 kg, allowing safe laboratory handling while preserving the structural integrity of the assembly.

- Support spacing (L_p): in the standard RFI test, the distance between supports is 2400 mm. In the present configuration, this spacing was reduced to 600 mm, corresponding to the average distance between two consecutive sleepers in real track conditions. This adjustment ensured that the end post of the IRJ was positioned exactly at mid-span, with the joint itself behaving as a cantilevered element between two support points, effectively replicating its in-situ boundary conditions.

- Articulated support geometry: the articulated supports used in this study had a radius of 30 mm and a contact width of 100 mm. These values were chosen to maintain the correct curvature and pressure distribution, scaled to the reduced specimen size, while still reproducing the kinematic conditions (free rotation and reaction balance) required by the RFI specification.

- Loading roller spacing (L_r): according to the RFI standard, the two loading rollers are positioned 1200 mm apart (approximately half the support span). In the adapted setup, the inter-roller distance was 150 mm, maintaining the same geometrical ratio between loading and support spans and ensuring a constant bending moment region centered on the joint.

- Load application mode: while the RFI procedure allows for load or displacement control, the present tests were conducted in force-controlled mode, applying a ramp load profile with an increase rate of 2 kN per second. This configuration provided precise control over load increments and avoided any risk of damaging the specimen, in line with the non-destructive testing philosophy of this campaign.

- Measurement setup: instead of a central deflection gauge, the displacement field was monitored by two potentiometric transducers placed 50 mm from the end post on either side of the joint. This layout was specifically designed to measure local vertical displacements of the IRJ under bending, rather than the global deformation of the beam, providing higher sensitivity to variations in bolt preload.

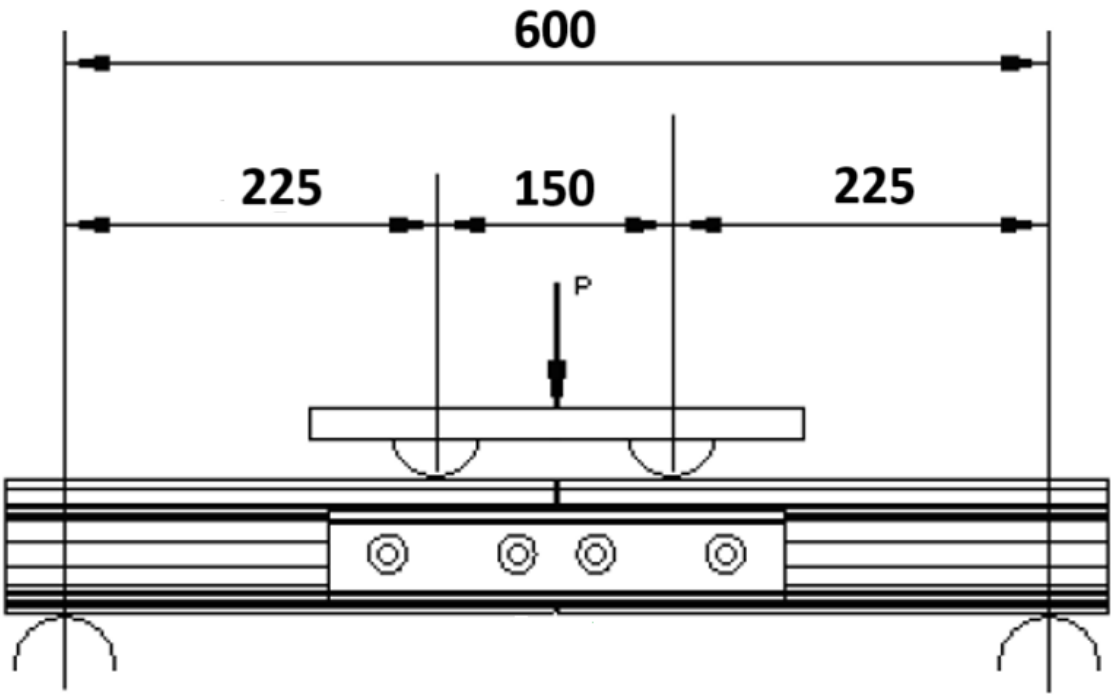

Figure 72. Four-Point bending test scheme on IRJ

5.2 Test preparation

This section outlines the preparation process of the specimen for the four-point bending test and details the configuration of the associated measurement setup.

5.2.1 Description of the available IRJ sample

Figure 73. IRJ specimen details

The IRJ specimen available for this study is of the 60 UNI type, with a total length of 1180 mm and a mass of approximately 150 kg. The assembly includes four bolts with irreversible locking nuts (visible in Figure 73).

Each bolt was originally tightened to a torque of about 960 Nm, corresponding to an axial preload of roughly 200 kN in the bolt shank. This value, not coincidentally, is the same preload used in the Abaqus numerical model to represent the initial bolt tension.

At first glance, the external appearance of the joint may not seem optimal; however, both its structural integrity and mechanical functionality were found to be fully preserved. The joint exhibited no visible structural defects, either in the rail sections or in the fishplates.

At the time the specimen was received, it was neither possible nor necessary to quantify the residual bolt preload, as all bolts appeared well preserved and firmly secured. The only detectable sign of degradation concerned a slight deterioration of the insulating layer and the end post. It is therefore reasonable to assume that the joint was removed from service due to a

loss of electrical insulation between the adjacent rail sections, while its mechanical performance remained entirely intact.

5.2.2 Modifications applied to evaluate preload influence

As discussed in the previous sections, the purpose of these tests — and of the overall study — is to evaluate the influence of bolt preload loss on the mechanical behavior of IRJ. Since the original irreversible locking bolts were not suitable for this type of investigation due to their intrinsic design, modifications to the joint assembly were required.

Figure 74. Original bolt anti-rotation collars and bolts extraction

The original bolts were therefore removed. First, the anti-rotation collars (visible in Figure 74) were cut off, and the bolts were then extracted manually using hammer blows. The original fasteners, with a diameter of 26 mm, were replaced by four M24 bolts. As the holes in both rails and fishplates had a diameter of 32 mm, the resulting radial clearance increased. However, given the static nature of the tests, a difference of 2 mm can be reasonably considered negligible with respect to the test outcome (this would not be the case in a tensile).

The decision to use M24 bolts instead of M27 was motivated by the intention not to reduce the existing clearances, but rather to slightly increase them, avoiding any artificial stiffening of the assembly that could have distorted the experimental results. The rationale behind this approach is clear: it is preferable to test a joint that is slightly more flexible than the original, rather than one that is unrealistically rigid.

Figure 75. Modified IRJ sample

Furthermore, to prevent thread yielding in the M24 bolts, the tightening torque was limited to 800 Nm, according to the manufacturer's specifications, corresponding to an axial preload (P_b) of approximately 170 kN. This value is derived from Equation 7:

$$P_b = \frac{T}{Dk_b} \qquad \text{Eq. 7}$$

where T is the bolt torque (set to 800'000 Nmm), k_b is the bolt torque coefficient (assumed as 0.2), and D is the new bolt diameter (24 mm in this case).

Both the torque and the axial force are slightly lower than those used in the actual joint and in the Abaqus simulations, but this deviation is considered minor and acceptable within the context of the test campaign. Once again, the guiding principle was the same: a slightly more flexible joint is preferable to one that is excessively stiff.

5.2.3 Instrumentation layout and sensor placement

The measurement system was designed to capture the local flexural response of the insulated rail joint (IRJ) under four-point bending. As shown in Figure 76, two linear potentiometric displacement transducers (Celesco Transducer Products, Inc., model PT1MA-2-UP-420R-C25) were installed to record the vertical deflection of the two rail ends.

Figure 76. Linear potentiometric displacement transducers set up

The sensors were positioned 50 mm from the end post on each side of the joint, allowing the relative vertical displacement between the two rail sections to be used as an indirect measure of the joint's flexural stiffness. The data acquisition was performed at a sampling frequency of 5 Hz.

Figure 77. Linear potentiometric displacement transducers

Each potentiometer was securely mounted to the test frame of the hydraulic rig and magnetically attached to the rail surface to ensure stable alignment and repeatable measurements throughout the loading sequence. The applied load was monitored using a load cell (AEP Transducers, model C8S 1MN, capacity 1000 kN) installed on the hydraulic actuator piston, ensuring high accuracy in force control during the test.

Figure 78. Load cell

Environmental conditions were continuously monitored using a mini data logger (Testo 147T) to record the ambient temperature, ensuring consistency in material behavior and sensor performance.

Data acquisition and processing were carried out through a dedicated control and monitoring system (Trio Sistemi e Misure Srl, model RT3), which synchronized load and displacement measurements in real time.

The bolt preload was adjusted using a torque wrench capable of delivering tightening torques between 200 Nm and 1000 Nm, enabling precise control of the preload level for each test configuration.

Figure 79. Torque wrench

All instrumentation was calibrated prior to testing by the P&P Laboratory in Seriate (Bergamo), ensuring traceability and measurement reliability.

5.3 Test procedure

The static bending tests were performed using the hydraulic testing frame shown in Figure 80, a reaction portal designed for both static and dynamic load applications. The test rig is equipped with a hydraulic actuator capable of delivering a maximum load of 500 kN (50 tonnes), with a stroke of 100 mm and a maximum piston velocity of 0.5 m/s. The system ensured precise control of both load amplitude and application rate throughout the test.

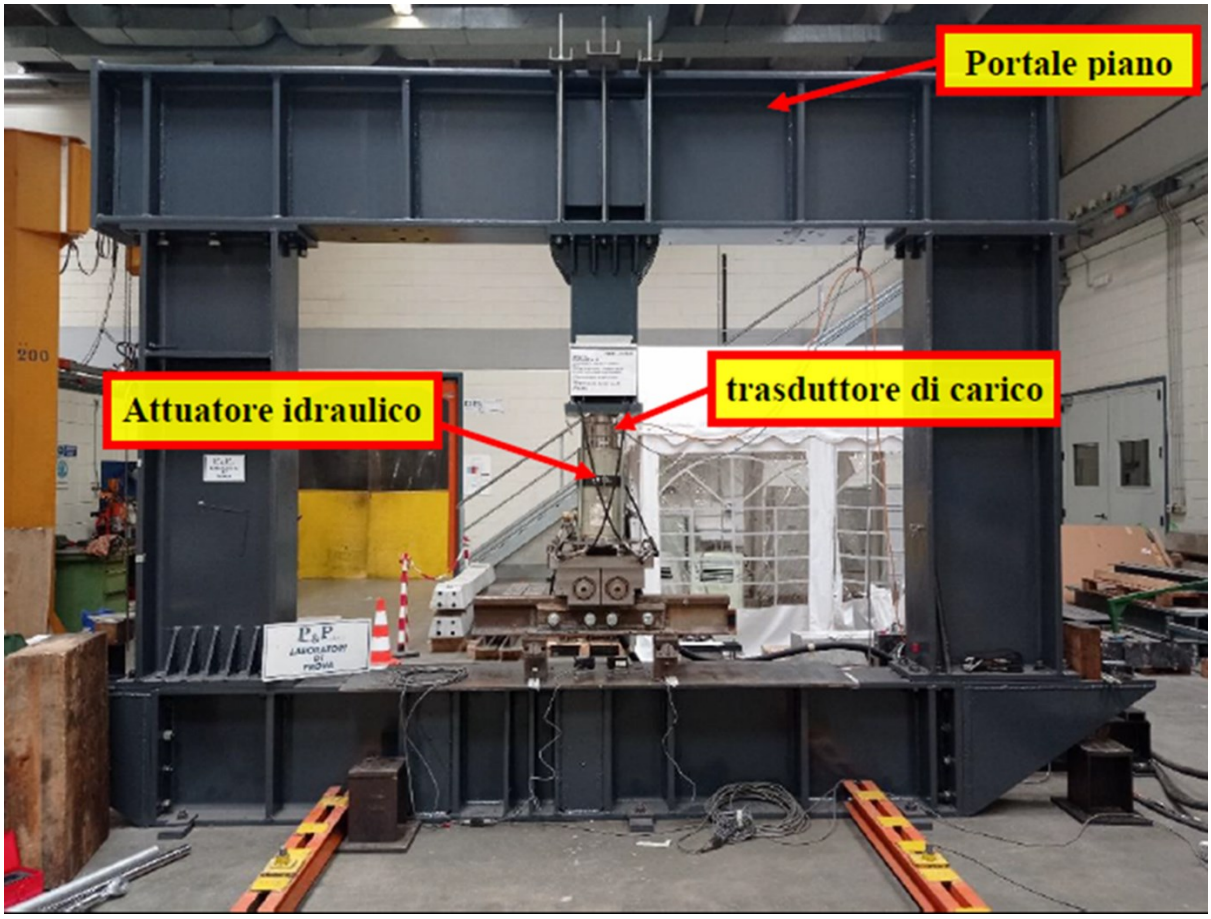

Figure 80. Hydraulic testing frame

The specimen was mounted on two articulated supports, as described in Section 5.1.1. Each support had a bearing width of 100 mm and a contact radius of 30 mm, positioned at a center-to-center distance of 600 mm, reproducing the typical sleeper spacing in track.

The loading unit consisted of two steel rollers, each with a diameter between 80 and 85 mm, spaced 150 mm apart, in accordance with the geometry adopted for the scaled-down test configuration.

Figure 81. Support

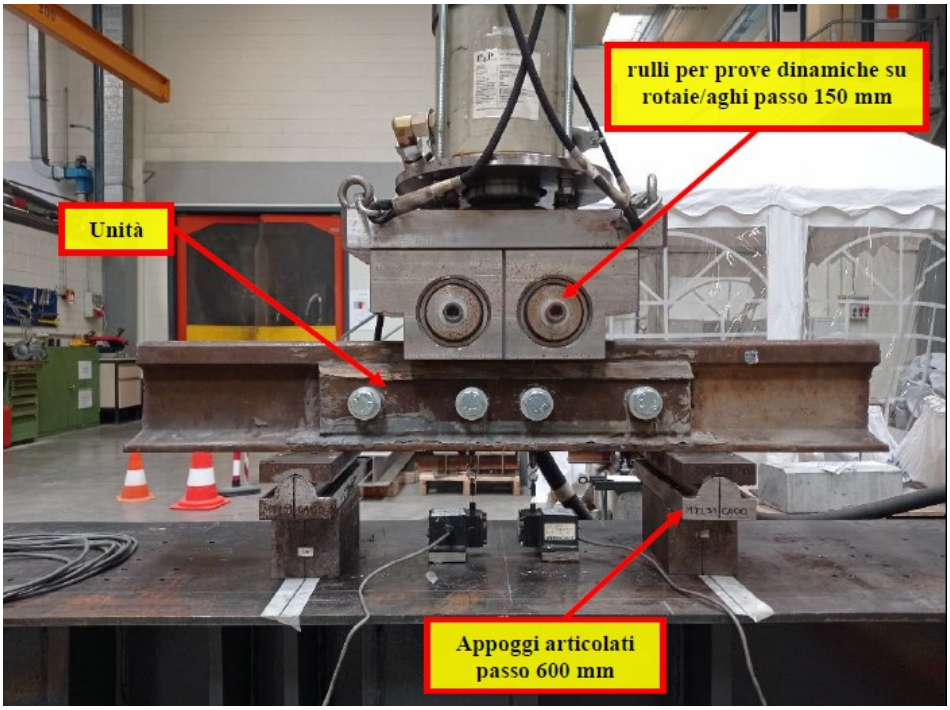

Figure 82. Loading unit

The tests were conducted in force-controlled mode, applying the load through the hydraulic actuator in the form of a progressive ramp profile (2 kN/s). The applied load corresponded to n-times half the weight of a Category D railway axle, in accordance with the EN 15528 classification. Specifically, three load levels were considered, equivalent to 11 tonnes, 22 tonnes, and 30 tonnes, corresponding approximately to 1×, 2×, and 3× the nominal axle half-load.

The bolt preload was independently imposed using a torque wrench, allowing controlled adjustment of the tightening torque for each test series. Comparative tests were performed under progressively decreasing preload conditions, corresponding to 100%, 80%, 60%, 10%, and 0% of the nominal preload value. This procedure enabled the systematic investigation of the influence of bolt preload loss on the flexural stiffness and mechanical response of the insulated rail joint under quasi-static loading.

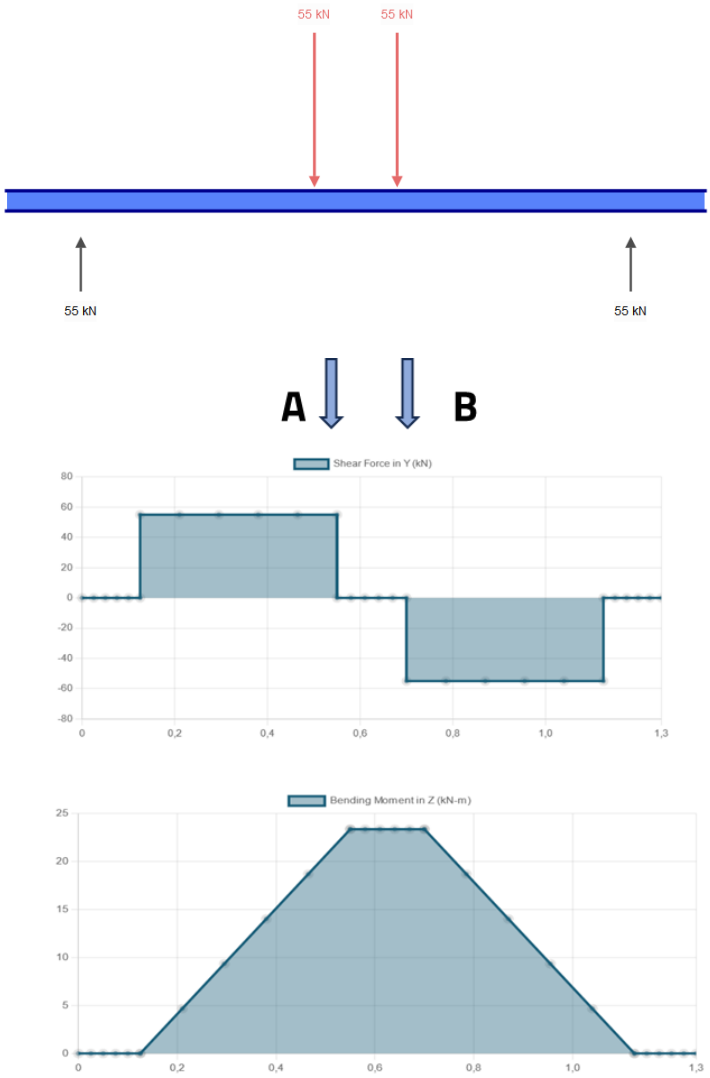

Figure 83. Shear force and bending moment diagrams

5.4 Static tests results

Excluding the preliminary calibration and setup trials, a total of seven tests were carried out under different combinations of bending loads and bolt preload levels.

A summary of all the test configurations is presented in the table below.

TEST NAME	BOLT PRELOAD	LOAD
100 A	100% (800 Nm)	11 Tonnes
80 A	80% (640 Nm)	11 Tonnes
60 A	60% (480 Nm)	11 Tonnes
10 A	10% (80 Nm)	11 Tonnes
100 B	100% (800 Nm)	11 Tonnes
200 B	100% (800 Nm)	22 Tonnes
300 E	0% (0 Nm)	30 Tonnes

Table 7. IRJ static tests

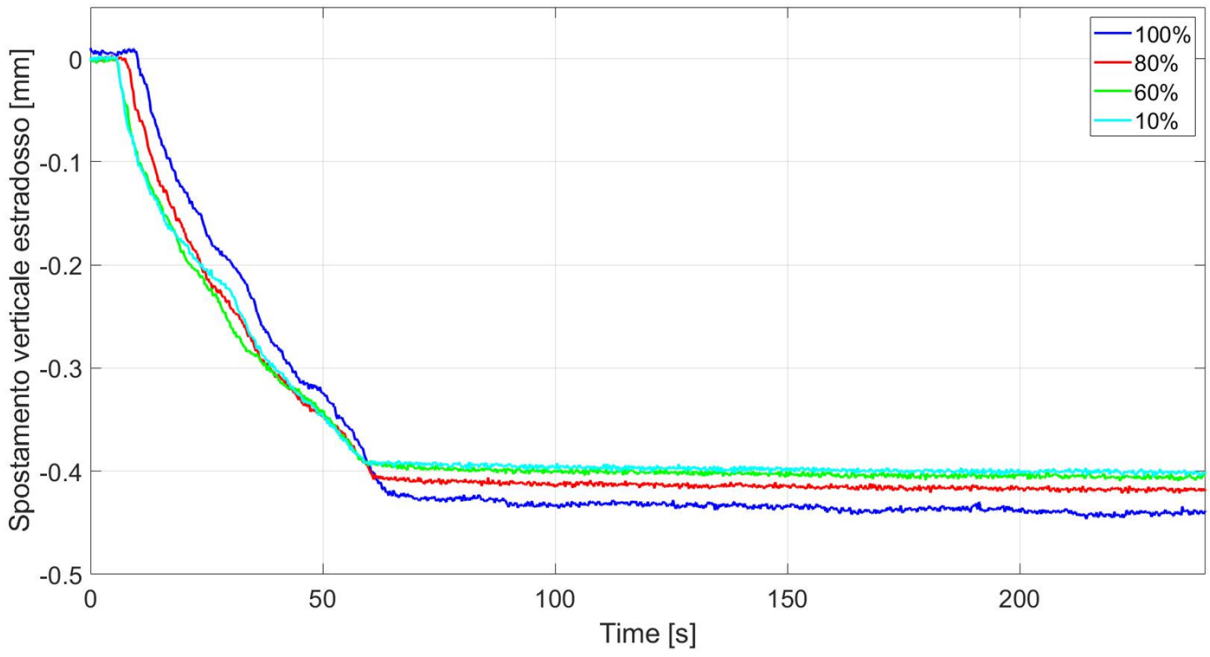

Figure 84. Comparative test between constant-load and variable-preload conditions

The first set of results, shown in Figure 84, compares tests 100A, 80A, 60A, 10A, performed under identical loading conditions—namely, a constant applied load of 11 tonnes—while progressively varying the bolt preload. Between consecutive tests, the desired preload level was adjusted using a torque wrench, after which the measurement instruments were reset to zero and the subsequent test was initiated.

As previously discussed, the main objective of these tests was to measure the vertical deflection at the rail ends using the two potentiometric displacement transducers. The graph in Figure 84 shows the time history of the average displacement recorded by the two sensors.

During the initial transient phase, the applied load of 110 kN was reached in approximately 55 seconds, consistent with the ramp-type load profile (increasing at 2 kN/s). Throughout this stage, the joint exhibited a gradual downward deflection, with a magnitude clearly in the order of tenths of a millimeter.

It should therefore be recalled that, as reported in Section 4.2, the FEM simulations predicted vertical displacements of the order of millimeters. This divergence between numerical and experimental results will be discussed in detail in a dedicated section later in this chapter.

Once the target load was reached and the transient regime completed, the joint response stabilized, and the deflection remained constant over time. The corresponding results are summarized in Table 8.

TEST NAME	BOLT PRELOAD	DEFLECION Δv
100 A	100% (800 Nm)	0.45 mm
80 A	80% (640 Nm)	0.42 mm
60 A	60% (480 Nm)	0.39 mm
10 A	10% (80 Nm)	0.39 mm

Table 8. Table 8. Test 100A, 80A, 60A, 10A summarized

The most interesting observation emerging from the results is that, once steady-state conditions are reached, the vertical deflection decreases as the bolt preload is reduced. Specifically, with 100% preload, the deflection reaches approximately 0.45 mm, whereas with 10% preload, it decreases to 0.39 mm. Although the joint clearly operates within the elastic range, this behavior

is noteworthy: despite being counterintuitive, the joint appears to become stiffer as the preload decreases.

It is also important to note that no appreciable difference is observed between the vertical displacement curves obtained in tests 60A and 10A. This suggests that, below approximately 60% of the nominal preload, the vertical response of the joint is no longer significantly influenced by the bolt tightening force.

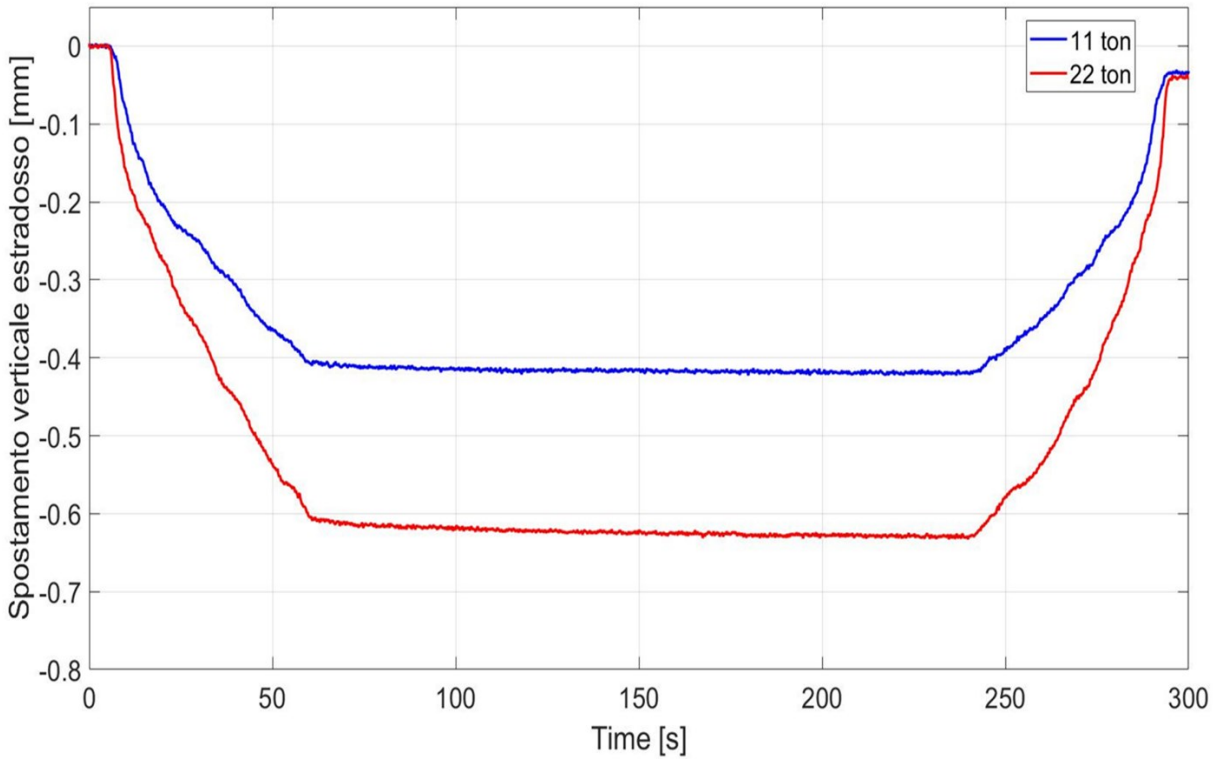

Figure 85. Joint nonlinearity

TEST NAME	BOLT PRELOAD	LOAD	DEFLECION Δ_V
100 B	100% (800 Nm)	11 Tonnes	0.45 mm
200 B	100% (800 Nm)	22 Tonnes	0.62 mm
300 E	0% (0 Nm)	30 Tonnes	0.72 mm

Table 9. Test 100B, 200B and 300E results

Further noteworthy results arise from the comparison between tests 100B and 200B. In this case, the applied load on the joint was varied—increased from 11 tonnes to 22 tonnes, i.e., doubled—while the bolt preload was kept constant at its maximum value of 800 Nm.

The results clearly show that the joint exhibits a nonlinear response to the increase in load: a linear rise in applied load does not produce a proportional increase in vertical displacement. Instead, as the load increases, the incremental deflection becomes progressively smaller, indicating a stiffening behavior of the joint under higher load levels.

Finally, an additional and particularly interesting test (300E) was carried out by completely loosening all the bolts and applying a load of 30 tonnes, nearly three times the maximum service load. Under these extreme conditions, the measured vertical displacement was approximately 0.72 mm. The difference between the two extreme cases — test 100A, with maximum preload and minimum load, and test 300E, with minimum preload and maximum load — is approximately 0.3 mm in vertical displacement.

Naturally, the test configurations listed in Table 7, whose results have been presented in this section, were repeated multiple times to verify the repeatability of the observed trends and to ensure the robustness and reliability of the experimental findings presented in this study.

5.5 Static tests discussion

This section discusses the results obtained from the static tests performed on the insulated rail joint (IRJ).

The most remarkable outcome is the reduction in joint deflection observed as the bolt preload decreases.

At first glance, this behavior appears highly counterintuitive. However, it must be emphasized that the system under investigation is not a conventional bolted connection, but a complex insulated rail joint, characterized by a heterogeneous material composition and a geometrically intricate interface between the rail and the fishplates. Therefore, deviations from the well-established behavior of traditional bolted assemblies are both plausible and physically meaningful.

In a standard bolted joint — such as a typical plate–bolt system — a reduction in bolt preload would normally lead to a clear decrease in the global stiffness of the assembly.

In contrast, the IRJ exhibits the opposite trend, showing an apparent stiffening as the preload is reduced. The explanation for this unconventional behavior lies in the complex redistribution of contact forces within the joint, as shown in Figure 86.

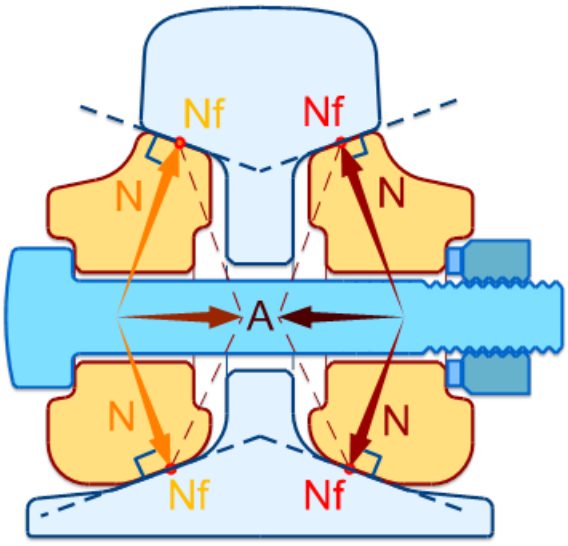

Figure 86. IRJ rail and fishplates contact force scheme

When the bolt preload decreases, the axial compressive forces (A) acting along the bolt axis are reduced in magnitude. Therefore, also as a result of the applied load, the inclination angle of the contact forces (N) between the fishplates and the rail head/foot increases. This geometric modification enhances the local wedging effect of the fishplates between the upper and lower rail surfaces.

Although this effect is subtle, it is sufficient to increase the effective resisting section of the joint under bending loads, leading to a localized stiffening of the IRJ in the vicinity of the connection. The result is a smaller measured deflection as the preload is progressively reduced.

Furthermore, the results reveal that the IRJ exhibits a nonlinear flexural response: as the applied load increases, the incremental deflection progressively decreases. For instance, at maximum preload, the joint deflects 0.45 mm under 11 tonnes, but only 0.62 mm under 22 tonnes—well

below the proportional value expected from linear scaling—and even under zero preload and 30 tonnes, the deflection remains limited to 0.72 mm.

This behavior is consistent with the contact-induced stiffening mechanism discussed earlier. Under higher external loads—and particularly when bolt preload is reduced—the fishplates tend to wedge more firmly between the rail head and foot. This process closes micro-gaps, activates additional bearing areas around the bolt holes, and increases normal and frictional contact forces at the plate–rail interfaces. The result is a redistribution of load paths and an increase in the local bending stiffness of the jointed section.

However, this apparent stiffening is not beneficial for the overall track superstructure. The local increase in rigidity concentrates stresses within the joint region, particularly at stress concentration points such as the bolt holes. These zones are historically known to act as crack initiation sites, where subsurface cracks can propagate at approximately 45°, often hidden beneath the fishplates. Such cracks can eventually reach the rail head, leading to catastrophic failures—including complete rail-head separation and train derailments, as tragically documented in incidents such as the Pioltello accident.

Therefore, while the observed stiffening effect may reduce visible deflection, it simultaneously raises the risk of internal damage accumulation, confirming that preload degradation has complex and potentially dangerous consequences for the long-term structural integrity of insulated rail joints. Bolts not only ensure that the fishplates remain correctly positioned and prevent any relative displacement, but, with high levels of preload, they also avoid localized stiffening of the joint by preventing the wedging effect between the rail head and foot. In this way, the load transmitted by the passing train is more evenly distributed along the joint, reducing stress concentrations and enhancing both the mechanical performance and durability of the assembly.

5.5.1 Comparison with FEM predictions

A critical comparison between the numerical simulations and the static laboratory tests highlights both convergences and divergences in the mechanical behavior of the insulated rail joint.

As expected, the absolute magnitude of the vertical deflections differs significantly between the two approaches. In the FEM track-level model, the joint is part of a larger structural system that

includes the ballast compliance, modelled through an elastic foundation, and the global bending of the rails. Consequently, a large portion of the millimetric deflections predicted by the FEM analysis can be attributed not to the joint itself, but to ballast compression and overall rail flexibility.

In contrast, the laboratory tests were performed on an isolated joint segment, excluding the influence of the ballast and sleepers. Therefore, the recorded displacements, typically in the order of tenths of a millimeter, represent the intrinsic stiffness of the jointed section alone. The discrepancy in absolute values between the two methods thus reflects different boundary conditions rather than an inaccuracy in the numerical model.

Beyond magnitude, the trend divergence between the two approaches is of particular interest. In the FEM simulations, a reduction in bolt preload led to a softer response and increased deflection—consistent with the behavior of a conventional bolted connection. Conversely, in the laboratory tests, a reduction in preload resulted in a stiffer joint response, with smaller deflections under the same load.

This apparent contradiction can be rationalized by considering the complex contact mechanics within IRJ. When preload decreases, the fishplates wedge more tightly between the rail head and foot, closing micro-gaps and activating additional bearing regions around the bolt holes. These local contact transitions effectively increase the resisting section under bending and reduce the measured deflection, despite the global reduction in frictional coupling. The current FEM model, which assumes idealized surface contacts and neglects bolt-hole clearances or plate wedging effects, is unable to capture this contact-mode switching and thus predicts a simpler, monotonic softening behavior.

From a modelling standpoint, the FEM is therefore not incorrect but rather answers a different question—it captures the track-level mechanical response, while the laboratory setup isolates the local joint mechanics. To reconcile the two perspectives and reproduce the experimental trends, future developments of the numerical model should include:

- Refined contact modelling, introducing finite-sliding surface-to-surface interactions with softened normal behavior (pressure–overclosure);
- Explicit bolt–hole clearances and initial micro-gaps to allow contact transitions;
- Inclusion of bolt shank and thread compliance for more realistic load transfer;
- Geometric imperfections, such as plate camber, hole ovality, and end-post misalignment, which can significantly affect the contact regime;

- And finally, a lab-replica FEM model, reproducing the four-point bending fixture and loading scheme, to directly calibrate against the static test curves.

Once calibrated, this refined model can be reintegrated into the full track simulation, enabling the quantification of how much of the total vertical deflection originates from the joint itself versus the ballast and rail system. Such an approach would bridge the gap between local experimental mechanics and global track behavior, enhancing both the predictive capability and the physical realism of the IRJ digital twin.

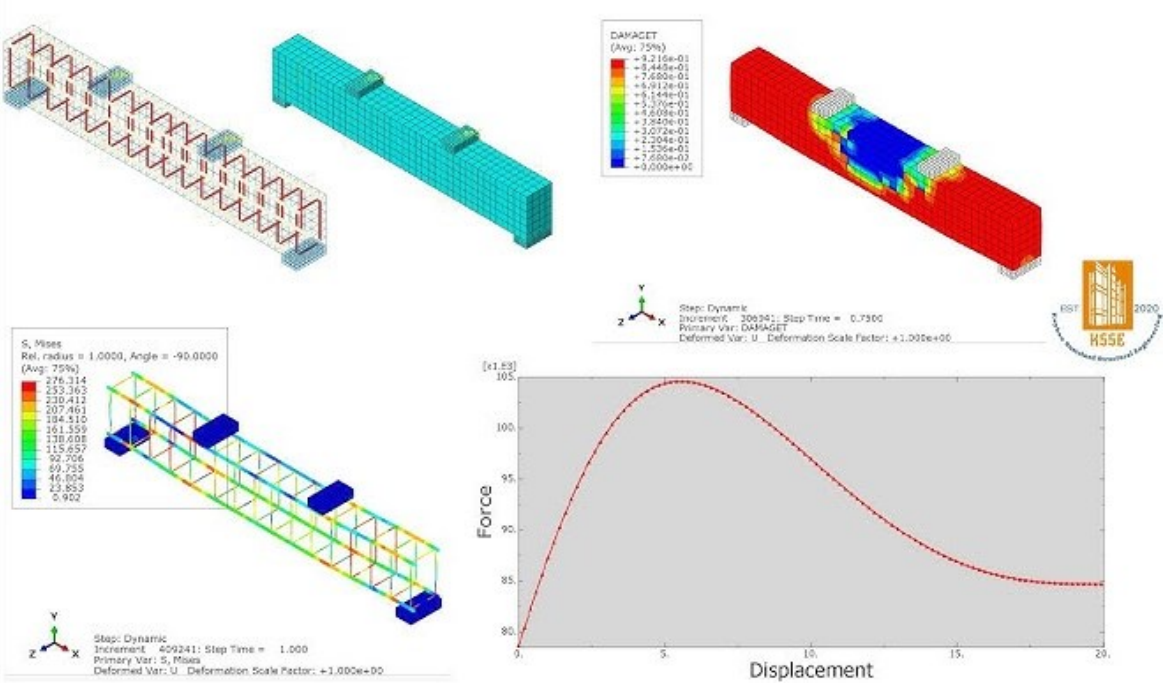

Figure 87. Example of four points bending test FEM model

6 Dynamic tests on IRJ

The Insulated Rail Joint (IRJ) represents one of the most critical discontinuities in the railway track, where complex dynamic interactions among rail sections, bolts, fishplates, and insulating materials can significantly influence the long-term performance and durability of the superstructure. Following the static investigations presented in Chapter 5, a complementary series of dynamic tests was conducted with two main objectives.

The first objective was to validate and confirm the findings of the static campaign, assessing whether the mechanical behaviour observed under quasi-static loading—particularly the influence of bolt preload on joint stiffness—remains consistent when subjected to time-varying and cyclic excitation. The second objective was to develop and assess reliable, repeatable experimental methodologies that could later be transferred to real track environments, supporting in-situ dynamic assessment of IRJs through vibration-based testing procedures.

This research aligns with the broader framework of Structural Health Monitoring (SHM), a field that has gained increasing importance as railway infrastructure continues to age and requires more predictive and cost-effective maintenance strategies. SHM techniques based on vibration analysis are particularly promising, as they provide a global, non-destructive means of evaluating a structure's health state [44]. By monitoring modal parameters—such as natural frequencies, damping ratios, mode shapes, and modal curvatures—it is possible to detect changes in the mechanical properties of the system, including variations in stiffness, mass, or energy dissipation.

In this context, Experimental Modal Analysis (EMA) was applied to IRJ specimens in the laboratory to determine how their modal properties evolve with bolt preload variation. This allowed for a deeper understanding of the joint's intrinsic dynamic stiffness and damping characteristics, and for the cross-validation of static test results. The outcomes of these analyses provide key input for improving the numerical model, enhancing its ability to predict both static and dynamic behaviour.

Looking ahead, the same experimental approach can be extended to the field through Operational Modal Analysis (OMA). Assuming that the ambient excitation produced by train passages can be modelled as a broadband stochastic input, OMA allows modal parameters to

be estimated from output-only measurements. Once identified, these parameters can be processed using data-driven techniques—such as Frequency Domain Decomposition (FDD) or machine learning algorithms—to distinguish environmental effects (temperature, humidity, traffic) from actual structural degradation.

The chapter is structured as follows: Section 6.1 outlines the modal analysis fundamentals; Section 6.2 describes the test preparation (set up and instrumentation); Sections 6.3 presents the modal parameter extraction; Sections 6.4 presents the modal testing campaign results; finally, Section 6.5 discusses the main findings and compares them with static tests results.

6.1 Modal analysis fundamentals

The dynamic behaviour of a mechanical system can be characterized by studying its response to harmonic excitation. The fundamental principle of modal analysis is that every structure can be represented as a combination of individual vibration modes, each defined by a natural frequency, a damping ratio, and a mode shape.

The starting point is the equation of motion for a multiple-degree-of-freedom system:

$$M\,\ddot{x}(t) + C\,\dot{x}(t) + K\,x(t) = F(t) \qquad \text{Eq. 8}$$

where M, C, and K are respectively the mass, damping, and stiffness matrices, x(t) is the vector of displacements, and F(t) is the external forcing vector.

Assuming a harmonic excitation of frequency ω, i.e. $F(t) = F_0\, e^{j\omega t}$, and a steady-state harmonic response $x(t) = X\, e^{j\omega t}$, the system can be rewritten in the frequency domain as:

$$(-\omega^2 M + j\omega C + K)\,X = F \qquad \text{Eq. 9}$$

The ratio between the response X and the applied force F defines the Frequency Response Function (FRF), which can be expressed as:

$$H(\omega) = \frac{X(\omega)}{F(\omega)} = \frac{1}{(-\omega^2 M + j\omega C + K)} \quad \text{Eq. 10}$$

This complex transfer function describes how each point of the structure responds to excitation over a range of frequencies. In experimental modal analysis, the FRF is estimated by measuring input forces and output accelerations (or velocities/displacements), generally in the form:

$$H(\omega) = \frac{Y(\omega)}{X(\omega)} \quad \text{Eq. 11}$$

where $Y(\omega)$ and $X(\omega)$ are the Fourier transforms of the output and input signals, respectively.

To reduce the influence of noise and ensure statistical accuracy, two estimators of the FRF can be used, depending on the measurement conditions:

- H_1 estimator: $H_1(\omega) = G_{xy}(\omega) / G_{xx}(\omega)$, where G_{xy} is the cross-power spectrum between output and input, and G_{xx} is the auto-power spectrum of the input. This estimator minimizes output noise and is most suitable for excitation-controlled tests.
- H_2 estimator: $H_2(\omega) = G_{yy}(\omega) / G_{xy}(\omega)$, which minimizes input noise and is preferable when force measurements are less reliable.

Once the FRF is obtained, peaks in the amplitude spectrum correspond to the natural frequencies of the structure, while the phase variation near resonance allows the estimation of the damping ratio. The mode shapes are then reconstructed from the relative responses of multiple measurement points, forming a complete modal representation of the system.

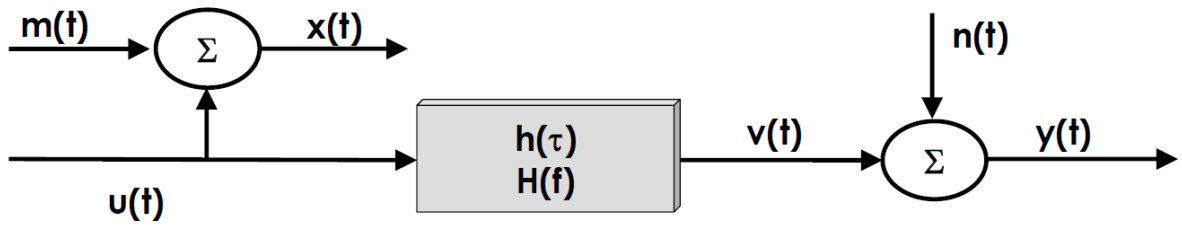

Figure 88. Model with input and output noise

In the context of this study, modal analysis proved to be an effective and complementary approach to validate and interpret the results obtained from static bending tests. While static testing provides a direct evaluation of the IRJ's global stiffness under quasi-static loading conditions, modal testing allows for the assessment of the same mechanical characteristics through the system's dynamic response.

Since the natural frequency ω_n of a system is proportional to the square root of the stiffness (k)-to-mass (m) ratio,

$$\omega_n \propto \sqrt{\frac{k}{m}} \qquad \text{Eq. 12}$$

an increase in natural frequency indicates a stiffer system, whereas a frequency decrease reflects loss of stiffness or increased compliance (with $\omega_n = 2\pi f_n$).

Therefore, the natural frequencies of a structure are intrinsically linked to its stiffness and mass distribution, any variation in the joint rigidity—such as that induced by changes in bolt preload or localized contact conditions—can be detected as a measurable shift in resonance frequency or damping ratio.

This makes modal analysis particularly valuable for cross-verifying static findings: if both approaches indicate consistent trends in stiffness variation, the reliability of the observed behaviour is reinforced; conversely, discrepancies between static and dynamic outcomes can reveal non-linearities, localized effects, or unmodelled contact phenomena that static testing alone may not capture. Furthermore, modal testing provides the additional advantage of being repeatable, non-destructive, and potentially applicable in the field, making it a promising diagnostic tool for future monitoring and maintenance of in-service IRJs.

6.2 Dynamic tests set up

6.2.1 IRJ installation

The modal analysis was performed on the same 60 UNI insulated rail joint previously tested under static and dynamic bending conditions. Before testing, the specimen was carefully

inspected to verify the integrity of the fishplates, bolts, insulating layer, and adhesive bond, ensuring that no structural defects or visible damage were present. All bolts were retightened using a calibrated torque wrench, reproducing the same preload conditions applied during the static campaign, so that differences in the response could be attributed exclusively to the testing method.

Figure 89. IRJ suspended from a pulley

In order to reproduce free–free boundary conditions and allow unrestricted vibration of the jointed rail segment, the specimen was suspended from a pulley using an overhead crane lifting rope, as shown in Figure 89: this configuration enabled the joint to vibrate freely when excited either by an impact hammer or an electrodynamic shaker, minimizing any artificial constraints that could alter its natural frequencies.

To prevent excessive rigid-body motion during excitation, a set of elastic cords was attached between the rail and the test frame columns, providing mild lateral stabilization without significantly affecting the dynamic characteristics of the system.

6.2.2 Accelerometer-based test layout

In the first configuration, the vibrational response of IRJ was measured using six single-axis piezoelectric accelerometers (PCB 393B31, Full-scale 4.9 [m/s^2], Bandwidth 0.1-200 [Hz]), arranged as in Figure 90. This layout ensured adequate spatial coverage of the jointed region and enabled the accurate reconstruction of mode shapes and local stiffness variations.

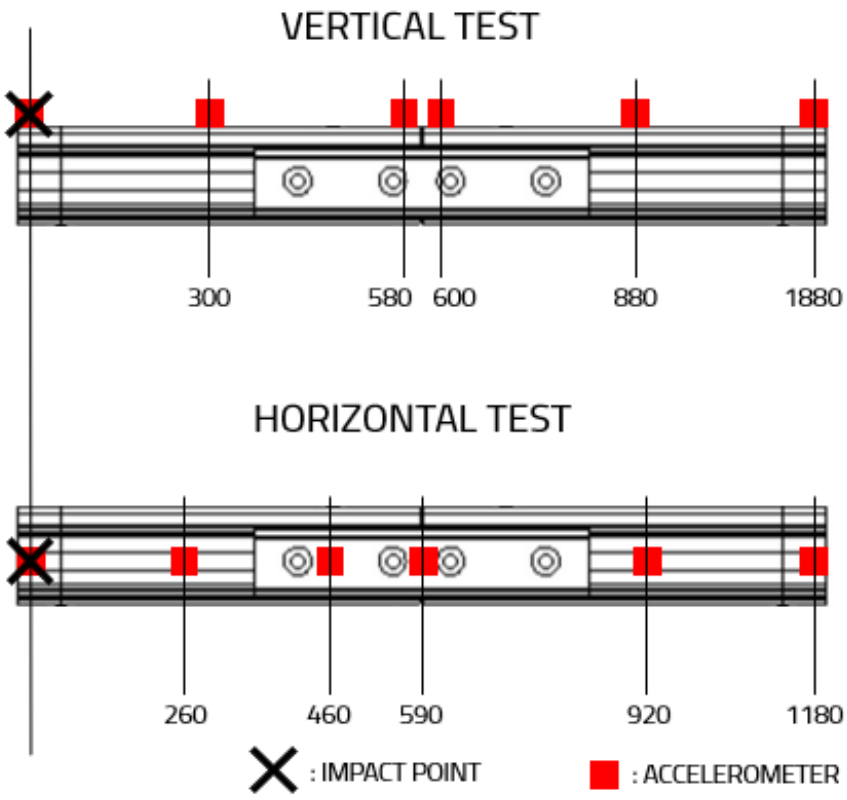

Figure 90. Layout of accelerometers

The accelerometers were mounted on the metallic surfaces using wax, providing reliable coupling without surface damage. The sensors were connected to a multi-channel data acquisition system, which collected data at a sampling frequency of 5125 [Hz].

The excitation was provided by an instrumented impact hammer (PCB 086C03), as seen in Figure 91). The force and acceleration signals were synchronized through the data acquisition system, and the Frequency Response Functions (FRFs) were calculated using H_1 estimators, which minimize output noise and are suitable for excitation-controlled testing.

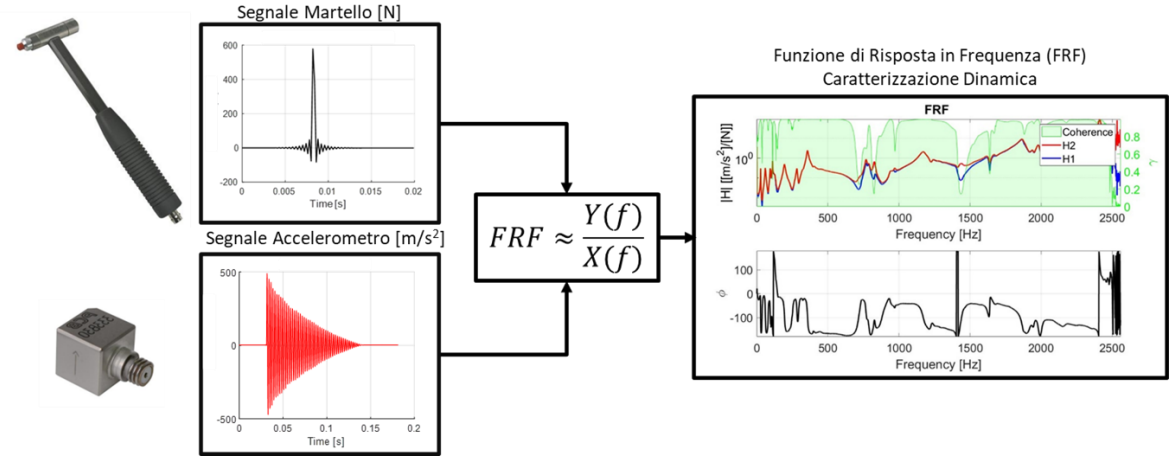

Figure 91. FRFs calculation through input and output signals

In the accelerometer-based modal testing campaign, the excitation forces were applied using an instrumented impact hammer in two orthogonal directions: vertically and horizontally, as illustrated in Figure 91. The vertical impacts were intended to reproduce the predominant bending excitation induced by the wheel–rail contact loads, while the horizontal impacts (applied parallel to the bolt axis) were performed to investigate the joint's in-plane dynamic response.

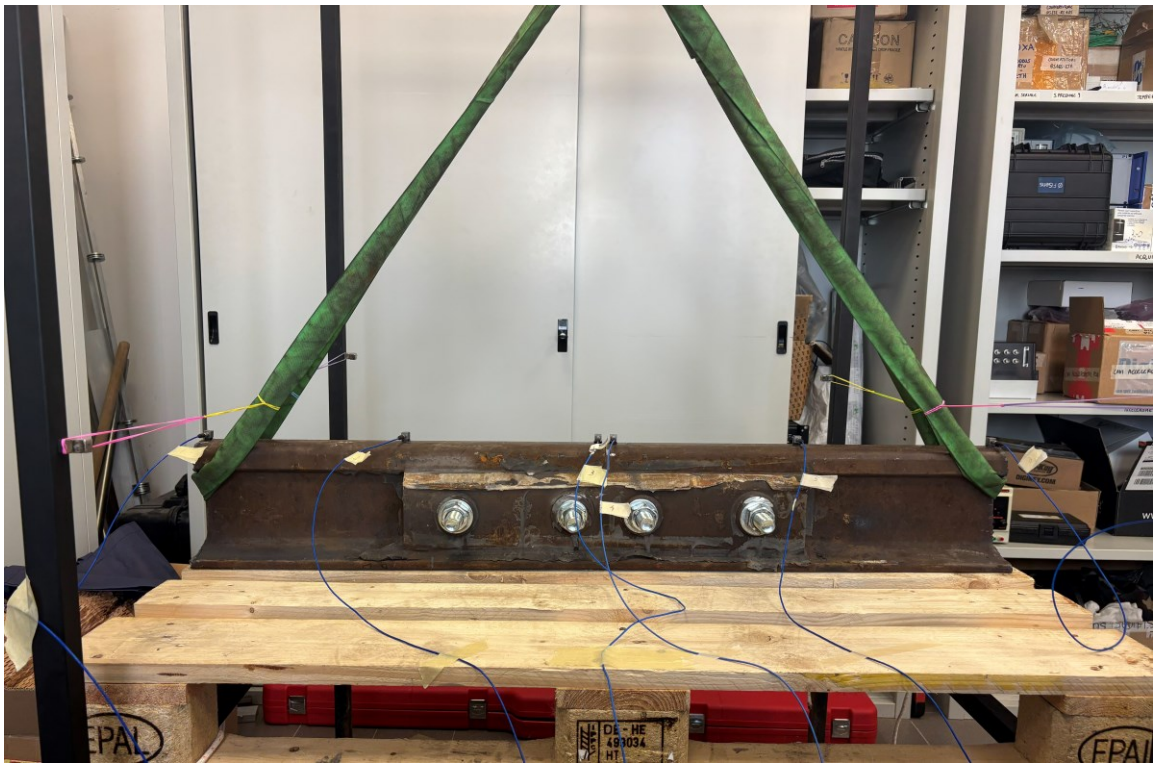

Figure 92. Vertical test set up

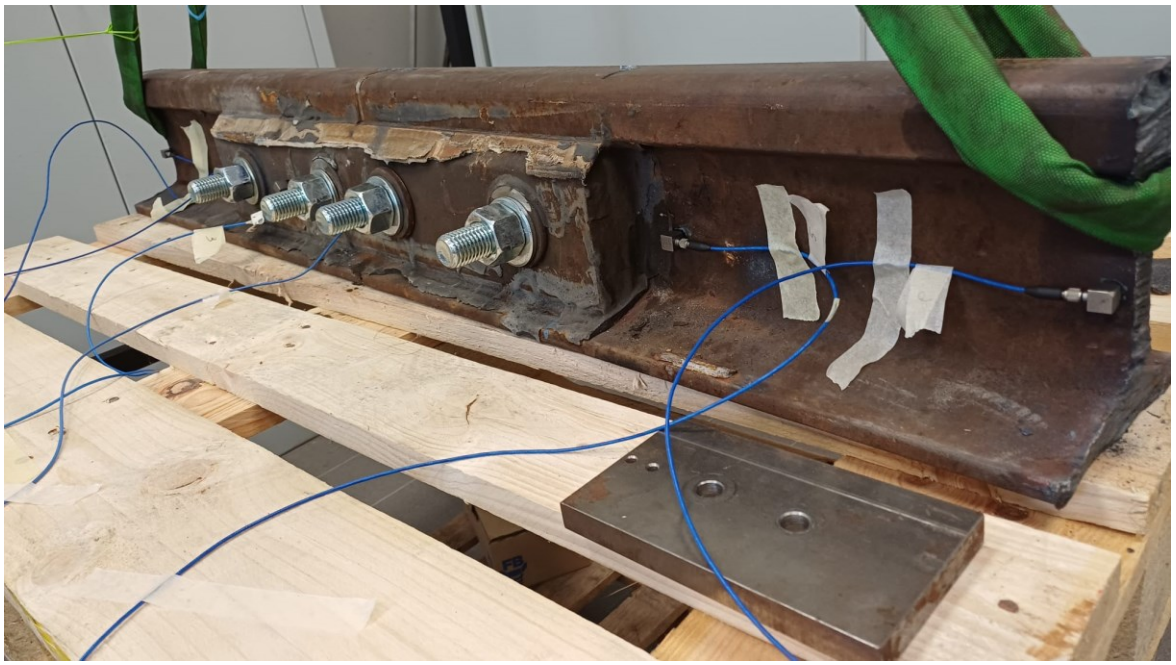

Figure 93. Horizontal test set up

This dual-excitation approach was motivated by the characteristic conical geometry of the railway wheel tread, which induces both vertical and lateral load components on the rail during wheel passage. Consequently, assessing joint stiffness and modal response in both directions provides a more comprehensive understanding of its dynamic behaviour under realistic service conditions.

Moreover, the horizontal excitation tests were particularly valuable, as they offered the opportunity to explore a less investigated stiffness component of insulated rail joints—one potentially sensitive to bolt preload and to the complex interaction between the rail web, the fishplates, and the insulating layers. The results obtained under varying preload levels may thus reveal new insights into the coupled bending–shear dynamics of the joint and its potential degradation mechanisms.

6.2.3 LiDAR-based test layout

In the second experimental configuration, the vibrational response of the insulated rail joint was measured using an optical, non-contact acquisition system based on the Ommatidia Q2 LiDAR sensor, shown in Figure 94. This instrument employs laser interferometry to perform high-

resolution, full-field vibration measurements, allowing the reconstruction of surface displacement fields without the need for physical contact or sensor mounting.

Figure 94. LiDAR Q2

Figure 95. LiDAR-based test layout

The LiDAR Q2 system used in this study provides sub-millimetric accuracy and was operated at a sampling frequency of 6000 Hz, selected to ensure reliable detection of all relevant resonance frequencies of the jointed section. This sampling rate exceeds more than twice the highest modal frequency observed in the campaign (approximately 2300 Hz), thereby satisfying the Nyquist criterion and preventing aliasing in the acquired vibration data. Its optical head was positioned approximately 2.5 m from the rail surface, aligned with the longitudinal axis of the joint, and oriented to scan a region covering both fishplates and the central insulated section.

Figure 96. IRJ region scanned by LiDAR

The Q2 LiDAR operates on a fundamentally different principle compared to traditional piezoelectric accelerometers: while accelerometers measure single-point acceleration responses at discrete locations (requiring physical coupling to the structure), the Q2 employs laser-based multi-point vibrometry and full-field metrology. Specifically, Q2 is capable of scanning at up to 25,600 points per second and capturing real-time vibration data across 65 simultaneous channels, as seen in Figure 96.

Each laser beam acts effectively like a contactless sensor, detecting surface displacement or velocity by means of Doppler or interferometric optical measurement, thereby avoiding the

mass-loading and mounting issues associated with accelerometers. The result is a high spatial resolution vibration map of the specimen—in this case the IRJ—covering not just locally at fishplates or bolts, but across rail head, web and foot. Furthermore, the system's optical nature allows for non-contact measurement, enabling rapid set-up and minimal intrusion on the structural behaviour.

Accelerometers offer several advantages, including simplicity, low cost, and well-established signal processing procedures, and they do not require special set-up conditions to obtain accurate results. In contrast, LiDAR-based measurements demand careful preparation of both the setup and the specimen, as the optical sensor must operate under optimal conditions to ensure accurate detection of surface displacements and reliable signal quality.

To maximize the quality of the Ommatidia Q2 LiDAR measurements, the IRJ specimen was surface prepared to improve the optical return from the scanned points. The Q2 provides, in addition to displacement/velocity signals, a reflectivity map of the scanned surface; low reflectivity leads to poor signal-to-noise ratio, intermittent dropouts, and unreliable tracking of point motion—especially on rusted steel and dark, non-uniform surfaces typical of in-service rails and fishplates.

Accordingly, the rail and fishplate surfaces within the scanning field were first cleaned to bare metal by lightly removing oxide with a handheld grinder, taking care not to alter geometry or contact interfaces.

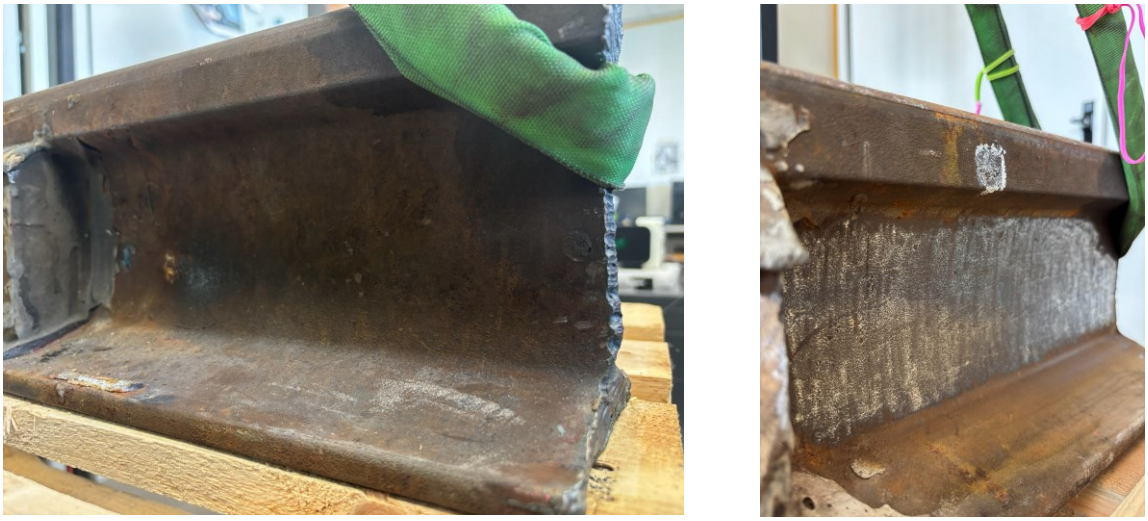

Figure 97. IRJ surfaces' cleaning

The prepared areas were then coated with a thin, removable matte white paint formulated for optical metrology. The matte finish was chosen to increase diffuse reflectance and reduce specular glare, ensuring a stable optical return over the full scan and minimizing measurement bias due to viewing angle. The coating was applied as a uniform, minimal-thickness layer to avoid any appreciable change in mass or stiffness and was kept away from functional interfaces (bolt seats, end-post contact zones) to avoid affecting mechanical behavior.

Figure 98. Painted IRJ

After preparation, a quick verification using Q2's reflectivity map confirmed a homogeneous, high-albedo field, enabling robust tracking of the 65 measurement points defined along the rail head, web, foot, and fishplates.

By combining the two approaches—traditional accelerometry and multi-channel LiDAR scanning—the study leverages the accuracy and temporal fidelity of accelerometers with the spatial completeness and non-invasiveness of the Q2 system. This dual approach enhances the

reliability of modal parameter extraction and supports a more detailed analysis of stiffness variations due to bolt preload loss.

6.3 Modal parameters extraction

In the present study, two distinct excitation strategies were employed to obtain the input signal for modal parameter extraction.

The first, used in accelerometer-based test layout, consisted of controlled impacts applied using the instrumented hammer (PCB 086C03), which allowed direct measurement of the input force and thus enabled the computation of Frequency Response Functions (FRFs) in the classical Experimental Modal Analysis (EMA) framework.

The second approach, used in LiDAR-based test layout, involved random, unmeasured excitations applied manually with a non-instrumented hammer (same load application point of instrumented hammer), effectively generating a broadband "white noise" excitation. This configuration, analogous to Operational Modal Analysis (OMA) conditions, allowed the evaluation of modal parameters through the system's output response only, using statistical techniques such as Frequency Domain Decomposition (FDD).

The extraction of modal parameters (natural frequencies, damping ratios, and mode shapes) allows the dynamic response of IRJ to be quantified in terms of its stiffness characteristics and potential local compliance.

Therefore, in this work, two complementary approaches were adopted:

- Experimental Modal Analysis (EMA) using accelerometer measurements with an instrumented impact hammer
- Operational Modal Analysis (OMA) using LiDAR data acquired under random excitation.

Although both techniques ultimately yield the same set of modal parameters, their underlying assumptions, data processing pipelines, and achievable spatial resolution differ significantly. A combined use of EMA and OMA enhances reliability, enables cross-validation, and provides richer physical insight into preload-dependent dynamic behaviour.

6.3.1 EMA using accelerometers and instrumented impact hammer

In the accelerometer-based campaign, modal parameters were extracted from the measured Frequency Response Functions (FRFs) between the input force provided by an instrumented impact hammer and the structural acceleration response recorded at multiple points along the joint. Under known excitation, the FRF can be computed as:

$$H(\omega) = \frac{Gxy(\omega)}{Gxx(\omega)} \qquad \text{Eq. 13}$$

where $G_{xy}(\omega)$ is the cross-spectrum between input force and output acceleration, and $G_{xx}(\omega)$ is the input autospectrum.

In this work, the H1 estimator was adopted, as it minimizes the influence of output noise and is widely recommended in hammer-based modal testing.

After computing the FRFs, modal parameters were identified using traditional peak-picking (PP) techniques. For lightly damped structures such as rails, resonance peaks are well-defined in both magnitude and phase, making PP an efficient and robust method. Natural frequencies are associated with the maxima of the magnitude of |H(ω)|, whereas damping ratios can be estimated using the half-power bandwidth method:

$$\zeta = \frac{\omega 2 - \omega 1}{2\omega_n} \qquad \text{Eq. 14}$$

where ω_1 and ω_2 are frequencies at −3 dB amplitude relative to the resonance peak at ω_n.

Mode shapes were assembled by stacking the complex FRF values corresponding to each sensor location at each identified resonance. Although the peak-picking approach is well suited for lightly damped metallic components and provided reliable estimates of the natural frequencies under varying bolt preload conditions, the use of only six accelerometers inherently limits the spatial resolution of the reconstructed mode shapes. With such a sparse sensor layout, only the global deformation pattern of the joint can be inferred, while localized effects—such as stiffness

variations around bolt holes, fishplate interfaces, or insulating layers—may not be adequately captured. For this reason, the accelerometer-based EMA was complemented by a LiDAR-based operational modal analysis, which enables dense spatial sampling over the jointed region and thus supports a more detailed and accurate identification of mode shapes and preload-dependent stiffness variations.

6.3.2 OMA using LiDAR and random excitation

In the LiDAR-based tests, no measurable input force was available, as the excitation was provided manually through non-instrumented tapping of the joint, producing a broadband (approximately white) random input. Under this assumption, modal extraction was performed using Frequency Domain Decomposition (FDD), a well-established operational modal analysis technique [45].

First, the output response matrix was converted into the Power Spectral Density (PSD) matrix, $G_{xx}(\omega)$. Applying the Singular Value Decomposition (SVD) yields:

$$\mathrm{Gxx}(\omega) = U(\omega)S(\omega)U(\omega)^{H} \qquad \text{Eq. 15}$$

where S(ω) is a diagonal matrix containing the singular values, U(ω) contains the corresponding singular vectors. Modal peaks appear as clear maxima in the first singular value $S_1(\omega)$, while the mode shape at a given natural frequency is given by the associated column of U(ω). Natural frequencies and damping ratios were extracted via peak-picking on the singular value plots.

The results obtained during the described test campaign and their processing are presented in the following section.

6.4 Modal testing campaign results

This section presents the dynamic characterization results obtained from the two experimental modal analysis approaches applied to the insulated rail joint.

First, Section 6.4.1 reports the outcomes of the Experimental Modal Analysis (EMA) conducted with accelerometers and an instrumented impact hammer, providing FRFs and highlighting the variation in resonance frequencies — and thus in the joint stiffness — associated with different bolt preload conditions.

Subsequently, Section 6.4.2 discusses the results of the Operational Modal Analysis (OMA) performed using the LiDAR Q2 system under random excitation, allowing high-resolution reconstruction of mode shapes. Together, these complementary datasets form a comprehensive basis for evaluating the influence of bolt preload on the dynamic behavior of insulated rail joints.

6.4.1 EMA results

The results obtained from the EMA approach are presented in the following section. As previously described, two excitation directions were investigated:

- vertical
- horizontal (parallel to the bolt axis)

For each excitation type, a comparative analysis was carried out between two preload conditions:

- zero preload (0%, 0 Nm)
- residual preload of 50% (400 Nm)

Each test was repeated multiple times, with preload being adjusted between measurements, to ensure result repeatability and strengthen the reliability of the observed trends.

The results of the vertically exciting EMA tests are presented in Figure 99 and summarized in Table 10. The Frequency Response Functions (FRFs) obtained under zero preload (blue curve) and 50% residual preload (red curve) were superimposed to enable direct comparison. With a sampling frequency of 5125 Hz, four distinct resonance peaks can be clearly identified below 2500 Hz, each associated with a natural frequency of the system.

A consistent trend emerges: the blue curve (no preload) is shifted toward higher frequencies compared with the red curve (50% preload). This behavior confirms the findings from the static bending tests—the joint exhibits a stiffer response when bolt preload is reduced.

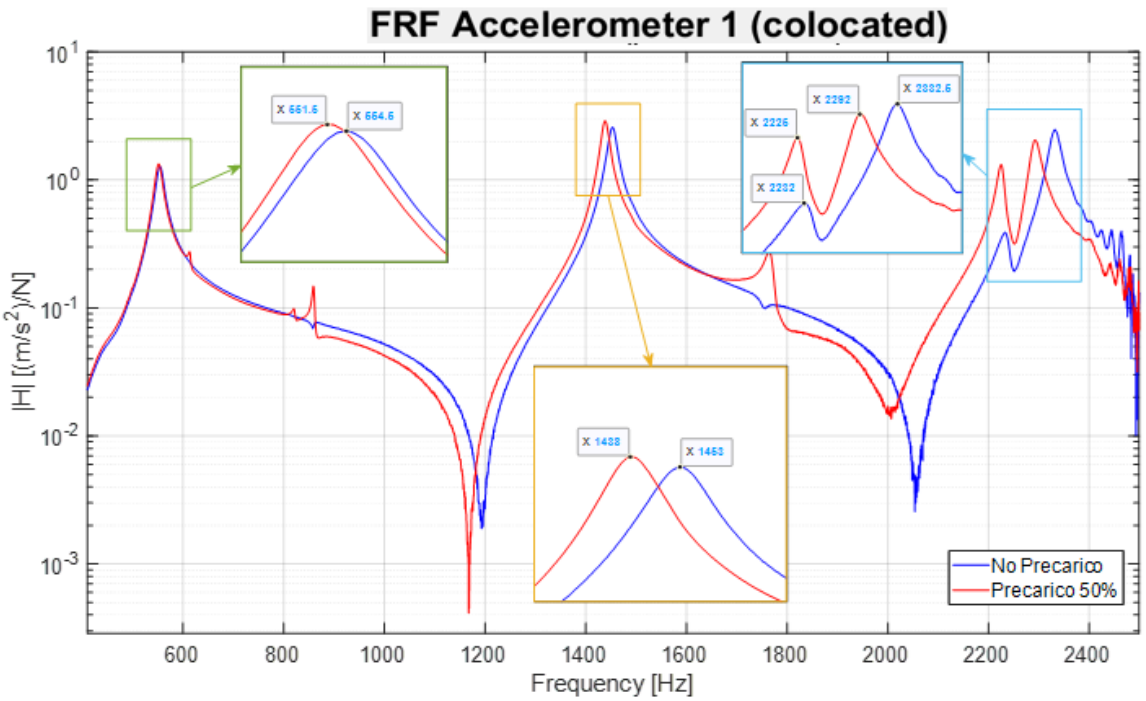

Figure 99. Vertical tests FRFs

Table 10 quantitatively reports the corresponding resonance frequencies for the two preload conditions, further supporting this observation.

NATURAL FREQUENCES	NO PRELOAD	50 % PRELOAD
f_1 [Hz]	554.5	551.5
f_2 [Hz]	1453	1438
f_3 [Hz]	2232	2225
f_4 [Hz]	2332.5	2292

Table 10. Resonance frequences in vertical tests

The results of the EMA tests with horizontal excitation are displayed in Figure 100 and summarized in Table 11. As before, the FRFs corresponding to zero preload (blue curve) and 50% residual preload (red curve) were superimposed for comparison. Five dominant resonance peaks are clearly identifiable below 2500 Hz.

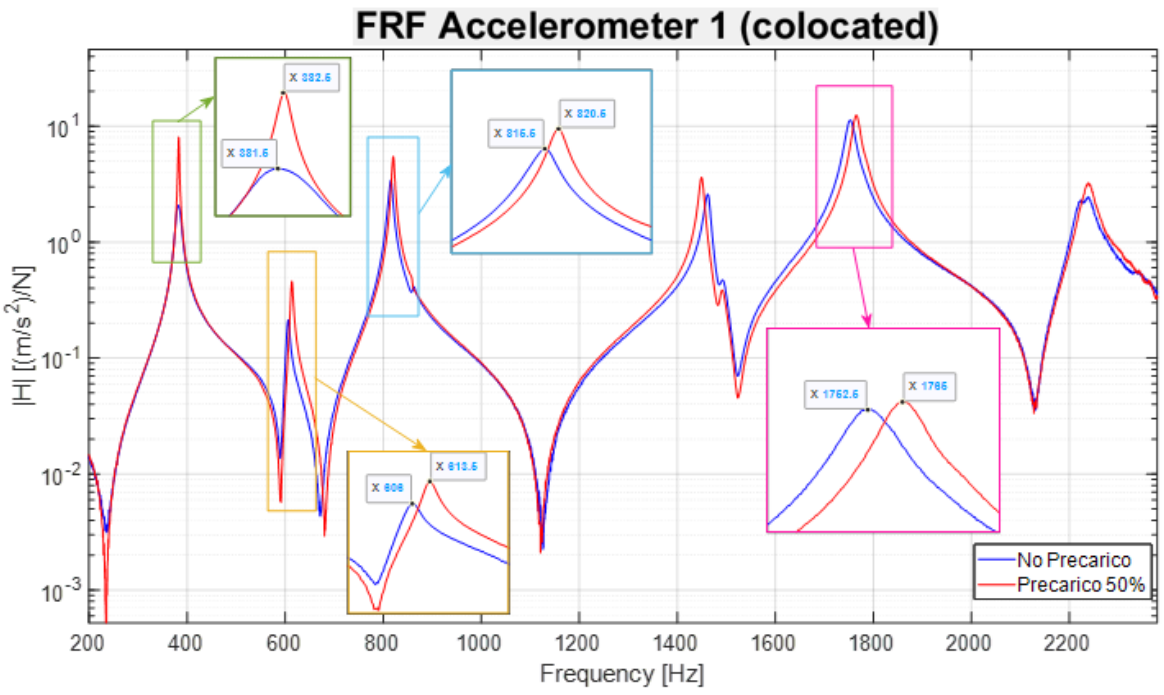

Figure 100. Horizontal tests FRFs

NATURAL FREQUENCES	NO PRELOAD	50 % PRELOAD
f_1 [Hz]	381.5	382.5
f_2 [Hz]	605	613.5
f_3 [Hz]	815.5	820.5
f_4 [Hz]	1462.5	1449
f_5 [Hz]	1753	1765

Table 11. Resonance frequences in horizontal tests

In this case, an opposite trend with respect to the vertical excitation tests is observed: the red curve is consistently shifted toward higher frequencies compared with the blue one. This behavior indicates that the joint exhibits a higher lateral stiffness when the bolts are properly pretensioned. The reason is physically reasonable: bolt preload enhances frictional contact and the lateral constraint provided by the fishplates, increasing the in-plane stiffness of the jointed region. Conversely, when preload is removed, clearances at the bolt holes become active and

sliding phenomena become more pronounced, resulting in lower resonance frequencies and thus reduced horizontal stiffness.

An additional and non-negligible effect—particularly noticeable at the first resonance peak—is the variation in damping due to preload. With higher bolt tension, the stronger frictional coupling and the reduced presence of micro-slips at interfaces lead to lower energy dissipation and, consequently, sharper resonance peaks. When the preload is lost, intermittent contact and increased frictional sliding introduce additional damping, broadening the peaks and reducing their amplitude. This observation highlights that bolt preload influences not only stiffness, but also the damping characteristics of the insulated joint.

6.4.2 OMA results

The results obtained through the OMA approach are presented in this section. In this case, only horizontal excitation was applied, and the modal parameters were compared between three preload conditions: zero preload (0%, 0 Nm), 25% and 50% residual preload (200 and 400 Nm).

The results of the Operational Modal Analysis performed with the LiDAR-based setup are presented in Figures 101–104.

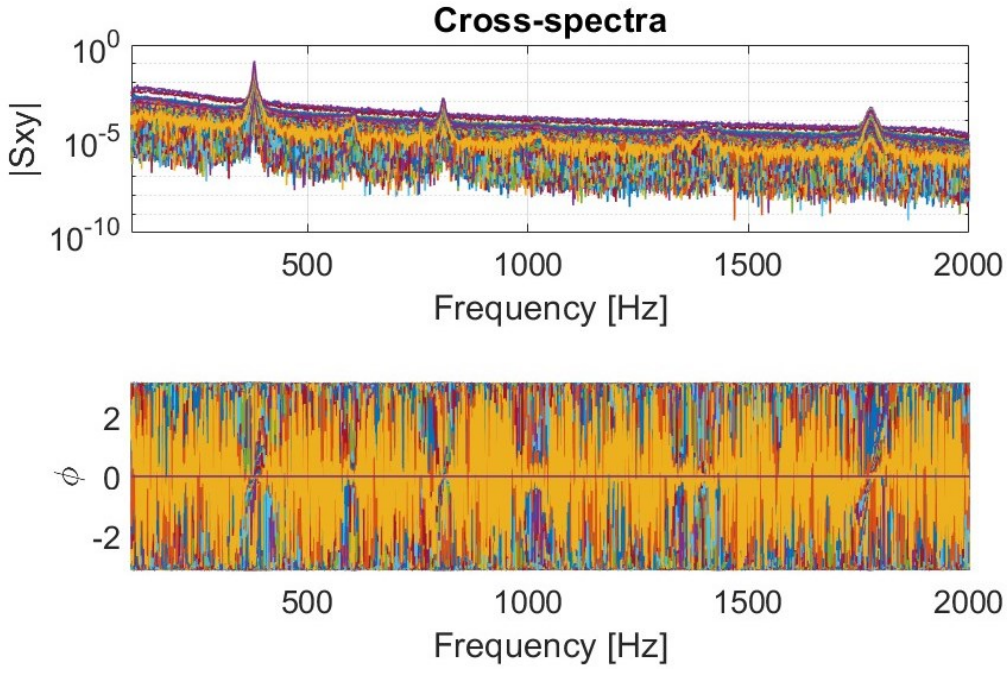

Figure 101. 65 measure points cross spectra matrix

Figure 101 shows the cross-spectra matrix obtained from the 65 scanned points. Clear amplitude peaks emerge around the resonance frequencies of the jointed section, confirming the presence of multiple well-defined vibration modes. These cross-spectra were subsequently processed using the Frequency Domain Decomposition algorithm.

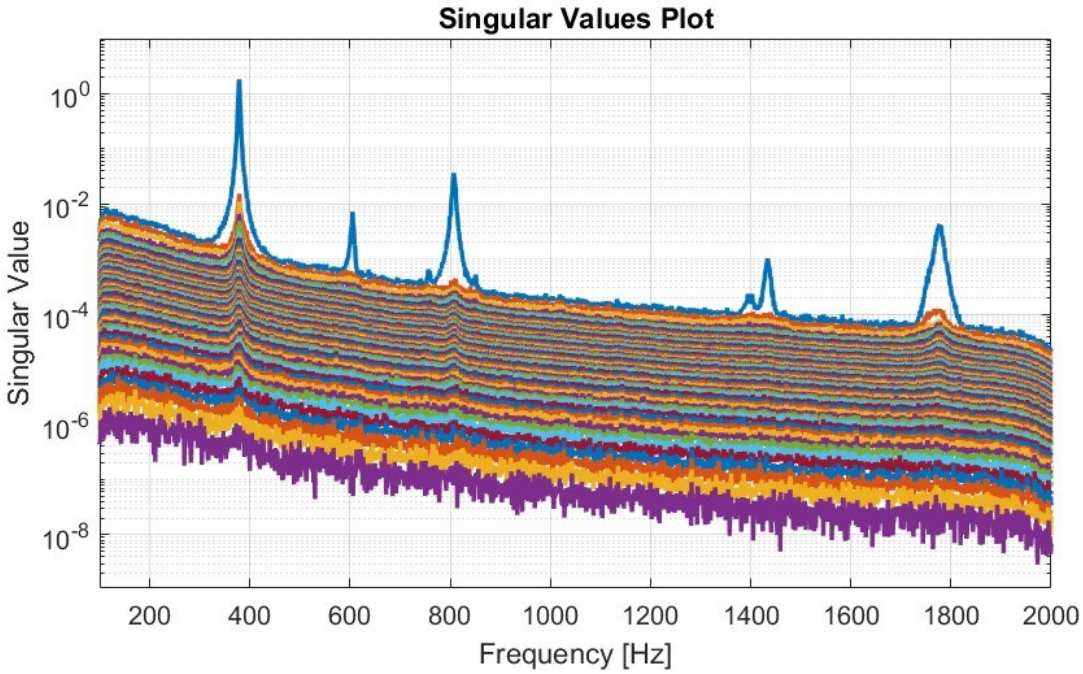

Figure 102. SVD for intermediate preload condition (200 Nm)

Figure 102 displays the singular values extracted through the Singular Value Decomposition (SVD) for the intermediate preload condition (200 Nm). The dominant modal contributions are highlighted by sharp peaks in the first singular value curve, indicating strong coherence across the measurement points and good excitation of the system despite the use of an uninstrumented hammer.

The comparison among the three preload configurations (0%, 25%, and 50%) is illustrated in Figure 103. Similar to the EMA results, a slight shift in natural frequencies is observed as the bolt preload increases: peaks corresponding to the joint resonances move toward higher frequencies as preload rises, indicating a progressive increase in joint stiffness. Although the magnitude of these shifts is modest, the trend is consistent and statistically repeatable across the full acquisition dataset.

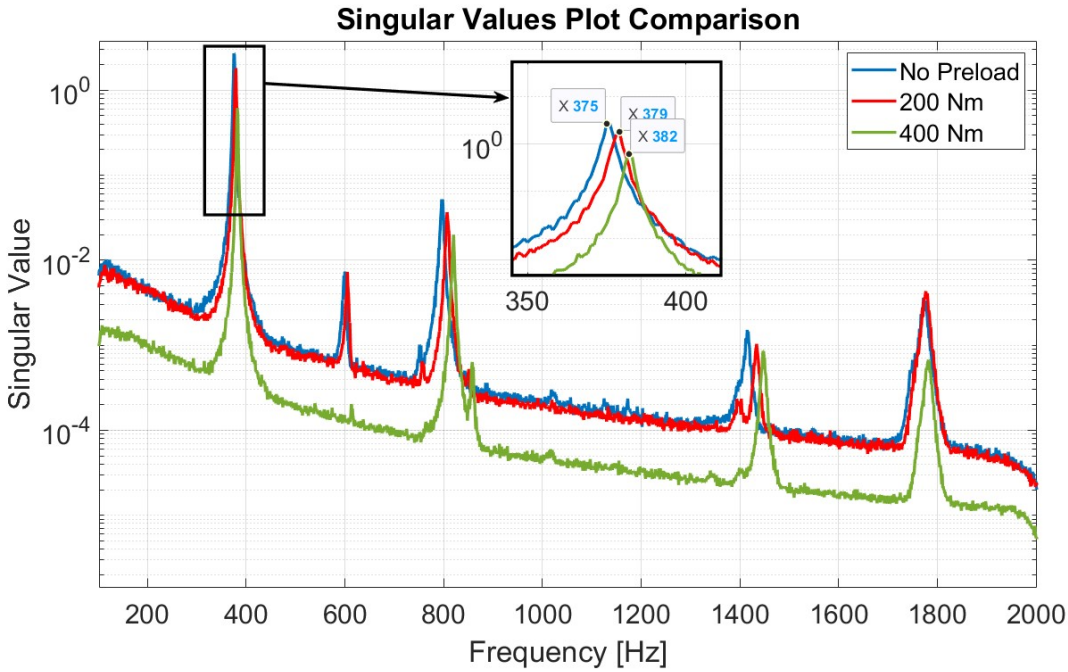

Figure 103. SVD comparison

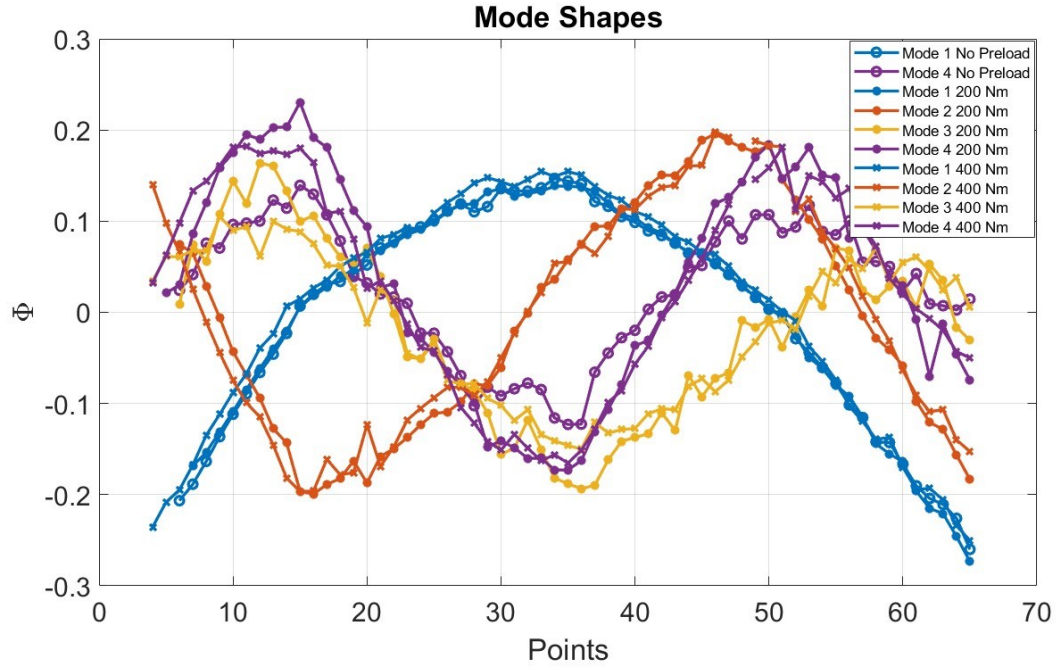

Figure 104. Mode shapes comparison

Finally, Figure 104 reports the mode shapes identified for the first four vibration modes at the three preload levels. While the overall modal topology remains consistent, confirming the structural integrity of the joint during testing, small variations in local deformation patterns can

be detected, particularly in the region of the fishplates and insulating layers where preload influences the mechanical coupling.

Most notably, the LiDAR-based system provides a significantly higher spatial resolution than the traditional accelerometer configuration: mode shapes are reconstructed over 65 measurement points instead of 6, enabling a far more detailed characterization of the joint's dynamic behavior and localized stiffness changes.

6.5 Modal tests discussion

The dynamic test results presented in this chapter provide a comprehensive validation of the findings obtained from the static bending campaign described in Chapter 5.

Both EMA and OMA approaches consistently demonstrated that bolt preload has a measurable influence on the stiffness of insulated rail joints, and thus on their modal behavior.

In particular, the vertical EMA tests confirmed the counterintuitive outcome already highlighted by the static analyses: lower bolt preload leads to a stiffer response in the vertical bending configuration. This phenomenon can be attributed to the wedging effect of the fishplates at the insulating gap. When the preload decreases, the jointed section is no longer fully constrained by bolt tension, and the applied load induces localized contact locking between the fishplates and the rail, which increases the apparent bending stiffness of the assembly. Conversely, when bolts are properly pretensioned, the joint behaves closer to a continuous rail, and its bending flexibility increases.

On the other hand, both horizontal EMA results and the higher-resolution OMA measurements clearly showed the opposite trend for lateral stiffness: an increase in bolt preload causes a corresponding increase in natural frequencies. In this case, the mechanical interpretation is fully consistent with common engineering expectations. Prestressed bolts improve frictional coupling, reduce joint looseness, and strongly constrain lateral movement of the fishplates relative to the rail web. Loss of preload introduces clearances and micro-slip phenomena, thereby reducing the horizontal stiffness of the insulated joint.

The OMA campaign further reinforced such observations, not only by confirming the frequency shift trends but also by revealing preload-dependent variations in local deformation patterns

and in damping behavior — aspects difficult to assess using only a limited number of accelerometers. These results demonstrate the advantages of LiDAR-based modal testing for detecting subtle changes in the dynamic response of jointed track components.

Overall, the combined experimental evidence suggests that dynamic modal analysis is a robust and sensitive tool for assessing bolt preload conditions and structural integrity in IRJs. The strong agreement between static and dynamic evaluations also provides confidence in the suitability of modal testing as a foundation for future condition-monitoring strategies, including potential field deployment for predictive maintenance.

7 Conclusion

7.1 General conclusions

The present work provided a comprehensive experimental and numerical investigation of insulated rail joints (IRJs), with a specific focus on the influence of bolt preload degradation on their structural performance under static and dynamic loading conditions. Through a combined methodology integrating Finite Element modelling, laboratory tests and modal analysis techniques, this work addressed a critical degradation mechanism that is frequently observed in service yet scarcely quantified in prior literature.

First, the numerical campaign demonstrated that the IRJ represents a strongly non-linear structural discontinuity, where complex interactions arise between dissimilar materials, frictional interfaces, geometric constraints and clearance phenomena. The loss of bolt preload was shown to significantly alter these interactions, leading to local variations in stiffness and stress redistribution in the jointed rail section. The model highlighted how the insulating gap and the presence of bolt holes cause strong stress concentrations—particularly dangerous because they can trigger subsurface crack growth beneath the fishplates, consistent with failures historically observed in service.

Experimental static four-point bending tests confirmed and expanded upon these numerical findings. Contrary to what would be expected for conventional bolted connections, a reduction in bolt preload increases the vertical stiffness of the IRJ. This apparently counter-intuitive behaviour was physically justified by the wedging mechanism of the fishplates between the rail head and foot: when bolt tension decreases, the normal contact forces rotate, enhancing interlocking and consequently stiffening the section locally. However, this effect is not beneficial: the artificially stiffened region leads to increased internal stress and reduced deformation compatibility with the surrounding track, potentially accelerating fatigue damage at the joint. This result emphasizes the necessity of maintaining high and stable bolt preload to mitigate premature deterioration.

To validate these outcomes under dynamic conditions and to explore the feasibility of field-applicable diagnostic approaches, a dedicated modal testing campaign was carried out. The first phase included Experimental Modal Analysis (EMA) with accelerometers and impact hammer excitation. The results revealed a clear directional dependency: under vertical excitation, a

reduction in bolt preload leads to an increase in resonance frequencies, confirming the rise in vertical stiffness associated with reduced pretension. In contrast, when the joint is excited horizontally, the opposite behavior emerges—proper bolt tension enhances frictional coupling and lateral constraint, resulting in higher stiffness, whereas reduced preload activates hole clearances and promotes relative sliding between components. These dynamic results therefore provide a coherent and powerful validation of the static test conclusions.

The second phase employed Operational Modal Analysis (OMA) with a LiDAR system, enabling high-resolution measurement of 65 spatial points without physical contact. The Frequency Domain Decomposition successfully identified multiple mode shapes and confirmed a consistent preload-dependent shift in natural frequencies. The enhanced spatial resolution yielded much more informative deformation patterns than accelerometers, demonstrating that LiDAR-based OMA is a promising and repeatable technique for real-track condition monitoring of IRJs. The ability to detect subtle modal variations linked to preload degradation opens the door to preventive maintenance strategies and structural health monitoring applications.

In summary, this thesis advances the state of the art in insulated rail joint (IRJ) research by:

- Demonstrating and experimentally validating the non-linear preload-dependent behaviour of IRJs
- Showing that preload loss leads to harmful stiffening in vertical flexure and softening in lateral shear
- Linking preload degradation to increased stress concentrations and potential crack initiation
- Introducing modal analysis as a diagnostic methodology for IRJ integrity monitoring
- Demonstrating the superiority of LiDAR-based modal acquisition for mode shape resolution

These findings highlight the central role of bolt preload stability in prolonging IRJ service life and strongly support the implementation of preload monitoring in railway maintenance frameworks.

7.2 Future developments

Building upon the findings of this research, two main directions for future work can be envisaged to further improve the understanding and the operational reliability of insulated rail joints.

The first concerns the evolution toward real-time preload monitoring. Since bolt preload has been demonstrated to strongly affect IRJ stiffness and mechanical integrity, establishing a continuous assessment framework would enable predictive maintenance strategies and reduce unexpected failures. Modern sensing technologies—such as strain-gauge–equipped smart bolts, low-cost force sensors, MEMS accelerometers, and magneto-mechanical displacement sensors—offer viable paths for integration into railway fastening systems at scale. Their installation in series along a railway network could allow continuous tracking of preload degradation and early detection of dangerous loosening phenomena, providing infrastructure managers with an automated diagnostic tool for the condition-based maintenance of IRJs.

The second development route involves advanced laboratory experimentation on a full-scale railway superstructure, using the newly commissioned test facility at the University of Parma (Figure 105).

Figure 105. Railway superstructure full-scale prototype

The setup includes ballast, sleepers, and two 6-m rails, each incorporating an IRJ, loaded by a full-dimension D2-category railway wheelset through a hydraulic actuator capable of both static and high-cycle dynamic loading. This infrastructure enables unprecedented testing scenarios: progressive preload loss, intentional damage at bolt holes, degradation of insulating layers, and ballast settlement effects can be introduced and monitored under millions of wheel passages. Such tests will allow tracking the long-term evolution of IRJ performance and validating damage indicators emerging from both static and modal analyses.

These two research avenues—one rooted in in-field monitoring technologies, the other grounded in controlled full-scale laboratory degradation—together pave the way for a next generation of insulated rail joint design and maintenance, aligning with the principles of predictive infrastructure management and safe mobility.

Funding

National Recovery and Resilience Plan (NRRP)
National Center for Sustainable Mobility
Spoke 4: Rail Transportation
WP4 "Digitization of railway transport"

Finanziato dall'Unione europea
NextGenerationEU

Ministero dell'Università e della Ricerca

Italiadomani
PIANO NAZIONALE DI RIPRESA E RESILIENZA

Bibliography

[1] *Transport safety performance in the EU: a statistical overview*. The Council, 2003.

[2] N. Kumar Mandal, M. Spiryagin, Q. Wu, and Z. Wen, "FEA of mechanical behaviour of insulated rail joints due to vertical cyclic wheel loadings," *Eng Fail Anal*, vol. 133, no. 1:105966, 2022.

[3] T. Watanabe, K. Goto, K. Matsuoka, and S. Minoura, "Validation of a dynamic wheel load factor and the influence of various track irregularities on the dynamic response of prestressed concrete sleepers," *Journal of Rail and Rapid Transit*, vol. 234, no. 10:1275-1284, 2019.

[4] M. Gallou, M. Frost, A. El-Hamalawi, and C. Hardwick, "Assessing the deflection behaviour of mechanical and insulated rail joints using finite element analysis," *Proc Inst Mech Eng F J Rail Rapid Transit*, vol. 232, no. 9, pp. 2290–2308, Oct. 2018, doi: 10.1177/0954409718766925.

[5] M. P. Papaelias, C. Roberts, and Davis C L, "A review on non-destructive evaluation of rails: State-of-the-art and future development," *Journal of Rail and Rapid Transit*, vol. 222, no. 4:367-384, 2008.

[6] A. Bracciali and G. Megna, "FMEA, monitoring, retrofit and redesign of insulated rail joints," *IOP Conf Ser Mater Sci Eng*, vol. 1306, no. 1, p. 012014, May 2024, doi: 10.1088/1757-899x/1306/1/012014.

[7] "Railway passenger transport statistics - quarterly and annual data," Sep. 2024.

[8] "Global rail sustainability report," 2023.

[9] K. Gholamizadeh, E. Zarei, and M. Yadzi, "Railway Transport and Its Role in the Supply Chains: Overview, Concerns, and Future Direction," in *The Palgrave Handbook of Supply Chain Management*, Palgrave Macmillan Cham, Ed., 2022, pp. 1–28.

[10] European Union Agency for Railways, "Report on Railway Safety and Interoperability in the EU," Jun. 2020.

[11] Rete Ferroviaria Italiana (RFI), "Proposta di revisione tariffaria sulla base di un modello econometrico e ingegneristico per il calcolo dei costi direttamente legati alla prestazione del servizio ferroviario.," Jan. 2022.

[12] N. Kumar Mandal and B. Peach, "An Engineering Analysis of Insulated Rail Joints: A General Perspective," Aug. 2010.

[13] A. D. Kerr and J. E. Cox, "Analysis and tests of bonded insulated rail joints subjected to vertical wheel loads," 1999.

[14] Z. Wen, X. Jin, and W. Zhang, "Contact-impact stress analysis of rail joint region using the dynamic finite element method," *Wear*, vol. 258, pp. 1301–1309, Mar. 2005.

[15] H. Yin, Y. Qian, J. R. Edwards, and K. Zhu, “Investigation of Relationship between Train Speed and Bolted Rail Joint Fatigue Life using Finite Element Analysis,” *Transportation Research Record Journal of the Transportation Research Board*, Nov. 2018.

[16] RFI, “2021 Annual report,” 2021.

[17] M. Marshall, R. Lewis, R. Dwyer-Joyce, F. Demilly, and Y. Flament, “Ultrasonic Measurement of Railway Wheel Hub–Axle Press-Fit Contact Pressures,” *Journal of Rail and Rapid Transit*, vol. 225, no. 3, pp. 287–298, 2011.

[18] Y. Chen, “The effect of proximity of a rail end in elastic-plastic contact between a wheel and a rail,” *Journal of Rail and Rapid Transit*, vol. 217, no. 3, pp. 189–201, 2003.

[19] K. Koro, K. Abe, M. Ishida, and T. Suzuki, “Timoshenko Beam Finite Element for Vehicle—Track Vibration Analysis and its Application to Jointed Railway Track,” *Journal of Rail and Rapid Transit*, vol. 218, no. 2, pp. 159–172, 2004.

[20] H. Kataoka, N. Abe, O. Wakatsuki, and Y. Oikawa, “A dynamic Stress Analysis of Joint Rail Using Finite Beam Element Model,” in *Proceeding of the 14th Japan National Symposium on Boundary Element Method*, 1997.

[21] M. Busquet, L. Baillet, C. Bordreuil, and Y. Berthier, “3D Finite Element Investigation on the Plastic Flows of Rolling Contacts—Correlation with Railhead Microstructural Observations,” *Wear*, vol. 258, no. 7, pp. 1071–1080, 2005.

[22] Z. Wen, X. Jin, and W. Zhang, “Contact-Impact Stress Analysis of Rail Joint Region Using the Dynamic Finite Element Method,” *Wear*, vol. 258, no. 7, pp. 1301–1309, 2005.

[23] Y.-C. Chen and L.-W. Chen, “Effects of Insulated Rail Joint on the Wheel/Rail Contact Stresses under the Condition of Partial Slip,” *Wear*, vol. 260, no. 12, pp. 1267–1273, 2006.

[24] E. Kabo, J. C. O. Nielsen, and A. Ekberg, “Prediction of Dynamic Train-Track Interaction and Subsequent Material Deterioration in Presence of Insulated Rail Joints,” *Vechicle System Dynamics*, vol. 44, pp. 718–729, 2006.

[25] N. Mandal and M. Dhanasekar, “Sensitivity Analysis of End Post Materials of Insulated Rail Joints Sing Finite Element Analysis,” in *9th International Conference on Contact Mechanics and Wear of Rail/Wheel System*, 2012, pp. 509–515.

[26] N. Mandal and B. Peach, “3D Stress Analysis of Insulated Rail Joints,” in *9th International Heavy Haul Conference, Shanghai, China*, 2009.

[27] T. Mazilu, I. Radu Răcănel, C. L. Ghindea, C. Radu Iuliu, and L. Mihai-Cornel, “Rail joint model based on the Euler-Bernoulli beam theory,” *Romanian Journal of Transport Infrastructure*, vol. 8, no. 2, 2019.

[28] M. Oregui, M. Molodova, A. Nunez, R. Dollevoet, and Z. Li, “Experimental Investigation into the Condition of Insulated Rail Joints by Impact Excitation,” *Exp Mech*, vol. 55, pp. 1597–1612, 2015.

[29] M. Oregui, Z. Li, and R. Dollevoet, “An investigation into the modeling of railway fastening,” *Int J Mech Sci*, vol. 92, pp. 1–11, 2015, doi: 10.1016/j.ijmecsci.2014.11.019.

[30] H. Xiao, G. Liu, D. Yan, Y. Zhao, J. Wang, and H. Wang, “Field test and numerical analysis of Insulated rail joints in heavy-haul railway,” *Constr Build Mater*, vol. 298, Sep. 2021, doi: 10.1016/j.conbuildmat.2021.123905.

[31] M. E. Carolan, D. Y. Jeong, and A. B. Perlman, “Engineering studies on joint bar integrity, part II: finite element analysis,” 2014.

[32] B. Talamini, D. Y. Jeong, and J. Gordon, “Estimation of the fatigue life of railroad joint bars.” [Online]. Available: https://proceedings.asmedigitalcollection.asme.org

[33] N. K. Mandal, “Plastic ratchetting of railhead material in the vicinity of insulated rail joints with wheel and thermal loads,” *Wear*, vol. 330–331, pp. 540–553, 2015, doi: 10.1016/j.wear.2015.01.003.

[34] A. K. Himebaugh, R. H. Plaut, and D. A. Dillard, “Finite element analysis of bonded insulated rail joints,” *Int J Adhes Adhes*, vol. 28, no. 3, pp. 142–150, Apr. 2008, doi: 10.1016/j.ijadhadh.2007.09.003.

[35] T. Pang and M. Dhanasekar, “Dynamic finite element analysis of the wheel rail interaction adjacent to the insulated rail joints.”

[36] K. Giannakos, “Mathematical analysis of the transient loads for a deformed joint or welding in a railway track.” [Online]. Available: http://www.orb-

[37] G. Bono, C. Focacci, and S. Lanni, *La sovrastruttura ferroviaria*. 1997.

[38] A. La Placa, F. Benelli, G. Bianchi, F. Freddi, and F. Giuliani, “Behaviour of supported and unsupported insulated rail joint under different preload conditions,” in *Transportation Research Procedia*, Rome, 2024.

[39] A. Nemeth and S. Fischer, “Laboratory test results of glued insulated rail joints assembled with traditional steel and fibre-glass reinforced resin-bonded fishplates.,” *Science and Transport Progress*, no. 3(81), pp. 65–86, Jun. 2019, doi: 10.15802/stp2019/171781.

[40] D. Peltier and A. Mathews, “Measuring degradation of bonded insulated rail joints.”

[41] P. Boyd, N. K. Mandal, N. Mandal, T. Bandula, N. Zong, and M. Dhanasekar, “Experimental investigation into the failure behaviour of insulated rail joints,” 2012.

[42] RFI, “Traversoni e traverse speciali in calcestruzzo vibrato, armato e precompresso per apparecchi del binario – specifica tecnica di fornitura.”

[43] RFI, “Giunzioni incollate isolanti – specifica tecnica di fornitura – Codifica: RFI TCAR SF AR 07 008 A.”

[44] F. Lucà, S. Manzoni, S. Pavoni, and M. Vanali, “OMA-based Approach for Structural Health Monitoring: the Case of Palazzo Lombardia.”

[45] R. Brincker and C. E. Ventura, *Introduction to Operational Modal Analysis*. 2015.